The interplay of differentially γ-carboxylated vitamin K dependent proteins constitute variable VKCFD1 phenotypes

Dissertation

zur

Erlangung des Doktorgrades (Dr. rer. nat.)

der

Mathematisch-Naturwissenschaftlichen Fakultät

der

Rheinischen Friedrich-Wilhelms-Universität Bonn

vorgelegt von

Suvoshree Ghosh

aus

Kolkata, India

Bonn, March 2021

Angefertigt mit Genehmigung der Mathematisch-Naturwissenschaftlichen Fakultät der Rheinischen Friedrich-Wilhelms-Universität Bonn

1. Gutachter: Prof. Dr. med. Johannes Oldenburg

2. Gutachter: Prof. Dr. rer. nat. Diana Imhof

Tag der Promotion: 27.10.2021

Erscheinungsjahr: 2021

Abstract

Vitamin K dependent coagulation factor deficiency type 1 (VKCFD1) is a rare hereditary bleeding disorder caused by mutations in γ-Glutamyl carboxylase (*GGCX*). VKCFD1 patients are treated with high dose of vitamin K, which corrects the haemostatic phenotype in most cases. In addition, these patients often exhibit non-haemostatic phenotypes such as skin hyperlaxity, skeletal and cardiac abnormalities. These phenotypes are most likely developed due to the undercarboxylation of one or more vitamin K dependent proteins. However, it remained elusive how *GGCX* mutations affect γ-carboxylation of VKD proteins and which undercarboxylated protein leads to the development of a specific phenotype.

In this PhD thesis, I have used CRISPR/Cas9 engineered *GGCX* knockout HEK293T cells to evaluate the effect of 22 GGCX missense mutations on γ-carboxylation of 9 different vitamin K dependent proteins with respect to various concentrations of vitamin K. For this evaluation a specific ELISA assay was established, where only functional, γ-carboxylated VKD proteins were detected. Furthermore, a GGCX *in silico* model was generated, where molecular docking was performed to identify the vitamin K hydroquinone binding site.

All GGCX mutations were categorized into responder and low responder mutations, thereby determining the efficiency of vitamin K supplementation. It was observed that all VKCFD1 patients have at least one vitamin K responsive GGCX allele that is able to γ-carboxylate clotting factors sufficient for a viable phenotype. For non-haemostatic phenotypes, the findings highlight that the deficiency to γ-carboxylate Gla-rich protein leads to skin hyper-laxity whereas facial dysmorphologies are caused by reduced γ-carboxylated MGP. Moreover, the vitamin K hydroquinone binding site in GGCX was identified, where mutations within this site severely affect γ-carboxylation efficiency.

With these new structural and functional data, the clinical outcome of each VKCFD1 genotype can be predicted thus enabling optimized treatment strategies.

Zusammenfassung

Vitamin K-abhängiger Gerinnungsfaktor-Mangel Typ 1 (VKCFD1) ist eine seltene erbliche Blutungsstörung, die durch Mutationen in der γ-Glutamyl carboxylase (GGCX) verursacht wird. Der Blutungsphänotyp wird mit hohen oralen Dosen Vitamin K (K) behandelt um diesen zu korrigieren. Zusätzlich weisen VKCFD1-Patienten häufig weitere Phänotypen wie extreme Faltenbildung der Haut, und/oder Skelett- und Herzanomalien auf. Diese Phänotypen werden wahrscheinlich dadurch verursacht, dass ein oder mehrerer Vitamin K abhängige Proteine nicht ausreichend γ-carboxyliert werden. Bislang weiß man nicht, wie Mutationen in der GGCX die γ-Carboxylierung von Vitamin K abhängigen Proteinen beeinflussen und welches Protein für den jeweiligen Phänotyp verantwortlich ist.

In der vorliegenden Arbeit habe ich mittels CRISPR/Cas9 generierte GGCX-Knockout HEK293T-Zellen verwendet, um die Auswirkung von 22 Missense Mutationen auf die γ-Carboxylierung von 9 verschiedenen Vitamin K abhängigen Proteinen zu untersuchen. Dafür wurde ein ELISA assay etabliert, indem funktionelles und durch die GGCX modifizierte Vitamin K abhängige Proteine detektiert werden. Darüber hinaus wurde ein GGCX *in silico* Modell erstellt, bei dem ein molekulares Andocken durchgeführt wurde, um die Vitamin K-Hydrochinon-Bindungstasche zu identifizieren.

Alle GGCX Mutationen wurden dahingehend kategorisiert, ob sie auf erhöhte Gaben von Vitamin K ansprechen, um somit die Therapierbarkeit mit Vitamin K einzuschätzen. Alle VKCFD1-Patienten haben mindestens ein funktionelles GGCX-Allel. welches auf Vitamin K anspricht um Gerinnungsfaktoren zu γ-carboxylieren. Dies reicht für einen lebensfähigen Phänotyp aus. Im Hinblick auf den nicht-hämatologischen Phänotyp fanden wir heraus, dass unzureichend γ-carboxyliertes Gla-reiches Protein die Ursache des Hautphänotyps. Der Mangel an γ-Carboxyliertem MGP Protein führt zu Gesichts-hyperplasien. Darüber hinaus identifizierten wir die Bindungstasche von Vitamin K-Hydrochinon- in der GGCX. Mutationen, die diese Bindungstasche ändern, führen zu den schwerwiegensten VKCFD1-Phänotypen.

Table of contents

List of abbreviations

°C	degree celsius
Aa	Amino acid
Amp	Ampicillin
C1	VKORC1
Cas	CRISPR associated
cDNA	copy/ complementary DNA
CO_2	Carbon dioxide
CRISPR	Clustered Regularly Interspaced Short Palindromic Repeats
crRNA	CRISPR RNA
C-terminus	Carboxy-terminus
d,h, min, s	Day, hour, minute, second
ddNTP	Dideoxyribonucleotide triphosphate
DNA	deoxyribonucleic acid
dNTP	deoxynucleotide triphosphate
DSB	Double strand break
dsDNA	Double stranded DNA
EC50	Effective concentration
E. coli	*Escherichia coli*
e.g.	exempli gratia, for example
ER	Endoplasmatic reticulum
ERGIC	ER-Golgi intermediate compartment 53 kDa protein
et al.	et altera
F	Factor (e.g. FII ,FX)
G	Gram
Gas6	Growth arrest-specific gene 6
GGCX	γ-glutamyl γ-carboxylase
Gla	γ-carboxy glutamate
Glu	Glutamate (glutamic acid)
GRP	Gla-rich protein
HEK	Human embryonic kidney cells
hFIX	Human FIX
HRP	Horseradish peroxidase
hVKORC1	Human VKORC1
hVKORC1L1	Human VKORC1L1
i.e.	id est
IC_{50}	Half maximal inhibitory concentration
IC_{80}	Eighty percent inhibitory concentration
Indels	Insertion and deletion
ISTH	International society of thrombosis and hemostasis
K>O	Vitamin K 2,3-epoxide
Kb	Kilo bases
kDa	kilo dalton
KH_2	Vitamin K hydroquinone
KO	knockout
L1	VKORC1L1
M	molar, mol per liter
m, µ, n, p	milli-, mikro-, nano-, pico-
MGP	Matrix Gla protein
MK4	Menaquinone 4

MPV	Mean platelet volume
mRNA	messenger RNA
Myc tag	polypeptide protein tag derived from the c-myc gene product
NHEJ	Non-homologous end joining
NQO1	NAD(P)H:Quinon akzeptor oxidoreduktase
Nt	Nucleotide
N-terminus	Amino terminus
OAC	Oral anticoagulant
OCN	Osteocalcin
PAM	Protospacer adjacent motif
PCR	Polymerase chain reaction
PDI	Proteindisulfide isomerase
pH	potential hydrogen
PLT	Platelet count
PRGP	Proline-rich Gla protein
ROS	Reactive oxygen species
rpm	Revolutions per minute (U/min)
RT	Room temperature
SD	Standard deviation
SEM	Standard error of mean
ssRNA	Single stranded RNA
TF	Tissue factor
TFPI	Tissue factor pathway inhibitor
TM domain	Transmembrane domain
TMG	Transmembrane Gla protein
UIBC	Unsaturated iron binding capacity
VKCFD1 / 2	Vitamin K clotting factor deficiency type 1 / type 2
VKD	Vitamin K dependent
VKOR	Vitamin K 2,3-epoxid reductase
VKORC1	Vitamin K 2,3-epoxide reductase complex subunit 1
w/v	weight per volume
WT	Wild type

1. Introduction

γ-Glutamyl carboxylase (GGCX) is a post-translational modifying enzyme located in the endoplasmic reticulum (ER) that converts specific glutamic acid residues (Glu) into γ-carboxyglutamic acid residues (Gla) (Figure 1) [1–5]. γ-Carboxylation specially takes place in vitamin K dependent (VKD) proteins which is required for their function. VKD proteins includes haemostatic proteins- Factors II (FII), VII (FVII), IX (FIX), X (FX), Protein C (PC), Protein S (PS) and Protein Z (PZ) [6–14] and non-haemostatic proteins- osteocalcin (BGLAP), matrix Gla protein (MGP), upper zone of growth plate and cartilage matrix associated protein (UCMA/GRP), growth arrest specific 6 (GAS6), proline-rich Gla proteins (PRGPs) 1 and 2, and transmembrane Gla proteins (TMGs) 3 and 4 [15–29].

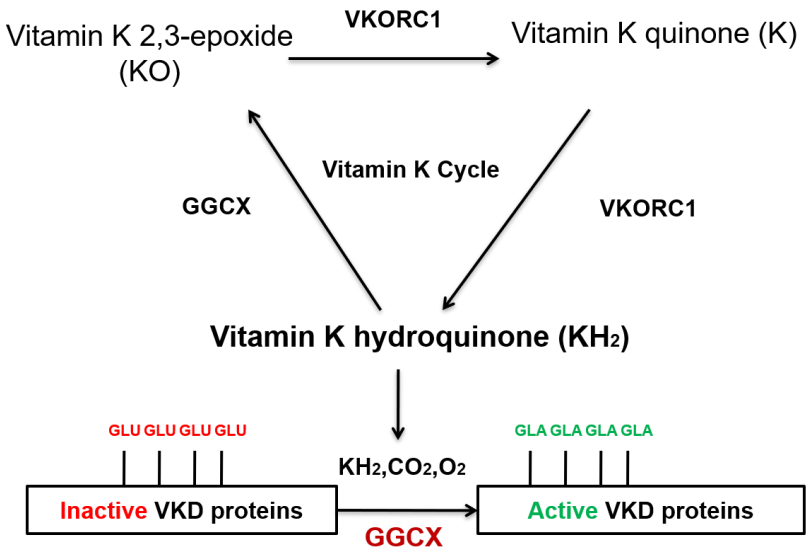

Figure 1: Schematic of γ-carboxylation process and vitamin K cycle. Inactive vitamin K dependent (VKD) proteins are post-translationally modified by GGCX into active state. γ-Carboxylation requires three co-substrates- vitamin K hydroquinone (KH_2), carbon dioxide (CO_2) and oxygen (O_2). Vitamin K 2,3- epoxide (KO) is formed by the epoxidase activity of GGCX which is recycled by vitamin K oxidoreductase complex subunit 1 (VKORC1) by a process called vitamin K cycle.

γ-Carboxylation is a vitamin K dependent process, where vitamin K hydroquinone (KH_2) is oxidized to vitamin K epoxide (K>O) by the epoxidase activity of GGCX [30]. K>O generated from this reaction is recycled back to vitamin K quinone (K) and further to KH_2 by another enzyme of the vitamin K cycle called vitamin K oxidoreductase complex subunit 1 (VKORC1)[31–34] in order to continue this post-translational modification.

1.1 γ-Glutamyl carboxylase (GGCX)

GGCX enzyme is encoded by the reverse strand of chromosome 2p11.2[35,36]. The longest transcript comprises of 15 exons which encodes for a 94 kDa protein (758 amino acid residues) [37] . It is a multi-pass transmembrane protein with its N-terminus in the cytoplasm and the C-terminus in the ER lumen and is expressed ubiquitously [38,39]. GGCX does not have higher homology to any known proteins.

1.2 Mechanism of γ-carboxylation

The mechanism of γ-carboxylation can be broadly divided into two steps- catalysis of vitamin K oxygenation and Glu γ-carboxylation. GGCX is a bifunctional enzyme which catalyzes both γ-carboxylation and epoxidation in a 1:1 stoichiometry [40]. The process of γ-carboxylation requires three co-substrates (vitamin K hydroquinone, CO_2, O_2) and a substrate (VKD proteins).

The energy from vitamin K hydroquinone (KH_2) oxygenation is used by GGCX to γ-carboxylate VKD proteins. The oxidation is performed by GGCX with its epoxidase activity. Dowd et al. proposed a base amplification model for γ-carboxylation which requires abstraction of hydrogen from Glu residues for initiating the process [41]. The mechanism of epoxidation driving γ-carboxylation is initiated by a weak base in GGCX, which deprotonates KH_2 enabling it to interact with O_2, thus forming a strong base intermediate (Figure 2). This strong vitamin K base (K^-) then abstracts hydrogen from Glu residues, which is a crucial and chemically challenging step. The intermediate carbanion then interacts with CO_2 forming Gla [42].

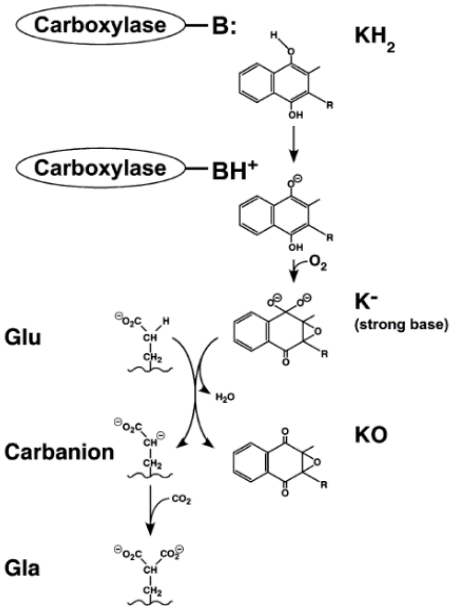

Figure 2: Schematic of mechanism of base amplification and γ-carboxylation. (Taken from Rishavy, M. A. et al., *Biochemistry*, 2006) Active site on γ-carboxylase (B:) deprotonates KH_2 which reacts with O_2 forming a strong base (K-). Deprotonation of Glu by this strong base results in carbanion formation, which reacts with CO_2 forming Gla, while the vitamin K base is protonated to form vitamin K epoxide (KO). [43]

1.2.1 Catalysis of vitamin K oxygenation by GGCX

As mentioned above vitamin K oxygenation is a crucial rate limiting step of γ-carboxylation. For a long time, it was believed that a cysteine is the catalytic base responsible for this rate limiting step, which was proven wrong as mutagenesis of all 10 cysteines in GGCX did not eliminate the vitamin K oxygenation activity [44]. Further chemical inactivation experiments suggested that histidine or lysine is a catalytic base. So, alignment of mammalian GGCX sequence with Leptospira homolog identified three conserved histidine and one lysine which were then mutated to alanine. Only the K218A mutant showed complete loss of oxygenase activity thus proving that this is the active site (Figure 3). The rescue experiments with amines also showed that K218 is the weak base in GGCX, which initiates the base amplification [43].

1.2.2 Catalysis of Glu γ-carboxylation by GGCX

Until now only one residue in GGCX is known to be involved in Glu γ-carboxylation. During the search for the catalytic base one conserved H160A did not affect oxygenation activity but showed 10-fold decreased Glu γ-carboxylation activity and also weak CO_2 binding. To decipher the specific role of H160 in Glu γ-carboxylation, short Glu containing peptide with tritium at the γ-carbon were checked for tritium release. H160A showed 10-fold reduction in tritium release which indicate its contribution to Glu deprotonation by the strong K base. It is

postulated that either H160 is involved in supporting Glu deprotonation by interaction with CO_2, which neutralizes the negative charge or it interacts with the original γ-carboxyl group resulting in indirect binding of CO_2, which is part of the reactions transition state [2 28] .

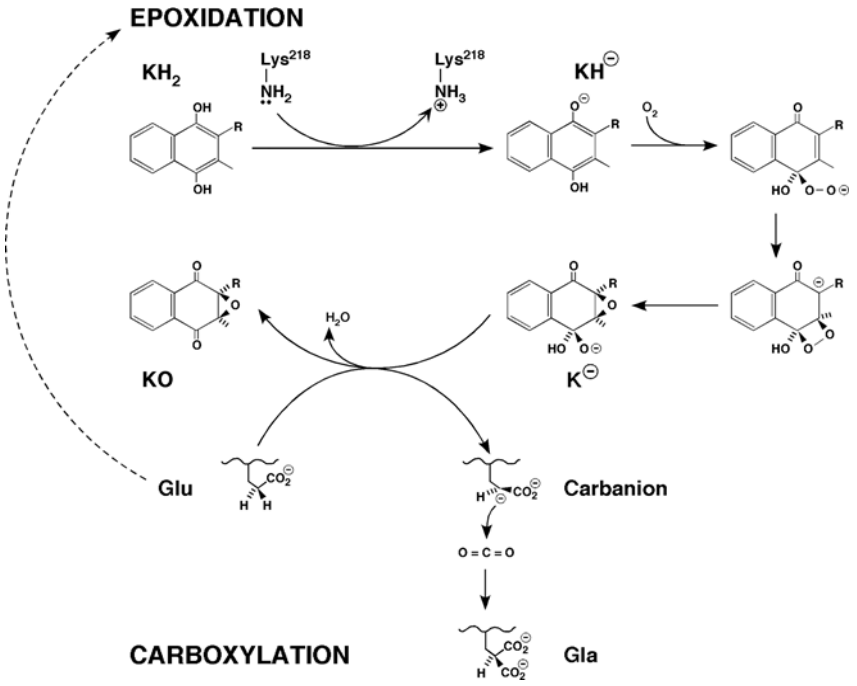

Figure 3: γ-carboxylation epoxidation coupling schematic. (taken from Rishavy, M. A. & Berkner et al, *Biochemistry* 2008) The γ-carboxylase (GGCX) is a bifunctional enzyme which has both an epoxidase that converts reduced vitamin K (KH_2) to vitamin K epoxide (KO) and a γ-carboxylase converts Glu to Gla. K218 is the known active site which acts as a weak base.[45]

1.2.3 Co-substrates of γ-carboxylation reaction

GGCX requires three co-substrates namely hydroquinone form of vitamin K, O_2 and CO_2. Until now the sites where three cofactors interacts with GGCX is unknown.

Vitamin K is a fat-soluble micronutrient and exits in two different natural forms; vitamin K_1 (phylloquinones) primarily found in green leafy vegetables (f.e. spinach and olive) and vitamin K_2 (menaquinone) found in trace amounts in animal products (f.e. egg yolks, cheese, and butter) (Figure 4). The daily requirement in normal population for vitamin K has been proposed to be 120 µg/day for men and 90 µg/day for women. From structural point of view, vitamin K has a hydrophobic poly-isoprenoid side chain which vary in bond saturation and length and common polar hydrophilic 2-methlyl-1,4-naphtoquinone ring which confers the catalytic activity. Vitamin K_1 has a phytyl side chain with only one unsaturated bond. Vitamin K_2 family (MK-n) is

divided into isoprenologs with number of prenyl units in the isoprenoid side chain. It is believed that variable tails of vitamin K might show differential anchoring in the ER membrane [2].

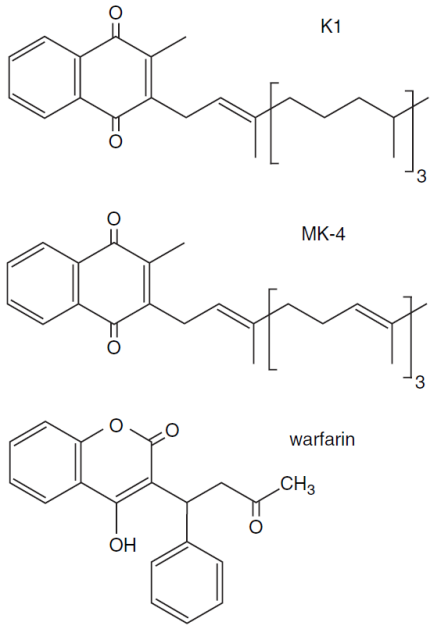

Figure 4: Schematic of different forms of K (taken from Berkner et al., *JTH* 2004) The structure of the different forms of vitamin K (K1, MK4) and the inhibitor of VKOC1 enzyme (warfarin).[46]

1.2.4 Interaction of VKD proteins with GGCX

The interaction of VKD proteins, the main substrate of γ-carboxylation, with GGCX is of specific interest (Figure 5). VKD proteins have variable propeptide sequence and a multiple number of Glu residues in the Gla domain which are γ-carboxylated. Two regions, the propeptide domain and the Gla domain of VKD proteins are directly interacting with GGCX. The propeptide domain of around 18 residues are initially recognized by GGCX and binds to its exosite. This binding event then places the Gla domain in the Gla binding site of GGCX where the γ-carboxylation takes place in a single binding event by processive mechanism.

The identification of natural occurring GGCX mutations L394R and W501S contributed to the knowledge of Gla and propeptide binding site residues in GGCX, which are in between 393-404 and 495-513 respectively [47] [48].

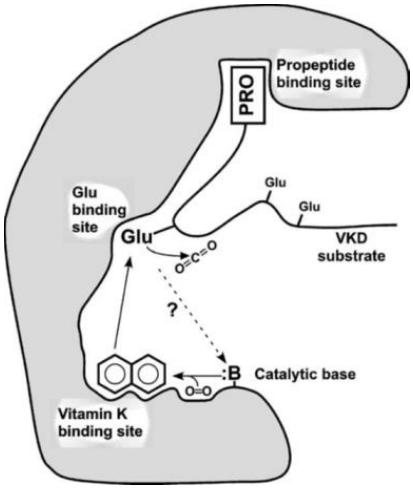

Figure 5: Schematic of the functional binding sites for VKD proteins in GGCX. (taken from Berkner et al., *JTH* 2004). Propeptide binding site, Glu binding site, vitamin K binding site and catalytic base. [46]

1.3 VKD proteins

VKD proteins undergoes γ-carboxylation by GGCX enzyme. Broadly, these proteins can be categorized into hepatic and extrahepatic VKD proteins [49]. Initially, it was believed that only specific haemostatic proteins involved in coagulation get γ-carboxylated. However, later it was found that other proteins involved in calcification undergo γ-carboxylation (BGLAP, MGP, and GRP). Then proteins like GAS6 were included known to have role in cell signaling followed by the addition of four novel membrane proteins i.e. the PRGPs and TMGs. Until now the function of PRGPs and TMGs are not clear.

Predominantly, VKD proteins have similar structural organization, where the N-terminal propeptide initially binds to GGCX and 3 to 16 Glu residues in the corresponding Gla domain are γ-carboxylated (Figure 6). After this modification in the ER, the propeptide is cleaved in the Golgi apparatus and the VKD protein is transported to its destined location. Apart from having different number of Glu residues in the Gla domain, these proteins differ in the length of the propeptide domain, which has variable affinity for GGCX [50].

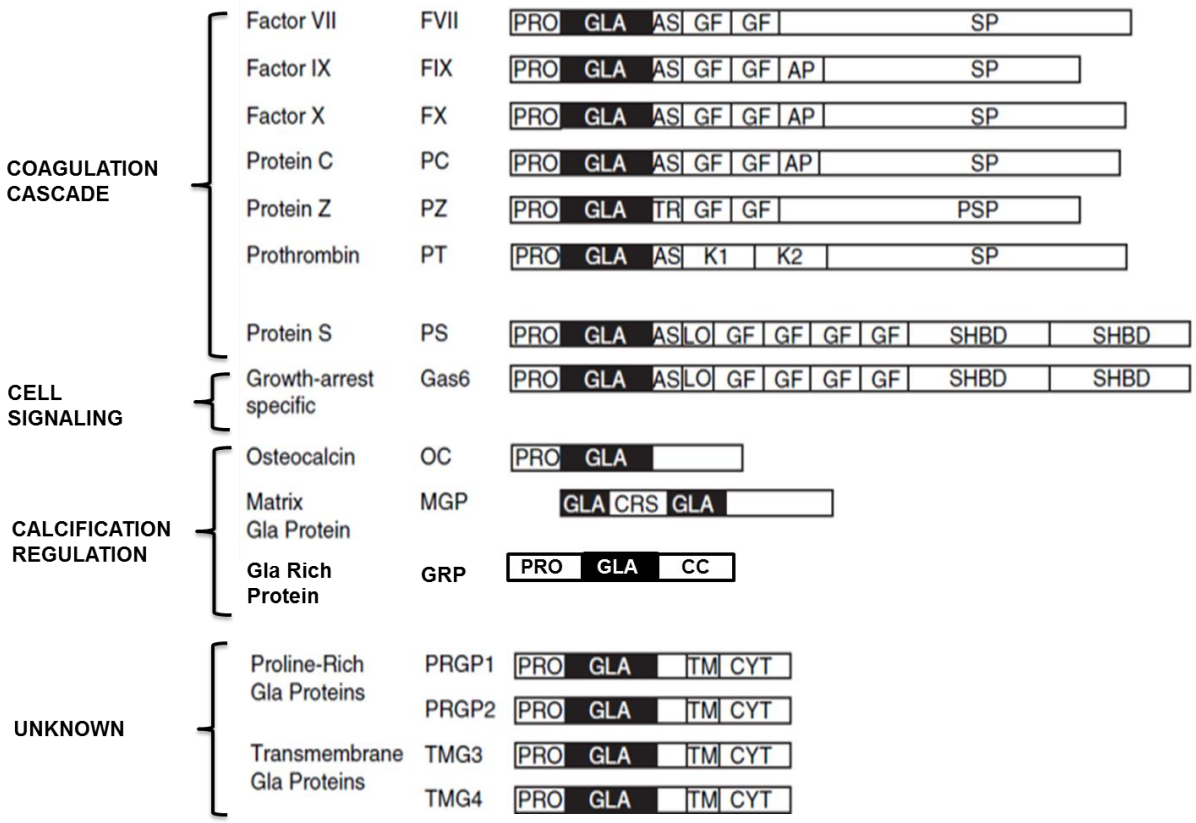

Figure 6: Schematic of different VKD proteins with their domain distribution (Taken and modified from K. L . Berkner and K. W. Runge, *J Thromb Haemost* 2004). FX, FVII, FIX, FX, PC, PS, and PZ functions as coagulation proteins. Gas6 has function in cell signaling, acts as a ligand of TAM receptor. Osteocalcin, matrix Gla protein and gla rich protein regulates calcification. Proline rich and transmembrane Gla proteins have unknown function.[46]

1.3.1 Coagulation cascade and VKD haemostatic proteins

Coagulation cascade is a series of complex reaction involving two types of pathways (extrinsic and intrinsic) and different phases (initiation and amplification) which ultimately leads to fibrin formation resulting in clotting [51–53]. This cascade includes different haemostatic proteins, mostly produced in the liver, which circulate as zymogens in the bloodstream and are later activated to serine proteases. A major number of clotting factors undergoes vitamin K dependent γ-carboxylation (Figure 7).

The extrinsic pathway is activated by tissue factor (TF), which is located in the tissue adventitia and after vascular injury it comes in contact with blood. TF has high affinity for FVII which forms a complex after vascular injury. This binding takes place in the presence of calcium which then activates FVII to FVIIa by trace amount of proteases such FVIIa, FIXa, FXa, and thrombin which circulates in the blood. The FVIIa-TF complex activates FX to FXa. The newly activated FXa forms complex with FVa in presence of calcium and phospholipids which converts

prothrombin to thrombin. The generation and release of thrombin takes place from the carboxyl-terminal of the precursor and the Gla and kringle-containing region which is from the amino-terminal is attached to the phospholipid. The formation of thrombin ultimately leads to generation of fibrin from fibrinogen.

The intrinsic pathway is longer which begins with endothelial collagen exposure activating FXII to FXIIa. FXIIa then activates FXI to FXIa which ultimately leads to FX activation (Figure 7).The formation of tenase complex from both extrinsic and intrinsic activates the common pathway which cleaves FII (prothrombin) to FIIa (thrombin) ultimately leading to the formation of fibrin from fibrinogen. The formation of fibrin is the final step in haemostasis, which stabilizes the platelet plug [54].

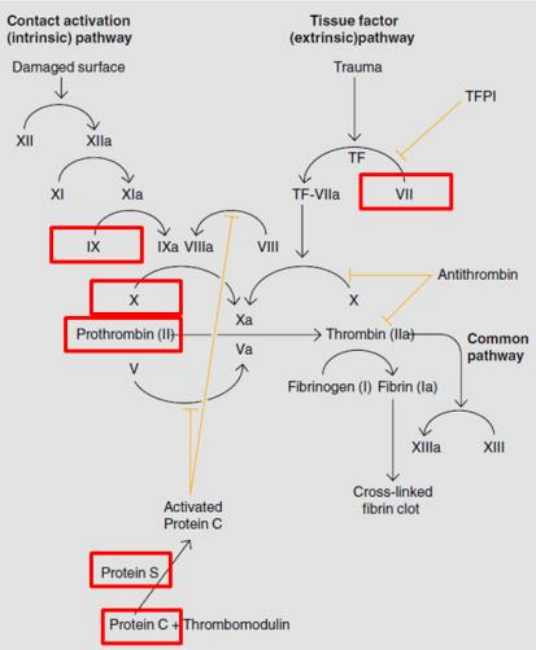

Figure 7: Coagulation cascade (taken and modified from Non-Vitamin K Antagonist Oral Anticoagulants: A Concise Guide, Shantsila E, Lip GYH, Cham (CH): Adis; 2016.). Coagulation cascade has two types of pathway (intrinsic and extrinsic). Several pro-coagulatory and anti-coagulatory factors works together for regulate this cascade. The coagulation proteins inside red boxes are undergoing γ-carboxylation.[55]

A negative feedback mechanism exists to regulate the cascade and prevent thrombosis in the form of anti-coagulation proteins namely, PS, PC, PZ. PZ circulates in the blood bound to the serine protease protein Z-dependent protease inhibitor (ZPI) which co-localizes to cell surface during coagulation and inhibits FXa. PC is another anticoagulant which acts on the complex feedback loop where thrombin inhibits its own production. Once the clot has been formed the

procoagulant activity of thrombin is reversed to an anticoagulant activity which binds to thrombomodulin. This thrombin-thrombomodulin complex then cleaves protein C and produces activated protein C (APC), which then cleaves FVa and FVIIIa making it inactive. Another anticoagulant PS acts a cofactor where it binds to APC and changes its position on the cell membrane. Apart from anti-coagulatory function, PC also has anti-inflammatory properties and PS also circulates in a bound form with C4BP which is a regulator of complement system [46].

Out of all the coagulation factors, seven proteins undergo the process of vitamin K dependent γ-carboxylation (FII, FVII, FIX, FX, PC, PS, and PZ). This multiple negatively charged Glu residues in the Gla domain increases the affinity for calcium binding, which then transforms the random coiled Gla domain into ordered structures. VKD proteins which has large number of Gla residues binds to several calcium ions thereby stabilizing the tertiary structure. This structure of calcium bound Gla domain helps it to bind to the cell surface by penetrating the lipid bilayer [46,56,57].

1.3.2 Non-haemostatic VKD proteins

Until now eight proteins are known to undergo γ-carboxylation whose function is not involved in coagulation cascade. Unlike coagulation proteins that are only functional when γ-carboxylated, uncarboxylated non-haemostatic proteins have function in normal physiology. Thereby, the balance between Glu and Gla form in non-haemostatic proteins has to be well regulated.

Three of the VKD proteins have function in regulation of calcification (BGLAP, MGP, and GRP). Other VKD proteins have role in cell signaling (GAS6) or have unknown functions (PRGPs and TMGs).

1.3.3 Expression and function of VKD calcification regulators

Osteocalcin (BGLAP)

The highest expression of BGLAP is in bone mainly by mature osteoblasts and early hypertrophic chondrocytes. It has role in bone mineralization and regulates osteoclast and osteoblast activity [49,58,59].BGLAP deficient mice were born with normal mendelian frequency and were phenotypically normal at birth. After six months they showed increased bone mass directly indicating its involvement in bone mineralization. This suggests that BGLAP deficiency might enhance osteoblast activity [60]. The role of BGLAP in osteoclast has been shown to be

independent of γ-carboxylation. Additionally, BGLAP also has hormonal function in endocrine tissues [61].

BGLAP has three Glu residues which undergoes γ-carboxylation, lowest number known until now. So, the Gla domain structures adopted by VKD proteins with a smaller number of Gla residues are slightly different from coagulation proteins. It was proposed by Berkner et al. that for BGLAP the Gla domain forms a helix which is surface exposed instead of an interior core, for the ease of calcium binding within the hydroxyapatite surface [46].

Matrix Gla protein (MGP)

MGP is highly expressed in the extracellular matrix and in calcified tissues and cartilages. In comparison to BGLAP, MGP is not expressed in osteoblast but during bone formation its levels were seen to be increased. MGP deficient mice were born normal with regular mendelian frequency but died after two months due to extensive arterial calcification leading to blood vessel rupture. Recently, it was shown that MGP deficiency has significant involvement in development of midfacial hypoplasia [62]. These mice showed shorter and abnormally mineralized nasal septum.

Presently, a great amount of information exists on the role of MGP in Vascular Smooth Muscle Cells (VSMCs). MGP is highly expressed in atherosclerotic plaques [63,64]. These high expressions of MGP in atherosclerotic plaques are calcium dependent. In one later study, the VSMC specific knock-in of MGP rescued the calcification phenotype of the MGP deficient mice, which was γ-carboxylation specific [65].

MGP have five Glu residues which undergoes γ-carboxylation. The propeptide domain in MGP is located in the C-terminus, following the Gla domain which is an arrangement different than the rest of VKD proteins (Figure 6).

Gla rich protein (GRP)

GRP is widely expressed in soft tissues and skeletal associated tissues. The expression of GRP increases in normal vasculature during calcification and it co-localizes with mineral deposits in chronic kidney disease (CKD) and diabetes mellitus patients [49]. It was postulated that GRP might interact with the HA crystals through the Gla domain. However, the GRP deficient mouse model showed normal skeletal development [66].

Interestingly, GRP also shows expression in skin and upon warfarin treatment uncarboxylated GRP accumulates in the epidermal and dermal microsomes. GRP have been also known to deposit in pathological conditions such as scleroderma and dermatomyositis [67,68]. Thus, under-carboxylated GRP might have a role in the development of ectopic calcification. GRP has 15 Glu residues which undergoes γ-carboxylation, the highest number known until now.

1.3.4 Other VKD proteins

GAS6

GAS6 is another VKD protein which possess growth factor-like properties and is a ligand for receptor tyrosine kinases of the TAM family (Tyro3, Axl and MerTK) [69–74]. GAS6 has a well-established role in cell signalling. Axl has the strong affinity for GAS6 followed by Tyro3 and Mer. Many studies have reported activation of PI3K pathway activation by GAS6/Axl binding which mediates the anti-apoptotic function in EC, VSMC, fibroblast etc.

The N-terminal Gla domain of GAS6 mediates the binding ability to anionic phospholipids at the cell surface which are exposed upon cell injury and apoptosis. The N-terminal Gla domain is followed by a disulphide loop, 4 epidermal growth factor domains and Sex Hormone Binding Globulin-like (SHBG-like) domain containing two sub domains which are structurally similar to globular modules of laminin A. This globular structure is typical for a protein which interacts with heparin sulfates, integrins and steroids. GAS6 have 40% sequence homology with PS. However, GAS6 is less sensitive to serine proteases unlike Protein S [75].

$Gas6^{-/-}$ mice are protected from pro-thrombotic stimuli suggesting a function of GAS6 on platelet biology [76]. Inactivation of Gas6 gene prevents arterial and venous thrombosis and confers protection against thromboembolism [77].

Proline rich or transmembrane gla proteins (PRGPs and TMGs)

The proline rich gla proteins-1 and 2 (PRGP1 and PRGP2) are the first identified single pass transmembrane proteins which undergo γ-carboxylation. Later additional two transmembrane proteins were added to this group, Transmembrane Gla proteins- 3 and 4 (TMG3 and TMG4). A handful number of studies exist for these VKD membrane proteins.

Unlike other VKD proteins which possess epidermal growth factors or disulfide loop these PRGPs has a small proline-rich cytoplasmic domain. These two proteins shows broad tissue expression, where PRGP1 showed highest expression in the spinal cord and PRGP2 showed

highest expression in the thyroid gland. Later two more proteins were added to this transmembrane group called the transmembrane gla protein-3 and 4 (TMG3 and TMG4).

Interestingly, PRGP1 is similar to TMG3 where both lack the signal peptide and their molecular mass is around 25.8 kDa and PRGP2 is similar to TMG4 where both have similar N-terminal hydrophobic sequence.

All four transmembrane Gla proteins bears PPXY motifs which interacts with WW domains which is present in a variety of proteins involved in signal transduction, protein turnover and cell-cycle progression [17]. PRGP2 and TMG4 possess a single PPXY motif within a consensus sequence P-P-P-P-Y, which was originally identified in WW domain-containing yes kinase-associated Protein. Later with the help of Glutathione S-transferase (GST) pulldown assay and co-immunoprecipitation, interacting candidates of TMG4 was identified. The interaction partners include membrane-associated guanylate kinase-related (MAGI-1, 3), Yes-associated protein (YAP) which are involved in hippo pathway [78].

1.4.1 Vitamin K dependent coagulation factor deficiency type 1 (VKCFD1)

Mutations in *GGCX* lead to a rare autosomal recessive bleeding disorder called Vitamin K dependent coagulation factor deficiency type 1 (VKCFD1) [79–93] (MIM number :277450). These mutations are heterogeneously distributed over the whole protein (Figure 8). VKCFD1 patients are characterized by decreased activity of VKD clotting factors that lead to spontaneous bleeding tendency from brain, nose or after surgery f.e. dental extraction. Mostly, in all patients FX activity is low whereas FII, FVII are reduced in some and FIX is reduced in minimum number of cases [37]. Oral administration of vitamin K_1 (K_1) increases clotting factor activities to normal range in most cases.

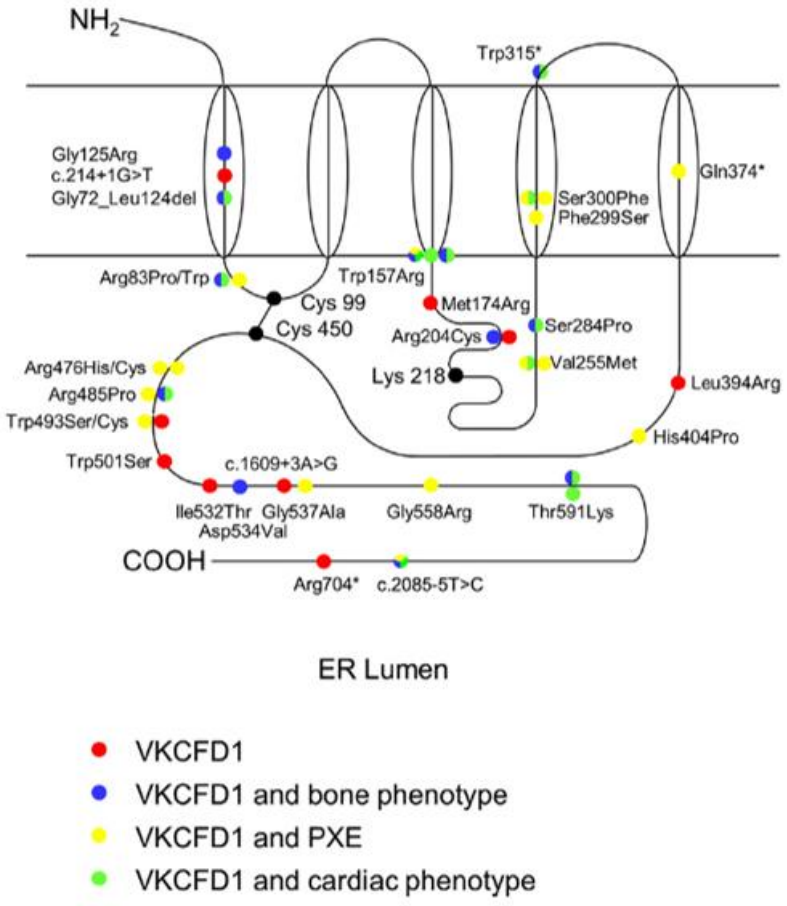

Figure 8: GGCX mutations causing VKCFD1 (taken from Watzka et al., *Thrombosis research*, 2014 [79]). The dots represent different mutations in GGCX which causes VKCFD1 bleeding phenotype (red), VKCFD1 and bone phenotype (blue), VKCFD1 and PXE phenotype (yellow), VKCFD1 and cardiac phenotype (green).

1.4.2 Non-haemostatic phenotype

Non-haemostatic phenotype in VKCFD1 patients can be broadly classified into skin, skeletal, and cardiac abnormalities, which varies with the degree of severity and age of onset. The VKD proteins responsible for these phenotypes remain elusive.

Most non-haemostatic abnormalities directs towards ectopic mineralization which are characterized by deposition of calcium crystals in multiple organs, such as the skin, kidneys, eyes, and blood vessels.

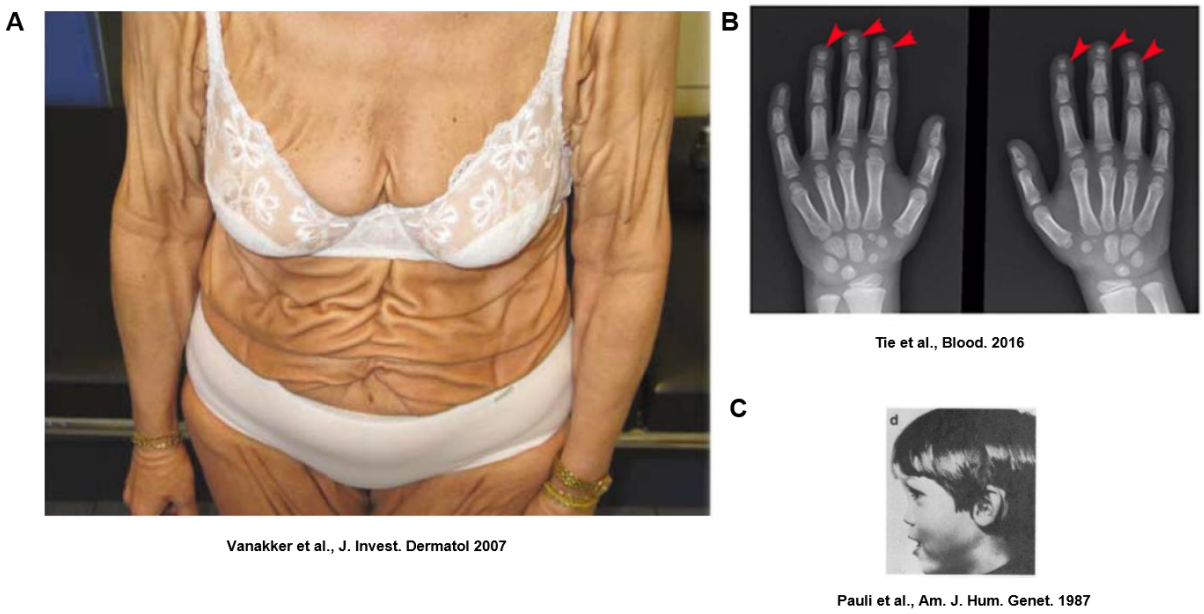

Figure 9: Non-haemostatic phenotype in VKCFD1 patients. **A,** Skin hyper-laxity[94]. **B,** Distal phalanges of the fingers (Keutel syndrome like phenotype) [88]. **C,** Midfacial hypoplasia.

Out of all the non-haemostatic phenotype, skin hyper-laxity has higher occurrence rate. The skin phenotype is collectively called pseudoxanthoma elasticum (PXE)-like phenotype which includes excessive skin folds and yellowish papules (Figure 9A). This name is derived from pseudoxanthoma elasticum due to the similarity in phenotypes. Classical PXE is an autosomal recessive disorder caused by mutations in *ABCC6* gene (ATP-binding cassette transporter, subfamily C member 6). This disorder is also characterized by calcification of elastic fibers in the skin, eyes, and cardiovascular system [95]. Although the clinical presentation is similar, PXE-like patients develop excessive skin folds mainly in the flexural areas, neck and trunk [37].

Skeletal phenotype is another non-hemostatic phenotype which includes midfacial hypoplasia (short nose with a flat nasal bridge), reduced bone mass density, stunted growth, and chondroplasia punctate. Another skeletal phenotype was brachytelephalangy of the fingers which is a feature of Keutel syndrome hence termed as Keutel syndrome-like phenotype (Figure 9B and C). Keutel syndrome is an autosomal recessive disorder caused by mutations in MGP gene [96]. The symptoms of classical Keutel syndrome are short terminal phalanges, calcification defects of the cartilage in nose, larynx, trachea and ribs and midfacial hypoplasia with a depressed nasal, neural hearing loss, and multiple peripheral pulmonary stenosis [96].

Cardiac phenotype includes congenital heart defects f.e. septal closure defects, persistent ductus arteriosus Botalli, Wolff–Parkinson–White syndrome and congenital supravalvular pulmonary stenosis and peripheral pulmonary artery stenosis [37]. There are also patients, which developed age associated cardiac abnormalities as atheriosclerosis.

However, there might be more phenotypes, which remains to be elucidated or is under diagnosed.

1.5 Aim of the study

The first aim of this study was to understand the pathological mechanism of VKCFD1. Therefore, a *GGCX*$^{-/-}$ HEK293T cell line was generated by CRISPR/Cas9 genome-engineering. This was followed by the establishment of an assay, where effects of GGCX mutations on γ-carboxylation of VKD proteins were measured based on different concentrations of vitamin K. With respect to the haemorrhagic phenotype this analysis will help to predict and provide better treatment of each GGCX genotype.

Due to lack of knowledge on the effect of *GGCX* mutations on non-haemostatic proteins, six VKD proteins were included into the study. This helped us to identify the causative protein for developing non-haemostatic phenotypes like skin, skeletal, and cardiac abnormalities.

The second aim of the study was to gain structural insights, as the first part involved screening of *GGCX* mutations effect, which is distributed throughout the protein. Hence, a GGCX *in silico* model was generated to check the distribution of these heterogeneous *GGCX* mutations. Based on the leads obtained from the *in vitro* data and mutation localization in the *in silico* model, vitamin K hydroquinone docking was performed and its binding site was identified.

2. Materials

2.1 Reagents and chemicals

All the chemicals used were purchased at *pro analysis* grade.

Agar	Sigma-Aldrich, Munich
Agarose	Biozym Scientific GmbH, Oldendorf
Ampicillin	Sigma-Aldrich, Munich
BigDye terminator	Life Technologies, Darmstadt
cOmplete mini, EDTA-free	Roche Diagnostics, Mannheim
DMEM, MEM, OptiMEM	Life Technologies, Darmstadt
DMSO	Merck, Darmstadt
DNA ladder (100 bp, 1 kb)	Fermentas, St. Leon-Rot
DNA loading dye	Fermentas GmbH, Leon-Rot
dNTPs	Fermentas GmbH, Leon-Rot
DreamTaq DNA polymerase	Fermentas GmbH, Leon-Rot
EDTA	Sigma-Aldrich, Munich
Ethanol	Merck, Darmstadt
Ethidium bromide	Fluka, Neu Ulm
FBS – SeraPlus	PAN Biotech, Aidenbach
Glycerol	Merck, Darmstadt
Glycine	Merck, Darmstadt
HPLC–grade water	Merck, Darmstadt
iProof High-Fidelity DNA Polymerase	Bio-Rad Laboratories, Munich
Isopropanol	Merck, Darmstadt
Lipofectamin 2000	ThermoFisher Scientific
LB broth (Lennox)	Sigma-Aldrich, Munich
LB broth with agar (Lennox)	Sigma-Aldrich, Munich
Methanol	Merck, Darmstadt
NEAA	Life Technologies, Darmstadt
NP-40	Sigma-Aldrich, Munich
Penicillin/streptomycin	Life Technologies, Darmstadt
PfuTurbo DNA polymerase	Agilent Technologies, Santa Clara, CA, USA
Proteinase K	Qiagen, Hilden
Precision plus dual color protein marker	Biorad laboratories, Munich
SDS	Sigma-Aldrich, Munich

SOC medium	Life Technologies, Darmstadt
Triton X-100	Sigma-Aldrich, Munich
Tween-20	Sigma-Aldrich, Munich
Vitamin K_1	Sigma-Aldrich, Munich

2.2 Laboratory equipment

3130xl capillary sequencer	Life Technologies, Applied Biosystems, Karlsruhe
Centrifuge (5430R-X)	Eppendorf, Wesseling-Berzdorf
Centrifuge (3-16PK)	Sigma Laborzentrifugen GmbH, Osterode am Harz
Chemi doc (Gel Doc XR+)	Bio-Rad Laboratories, Munich
Microscope	Carl Zeiss Microscopy GmbH, Göttingen
Nano-Drop ND 1000	Peqlab Biotechnologie GmbH
Neubauer chamber	Neubauer, DE
Power supply	Biometra, GE healthcare, Munich
Thermomixer	Eppendorf, Wesseling-Berzdorf
Thermocycler (MJ Research)	Bio-Rad Laboratories, Munich
Thermocycler (T3000)	Biometra, GE healthcare, Munich
Water bath (Thermostat 2761)	Eppendorf, Wesseling-Berzdorf
96-well plate reader	Synergy 2, BioTek Germany, Bad Friedrichshall
ELISA washer	Biotek (Elx50), Germany

2.3 Consumables

Labware:

Centrifuge tubes (15 and 50ml)	Greiner Bio-One GmbH, Solingen
CryoTube vials	VWR International GmbH, Langenfeld
Filtertips, 10, 200, 1000 µl	Sarstedt, Nürbrecht
Petri dishes	Greiner Bio-One GmbH, Solingen
PCR 8-stripes	Thermo Fischer Scientific, Waltham, MA, USA
Plates for cell culture (12, 24 and 48-well)	Greiner Bio-One GmbH, Solingen
Serological pipettes	Sarstedt, Nürbrecht
Reaction tubes (1,5 and 2 ml)	Eppendorf, Wesseling-Berzdorf
96 well Maxisorp weiß Fluoro nunc ELISA plate (14011184)	Thermoscientific fischer

2.4 Vectors

pIRES	Clontech, Saint-Germain-en-Laye, France

2.5 Antibodies

Rabbit Anti-Myc Polyclonal	Applied biological materials (G077)
Rabbit Anti-GGCX Polyclonal	Antibodies online (ABIN2781826)
Goat Anti-GGCX Polyclonal	Invitrogen (PA5-19155)
Rabbit Anti-GGCX Monoclonal	Abcam (ab170921)
Mouse Anti-Gla Monoclonal	Loxo-Sekisui (REF 3570)
Mouse Anti-PDI Monoclonal	Thermoscientific (MA3-019)
Mouse Anti-Gla specific MGP Monoclonal	Gift from Prof. Leon Schurgers, CARIM, University Maastricht, The Netherlands (G8A.1 lot3)
Sheep anti-human prothrombin	Affinity biologicals (SAFII-AP)
Goat anti-human Factor X	Affinity biologicals (GAFX-AP)
Goat anti-human Factor IX	Affinity biologicals (GAFIX-AP)
Mouse anti-ERGIC-53	Santa Cruz Biotechnology
Rabbit anti-mouse HRP-conjugated	Dako, P0260
Rabbit anti-goat HRP-conjugated	Dako, P0160
Goat anti-rabbit HRP-conjugated	Santa Cruz Biotechnology (sc-2305)

2.6 Buffers and solutions

1x DreamTaq buffer	100 µl 10x DreamTaq buffer, 20 µl 10 mM dTNP mix, 880 µl ddH_2O
50x TAE buffer	2 M Tris pH 8.5, 50 mM acetic acid, 50 mM EDTA
Blocking solution	2.5 g skim milk powder, 50 ml TBS-Tween, 25 µl Tween-20
Lysis buffer for western blot	50 mM Tris base pH 8.0, 150 mM NaCl, 1% NP-40
TBS-Tween	100 ml 10xTBS, 900 ml a.d., 50 µl Tween-20
Running buffer for western blot	1x Tris-Glycine
Stripping buffer	7.5 g Glycine, 0.5 g SDS, 5 ml Tween-20, pH 2.2 (heating at 30°C)
10x PBS	80 g NACl, 2 g KCl, 14 g Na_2HPO_4, 2 g KH_2PO_4, 1000ml ddH_2O
Coating buffer (pH:9)	1.59 g Na_2CO_3, 8.4 g $NaHCO_3$, 500ml ddH_2O

ELISA Wash buffer (pH7.4)	300mM $MgCL_2$:10ml, 10X PBS: 100ml, Tween 20: 500µl in 900ml Aqua dest
ELISA blocking buffer	2 % BSA, 0.05 % Tween-20, 1x PBS
ELISA sample dilution buffer	0.1 % BSA, 1x PBS
ELISA antibody dilution buffer	0.1 % BSA, 0.05 % Tween-20, 1x PBS
4 % Paraformaldehyde (PFA)	40 g Paraformaldehyde, 800 ml 1x PBS
Immunostaining Blocking buffer	10 % FBS, 0.1 % Triton-X, 90 % PBS
Immunostaining antibody dilution buffer	1 % FBS, 0.1 % Triton-X, 99 % PBS

2.7 Software

Dissertation preparation	• Microsoft Office 2010 • Citavi 6 (Swiss Academic Software GmbH, Wädenswil, Switzerland)
Primer design	• Oligo-Calc (www.basci.northwestern.edu/biotools/oligocalc.html)
Sequence analysis	• Geneious (10.1.2)
Sequence search	• BLAST (Basic Local Alignment Search Tool) (www.ncbi.nlm.nih.gov/BLAST/) • Uniprot (https://www.uniprot.org/) • Pubchem (https://pubchem.ncbi.nlm.nih.gov/) • PDB (https://www.rcsb.org/)
Data analysis	• GraphPad Prism 8 (version 8.3.1, GraphPad Software Inc.,La Jolla, CA, USA)
Image analysis	• Zen 2.6 (blue edition)
In silico analysis	• YASARA platform (version 18.4.24) [97]

- ITASER (https://zhanglab.ccmb.med.umich.edu/I-TASSER/) [98]
- H-DOCK (http://hdock.phys.hust.edu.cn/) [99]

2.8 Commercial kits

Plasmid Mini kit, Thermo Scientific

Plasmid Midi Kit, Qiagen, Hilden

Qiaquick Gel Extraction Kit, Qiagen, Hilden

2.9 Media for bacterial and mammalian cell culture

LB broth (Luria-Bertani) was used for growing bacterial culture. 10 g of LB broth or 17.5 g of LB with agar was dissolved in 500 ml of ddH_20 which was autoclaved and stored at 4°C.

Complete DMEM (including 4.5 g/l D-glucose, L-glutamine and pyruvate) was supplemented with 1% v/v penicillin/streptomycin, 1% v/v NEAA and 10% FBS which was used for maintaining HEK293T cells. Freezing medium contained 50% complete DMEM medium, 40% FBS and 10% sterile DMSO.

2.10 Primers

List of primers is given in the appendix were designed using online software tools and synthesized in desalted quality (HPSF) by Eurofins MWG Operon (Ebersberg).

3. Methods

3.1.1 Cloning: Construction of human GGCX/VKD protein expression vectors

The wildtype (wt) human *GGCX* (*hGGCX*) cDNA was cloned into multiple cloning site B of the bicistronic expression vector pIRES by restriction free cloning using Phusion polymerase. cDNAs of VKD proteins (*F2, F7, F9, F10, PC, PS, PZ UCMA/GRP, MGP, BGLAP, PRGP1, TMG4, GAS6)* were cloned into multiple cloning site A of pIRES together with a c-myc tag at the C-terminus of each protein. *GGCX* mutations (mut) were introduced by site directed mutagenesis using Pfu-turbo polymerase. All the above mentioned cDNAs were analyzed by Sanger sequencing. Figure 10 and table 1 contain the steps of cloning procedure and the above-mentioned PCR reactions conditions respectively.

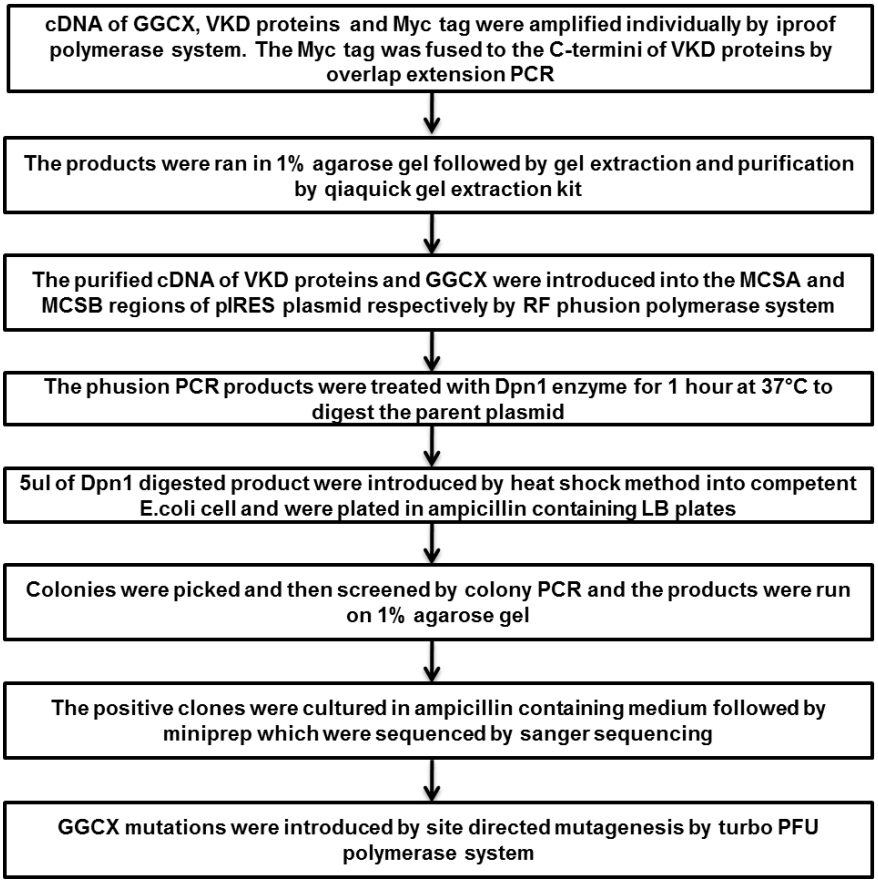

Figure 10: Flowchart depicting the overall procedure of cloning of VKD proteins and GGCX.

Table 1: PCR reaction and cycler conditions

Type of PCR	Reaction condition	Cycler conditions			
iProof PCR (HF-iProof polymerase system)	5x HF buffer- 4 µl dNTP Mix- 0.4 µl Forward primer-0.5 µl Reverse primer- 0.5 µl Template DNA (10 ng/µl) -1 µl iProof polymerase(5 U/µl)-0.25 µl ddH_2O-12 µl Total -20 µl	Step 1	98°C	30 s	
		Step 2	98°C	10 s	Repeat 30x
		Step 3	55-65°C	30 s	
		Step 4	72°C	1 min/kb	
		Step 5	72°C	10 min	
Restriction free (Phusion polymerase system)	5x HF buffer- 4 µl dNTP Mix-1.6 µl Forward primer-0.5 µl Reverse primer- 0.5 µl Template DNA (10 ng/µl) -1.5 µl iProof polymerase(5 U/µl)-0.5 µl ddH_2O-11.5 µl Total -20 µl	Step 1	98°C	30 s	
		Step 2	98°C	10 s	Repeat 35x
		Step 3	55-65°C	30 s	
		Step 4	72°C	1 min/kb	
		Step 5	72°C	10 min	
Site directed mutagenesis (Pfu-turbo polymerase system)	1x PFU buffer - 23 µl Template (10 ng/µl)- 1 µl Forward primer- 0.5 µl Reverse primer- 0.5 µl PFU Polymerase(2.5 U/µl)-0.5 µl ddH_2O- 11.5 µl Total- 25 µl	Step 1	95°C	3 min	
		Step 2	95°C	30 s	Repeat 15x
		Step 3	60°C	1 min	
		Step 4	68°C	2 min/kb	
		Step 5	95°C	30 s	Repeat 15x
		Step 6	60°C	1 min	

		Step 7 **68°C** **2 min/kb + 2 min**
Colony PCR (Dream Taq polymerase system)	**1x Dream buffer- 2.5 µl** **Forward primer- 0.5 µl** **Reverse primer- 0.5 µl** **Formamid- 0.3 µl** **Colony- 1 µl** **DNA polymerase(5 U/µl)- 0.4 µl** **ddH_2O- 11 µl** **Total - 25 µl**	**Step 1** **95°C** **5 min** **Step 2** **95°C** **30s** **Step 3** **55-65°C** **30s** **Step 4** **72°C** **1 min/kb** **Repeat 35x** **Step 5** **72°C** **7 min**
Sequencing reaction	**5x BigDye sequencing buffer- 1.5 µl** **Sequencing primer (5 µM)- 0.5 µl** **BigDye Terminator sequencing mix- 0.5 µl** **Diluted PCR product- 2 µl** **ddH2O 6.5 µl** **Total 11 µl**	**Step 1** **96°C** **1 min** **Step 2** **96°C** **10 s** **Step 3** **50°C** **5 s** **Repeat 35x** **Step 4** **60°C** **4 min**

In the following section, detailed protocols of three major steps of cloning (gel extraction, sequencing, and plasmid isolation) are described.

3.1.2 Gel extraction

The correct sized bands were excised with a clean scalpel. 750 µl of QG buffer was added and incubated at 50°C for 10 minutes. Once the gel had dissolved, 250 µl of isopropanol was added to the samples and mixed well. Then the samples were transferred to a QIAquick spin column and were centrifuged for 1 minute at 13,000 rpm. The flow-through was discarded followed by washing the column with 750 µl of PE buffer and centrifuged using the same condition. The flow-through was discarded and the columns were centrifuged again to remove the residual wash buffer. The column was then placed on a fresh 1.5 ml microcentrifuge tube. 30 µl of H_2O was added and incubated for 1 minute followed by centrifugation for 1 minute at 13,000 rpm.

The flow-through contains the megaprimer those concentration and purity was measured by nanodrop which was then used as an insert for phusion PCR.

3.1.3 Sequencing

The sequencing PCR was performed according to the conditions mentioned in table 1 with the respective gene primers to cover the complete sequence. The products were subsequently purified by EtOH/NaAc precipitation (10 µl of the sequencing reaction product, 50 µl 96 % EtOH, 10 µl dH_2O and 2 µl of 3M NaAc pH 4.6). These products were centrifuged for 4°C at 4000 rpm for 45 minutes. The supernatant was discarded followed by centrifugation of the empty stripes in an inverted manner. The pellet was washed once with 200 µl of 70% EtOH and were centrifuged for 10 minutes at the same centrifugation conditions and air-dried. Samples were stored at -20° C until they were resuspended in 15 µl water and loaded on the capillary sequencer.

3.1.4 Isolation and purification of bacterial plasmid DNA

The positive clones obtaining from cloning were grown overnight in LB containing ampicillin. These cultures were pelleted next day by centrifugation at 4000 rpm for 20 minutes at RT. The pellet was resuspended in 250 µl resuspension solution containing RNase followed by lysis with 250 µl lysis solution for 5 minutes at RT. The lysis was then stopped by 350 µl neutralization solution and mixed immediately by inverting the tubes 4-6 times thoroughly. The solution was centrifuged at 13,000 rpm for 5 minutes in RT to pellet the debris and chromosomal DNA. Then the supernatant was transferred to the GeneJET spin column which was centrifuged for 1 minute. The flow-through was discarded and 500 µl of wash solution was added which was centrifuged for 1 minute with same conditions mentioned earlier. The flow-through was discarded and the above washing step was repeated. Then the GeneJET spin column was transferred to a 1.5 ml microcentrifuge tube and 50 µl of H_2O was added and incubated for 2 minutes followed by elution by centrifugation for 2 minutes. The eluted plasmid concentration was measured using nanodrop which was then stored at -20°C for later usage.

For obtaining higher concentration of the plasmid midiprep was performed with similar steps of resuspension, lysis, neutralization, and washing using midiprep plasmid isolation kit from Qiagen.

3.2.1 Cultivation of mammalian cells

HEK293T cells were obtained from ATCC. Cells were routinely tested for the absence of mycoplasma contamination (PlasmoTest from Invivogen and PCR-based).

These cells were maintained in DMEM containing 10% fetal bovine serum and 1% penstrep 1% non-essential amino acid in 10cm dishes and were splitted at regular interval in a 1:10 or 1:5 ratio up to passage 25. Confluent cells grown in a 10cm dish were stored in a cryovial in liquid nitrogen for longer time in freezing medium. These vials were first stored in a cooling container (Mr Frosty) at -80°C overnight then transferred to liquid nitrogen.

3.2.2 Generation of *GGCX*$^{-/-}$ HEK293T cell line

A *GGCX*$^{-/-}$ HEK293T cell line was generated by CRISPR-Cas9 gene editing technology. The target crRNA sequence and the vector used were CCTACGTCATGCTGGCCAGCAGC and pRZ-Cas9-mCherry, respectively [100]. Genetic profile of single cell colonies were validated twice by MiSeq next generation deep sequencing. Absence of GGCX protein was verified by Western Blot using anti-GGCX antibody as described in the following section.

3.2.3 Western blot

For western blot, lysates were collected from HEK293T wt and *GGCX*$^{-/-}$ cells (1.1* 10^6) in 150 µl NP-40 buffer containing protease inhibitor from a 6-well plate after 24 hours of seeding. The samples were then diluted in 1:1 dilution in sample dilution buffer and heated for 5 minutes at 85°C. The chamber was assembled followed by addition of the transfer buffer. 40 µl of samples and 5 µl of marker were loaded on the wells. The gel was run for 225 V for 40 minutes. Then the proteins were transferred to the nitrocellulose membrane. The membrane and Whatman filter paper were soaked in methanol and transfer buffer respectively which were then sandwich along with the gel and run at 250 mA for 1 hour at 4°C. After the transfer, the membrane was blocked with milk overnight at 4°C. Following day, the membrane was washed 3 times on an oscillator and incubated with GGCX antibody in 1:1000 dilution prepared in 5 % milk and incubated overnight at 4°C. The membrane was then washed 3 times and incubated with anti-rabbit HRP antibody prepared 1:10,000 dilution in TBST for 2 hours at RT. The membrane was washed for 3 times. Then the substrate solutions were prepared in 1:1 dilution in dark which was added onto the membrane. The membrane was detected in chemidoc with Chemi Hi-sensitivity and auto exposure time settings. The membranes were then washed and stripped for detecting the house keeping gene ERGIC-53 as a loading control. It was incubated for 2 hours with anti-ERGIC antibody prepared in 1:500 dilution in TBST. The blocking, secondary antibody incubation, washing and detection steps were similar as mentioned earlier.

3.2.4 Expression of GGCX and VKD proteins in *GGCX*$^{-/-}$ cell line

HEK293T *GGCX*$^{-/-}$ were seeded in DMEM containing 10% heat inactivated fetal bovine serum and 1% non-essential amino acid. Different cell plate formats and cell number were tested as mentioned in the table.

Table 2: Plate format and transfection conditions

Plate format	Cell number	Transfection	
		DNA	Lipofectamine
12-well	500,000	1000ng	5µl
24-well	250,000	500ng	2.5µl
48-well	125,000	250ng	1 µl

Finally, for the analysis of the mutants 48 well format was used for seeding. After 24 hours, cells were transfected at a confluency of 80-90 % with pIRES vector containing *GGCX wt/mut* and VKD proteins by lipofectamin 2000 (ThermoFisher, #1875897). After four hours of transfection medium containing different concentrations of K_1 (Sigma Aldrich, V3501) was added to the wells. Different dilutions series of K_1 were tested (logarithmic and half-logarithmic) and finally the following concentration were used- 0.1µM, 0.3µM, 1µM, 3.16µM, 6.32µM, 10µM, 31.6µM, and 100µM.

After 48 hours of incubation, 350 µl cell medium were collected to measure γ-carboxylation of the VKD protein. For GGCX antigen levels, cell lysates were collected in Nonidet P-40 buffer (NP-40; 150mM sodium chloride, 1% NP-40, 50mM TRIS base, pH 8.0) containing protease inhibitors. These lysates were collected in different amounts of buffer and was accordingly diluted for two different ELISAs based on VKD proteins localization as mentioned in table no 3.

Table 3: ELISA conditions for different VKD proteins

VKD protein	Prot. Location	VK conc	Cell lysate in NP-40 buffer	Gla LISA	Sample dilution	GGCX ELISA	Sample dilution
FX	Secretory	0.1µM-100µM	80µl	Medium	1:6	Lysate	1:5
FII	Secretory	0.1µM-100µM	80µl	Medium	1:6	Lysate	1:7
PROC	Secretory	0.1µM-100µM	80µl	Medium	1:6	Lysate	1:5
GRP	Secretory	0.01µM-100µM	80µl	Medium	1:6	Lysate	1:7
MGP	Secretory	0.1µM-100µM	80µl	Medium	1:6	Lysate	1:3.5
BGLAP	Secretory	0.1µM-100µM	80µl	Medium	Undiluted	Lysate	1:5
PRGP1	Membrane	0.1µM-100µM	120µl	Lysate	1:10	No signal	No signal
TMG4	Membrane	0.1µM-100µM	120µl	Lysate	1:10	Lysate	1:6
GAS6	Secretory	0.1µM-100µM	80µl	Medium	1:6	Lysate	1:5

3.3.1 Establishment of ELISA for measuring γ-carboxylation (GLA elisa)

Initially different myc antibodies were tested from Santa Cruz, Molecular probes, ThermoScientific, and Antibodies online. The best anti c-Myc antibody (ABIN2688146) based on the luminescence signal and its signal-to-noise ratio, was used for the final sample measurement. Different dilution ranges were tested as mentioned in table 4.

Table 4: Testing and dilution conditions of ELISA

Reagent	Testing dilution	Final dilution
Primary coating antibody (Myc AB)	1:300, 1:500, 1:1200	1:1200
Primary detection antibody (Gla AB)	1:500, 1:1000, 1:2000	1:2000
Sample dilution range	1:5-1:10	1:6

96 well ELISA plates were coated with 100 µl of diluted capture antibody in prepared coating buffer and incubated overnight at 4°C. This was followed by 3 times washing using ELISA washer and then blocked with 200 µl of 2% BSA and incubated for 2 hours at RT. The wells were washed 3 times and were incubated with samples prepared in sample dilution buffer according to the dilution mentioned in the table 3. Samples were incubated overnight in 4°C. The following day samples were aspirated and washed 1 time manually followed by incubation with primary detection Gla antibody for 3 hours at RT. The wells were then washed 3 times and incubated with rabbit anti-mouse HRP at a dilution of 1:2000 for 1 hour. The substrate was prepared in 15 ml falcon covered with aluminum foil and incubated for 20 minutes on a shaker (A:B=99:1). This preparation was precisely done 20 minutes before 1 hour incubation of the secondary antibody was over. Then the plates were washed for 3 times followed by addition of the substrate. The luminescence was measured in an ELISA plate reader at 460/40 with optics in top position and gain at 135.

3.3.2 Establishment of ELISA for measuring GGCX antigen

The GGCX antigen levels were measured by another sandwich ELISA. Coating, washing, blocking, and detection were performed in a similar manner as mentioned above. The capturing and detection antibody dilution was 1:250 and 1:2000 respectively. Cell lysates were diluted in sample dilution buffer. The detection antibody against GGCX (ThermoFisher, PA5-19155) was incubated for 3.5 hours followed by a rabbit anti-goat-HRP antibody (Dako, P0160) for 1 hour. The GGCX antigen levels were quantified by GGCX wt standard curves run in parallel on each plate. The GGCX antigen levels were calculated by GEN5 software by 4 parametric curve formulas.

3.3.3 Generation of standard curve

Different plasmids were transfected in 10cm plates for generation of the standard curve which contained only the GGCX cDNA. But for these plasmids the luminescence signals were much higher than the 48 well plate wt GGCX samples. Then the bicistronic plasmids containing both F2 or GRP and GGCX wt were transfected and the lysates were collected after 48 hours where the medium was eliminated and 2 ml NP-40 buffer containing protease inhibitor were added to the 10cm plates and incubated for 5 minutes at 4°C. The lysates were then collected in 2 ml microcentrifuge tube and centrifuged at 13,000 rpm for 10 minutes at 4°C followed by transfer of the supernatant in a fresh tube. These lysates were tested in different dilution series. Finally, the pIRES plasmid containing both GRP and GGCX was used as final standard curve with seven dilution series and 2 times dilution between each interval as this standard curve covered the range of 48 well plate wt GGCX samples.

3.3.4 Measurement of FVII clotting factor activity

HEK293T *GGCX*$^{-/-}$ cells were seeded on 24 wells in DMEM containing 10% heat inactivated fetal bovine serum and 1% non-essential amino acid and after 24 hours it was transfected with pIRES vectors using Lipofectamine. Medium was changed to OptiMem containing 5% BSA including 10 µM K_1 after 4 hours. This was done to express FVII under serum-free conditions. After 72 hours medium was collected for measuring FVII clotting factor activity by using Atellica coagulometer (Siemens). Sample aliquots were added to Factor FVII-depleted plasma. Activities were normalized to a calibration curve of standard pooled plasma.

3.4 Immunofluorescence staining

HEK293T *GGCX*$^{-/-}$ cells were seeded on cover slips that were coated with gelatin (Sigma-Aldrich, G1890). 0.1 g of gelatin was added in 100 ml of ddH_2O and was autoclaved before use. Different cell dilutions were tested ranging from 250,000 to 500,000 and finally 300,000 cells were used for transfection at confluency of 70-80%. After 24 hours cells were transfected with vectors containing *GGCX wt/mut*. 24 hours post transfection cells were washed 3 times with PBS and fixed for 10 minutes in 4% paraformaldehyde solution at RT followed by blocking with 10% FBS for 30 minutes. Cells were incubated overnight with an anti-GGCX antibody (Abcam, ab170921). ER-staining was performed using an antibody targeting PDI (Protein disulphide isomerase; ER protein; ThermoFisher, MA3-019), or clotting factors FII, FIX, FX (Affinity Biologicals, SAFII-AP, GAFIX-AP, GAFX-AP). After 4 hours, 10 µM K_1 was added when GGCX was stained with clotting factors. Cells were washed 3 times with PBS followed by 30 minutes blocking and then incubated with respective secondary Alexa Fluor 488 or 594-labelled antibodies for 1 hour at RT. Mounting was performed with ProLong Glass (Thermo Fisher, P36983) that included NucBlue for nucleus staining. The exposure time used for the red filter was 80 psec for all GGCX mutations.

3.4.1 Image analysis

The images were analyzed and co-localization was calculated by Pearson´s correlation coefficient using Zen software. The region of interest (ROI) was drawn where individually cells were marked by using ‘draw Bezeier’ in the co-localization analysis tab. The colocalization parameters were set by Costes and the table showing the colocalization correlation coefficients was generated. 10 cells were analyzed for each condition and the mean and SD was plotted in Prism.

3.5.1 Generation of GGCX *in silico* model

Due to absence of crystal structure or homology to any other protein, a GGCX *in silico* model was established based on threading method. As mentioned above GGCX is a transmembrane (TM) protein located in the ER. So prediction of the TM domain residues and the secondary structure residues using different prediction servers was performed (Table 5 and 6). Then the TM results were analyzed to find the most consensus residues.

Table 5: Prediction of transmembrane domains in GGCX using different prediction server

SERVER	TM1	TM2	TM3	TM4	TM5	TM6	TM7	TM8	TM9	TM10	Total TM reported
EMBOSS		114-136			189-215		276-302		361-389		4TM
TMHMM		123-145		160-182	195-214	249-271	278-300				5TM
PRED-TMR2	61-79	114-133			197-216	252-272	278-299				5TM
PHILIUS		116-144		160-181	197-216	253-272	283-305				5TM
PSIPRED	61-81	116-140			196-220	249-272	278-297	300-319	359-383		7TM
TMPRED	61-82	116-134	129-152	159-177	199-215	254-272	259-285	294-313	362-379		9TM
TOPCONS	61-83	111-131	133-153	161-181	196-216	250-270	274-294	296-316	360-380		9TM
OCTOPUS	61-84	118-132	134-148	161-181	196-216	249-269	280-294	296-310	360-380		9TM
POLYPHOBIUS	61-85	69-83	116-149	161-180	197-216	250-272	282-296	298-312	362-380		9TM
SPOCTOPUS	61-86	118-132	134-148	161-181	196-216	249-269	280-294	296-310	360-380		9TM
SCAMPI	61-87	111-131	133-153	161-181	197-217	252-272	274-294	296-316	362-382	689-709	10TM
Consensus TM residues	**61-81**	**116-131**	**134-148**	**161-177**	**199-214**	**254-269**	**283-294**	**296-310**	**362-379**	**-**	

Table 6: Prediction of secondary structures in GGCX using different prediction server

SERVER	1	2	3	4	5	6	7	8	9
compbio (jpred)	63-84	112-156		159-174	197-218	250-270	276-292	299-308	361-382
	62-84	112-157		159-174	197-217	250-270	276-294	299-308	361-382
	64-85	112-153		159-174	197-219	251-270	274-290	299-305	360-382
predictprotein.org	62-85	112-131	133-152	160-177	197-219		247-294	298-310	361-382
predictprotein.org (TM helix)	61-84	113-131	137-154	160-175	197-218	251-273		292-309	362-379
bioinf.cs.ucl.ac.uk	64-84	115-155		159-173	197-216	241-270	277-286	298-306	360-376
YASPIN		113-127		163-173	199-206		287-291	302-208	
Consensus secondary residues	**64-84**	**115-127**	**137-152**	**163-173**	**199-206**	**251-270**	**277-286**	**302-305**	**362-376**

Subsequently GGCX protein sequence was submitted into ITASER [98] without any constraint for generating the model based on threading method. The model1 with the best C-score was used for further analysis but its N- and C-termini had the same orientation (Figure 12). This

contradicts with previous findings where it has been demonstrated that the N-terminus of GGCX lies on the cytoplasmic side and the C-terminus on the ER luminal side i.e. they have opposite orientation to each other [38]. Therefore, amino acid residues 1-120 were re-modeled separately in ITASSER and manually replaced onto the previous model to achieve the correct orientation of the N- and C-termini. A membrane embedded simulation was performed on the final re-modeled structure in a phosphatidylcholine bilayer in order to equilibrate the model using md_memsim macro embedded in YASARA [97]. After equilibration the TM residues were marked and matched with the earlier performed TM prediction analysis. This comparison showed that the most of the predicted residues were included along with additional residues in TM which were in disordered state.

3.5.2 Docking of vitamin K hydroquinone as ligand on GGCX *in silico* model

So, this above GGCX model was used as a receptor on which vitamin K hydroquinone docking was performed. So first the 2D structure of vitamin K hydroquinone (Figure 11) was downloaded from Pubchem and convert it into PDB file which was then labeled as ligand and the equilibrated GGCX model was the receptor.

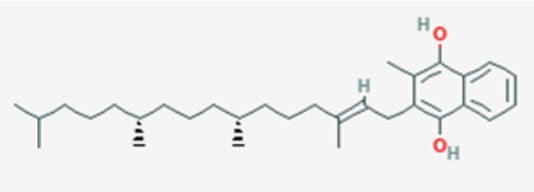

Figure 11: 2D structure of Vitamin K_1 hydroquinone used as ligand for docking (PubChem CID: 5280585).

The docking was performed using autodock module in YASARA. 29 docking poses were reported which were then analyzed. The selected docked complex was further subjected to the membrane embedded simulation for further equilibration and subsequent production phase stretching to a total of 250 ns.

3.5.3 Introduction of mutation in the GGCX *in silico* model

Two mutations were introduced in the GGCX structure by swapping the amino acid residues separately (GGCX:p.(M174R), GGCX:p.(S300F)). These mutated GGCX receptor along with the selected final docking complex were further simulated for >100 ns in order to understand the structural effect of the mutations on GGCX.

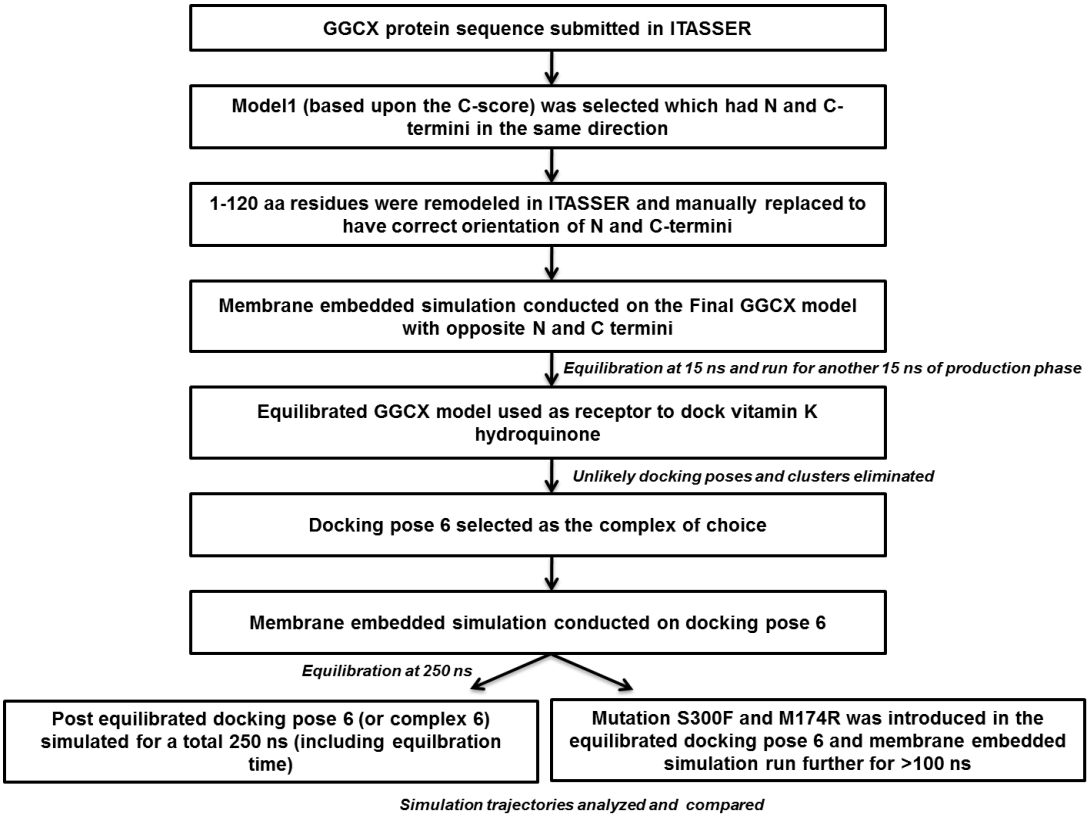

Figure 12: A flowchart of how the GGCX *in silico* model was generated and which analysis was performed to generate KH_2 docking.

4. Results

4.1 Evaluation of γ-carboxylation of VKD proteins

The aim of the study was to evaluate the γ-carboxylation efficiency of *GGCX* mutations causing VKCFD1 on different VKD proteins in a cellular model. Since GGCX is highly expressed in all mammalian cell lines, a *GGCX*$^{-/-}$ cell was generated in HEK293T. HEK293T cell line was chosen because it has functional vitamin K cycle where all VKD proteins get γ-carboxylated.

The *GGCX*$^{-/-}$ cell line was generated by CRISPR-Cas9 mediated gene editing. The single cell clone with a deletion of 46 nucleotides in exon 8 was validated by sequencing (Figure 13A). Further the absence of alternatively spliced GGCX was verified by western blot (Figure 13B).

Figure 13: CRISPR/Cas9 gene mediated generation of *GGCX*$^{-/-}$ HEK293T cell line. A, A *GGCX*$^{-/-}$ HEK293T cell line was generated by CRISPR-Cas9 gene editing technology. The target crRNA sequence used to generate the human *GGCX*$^{-/-}$ cell line was CCTACGTCATGCTGGCCAGCAGC. The deletion of 46 nucleotides in exon 8 was verified by next generation sequencing (NGS) **B,** Absence of GGCX protein was verified by Western Blot using anti-GGCX antibody. ERGIC-53 was used as loading control. (from Ghosh et al. *JTH* 2021, [101])

An assay was developed to measure the effect of GGCX mutations causing VKCFD1 on γ-carboxylation of VKD proteins by ELISA (Figure 14). For this assay VKD proteins were tagged in the C-terminus with c-myc tag in order to capture these proteins in a similar manner through the same antibody. Nine VKD proteins were selected for analysis, where three represented

haemostatic proteins and six non-haemostatic proteins. Out of three haemostatic proteins two were pro-coagulant with highest (FX) and lowest affinity (FII) for GGCX and one was anticoagulant protein (PC). Out of the six non-haemostatic proteins, three have known function in calcification regulation (BGLAP, MGP, GRP) and one protein (GAS6) have role in cell signalling (Figure 14B). The remaining two proteins represented transmembrane gla proteins with unknown function (PRGP1 and TMG4). These VKD proteins along with *GGCX* wt or muts were introduced into multiple cloning site A and B, which were under the same promoter. These two genes were similarly expressed in an equimolar 1:1 ratio from the same transcript by the help of internal ribosomal entry site.

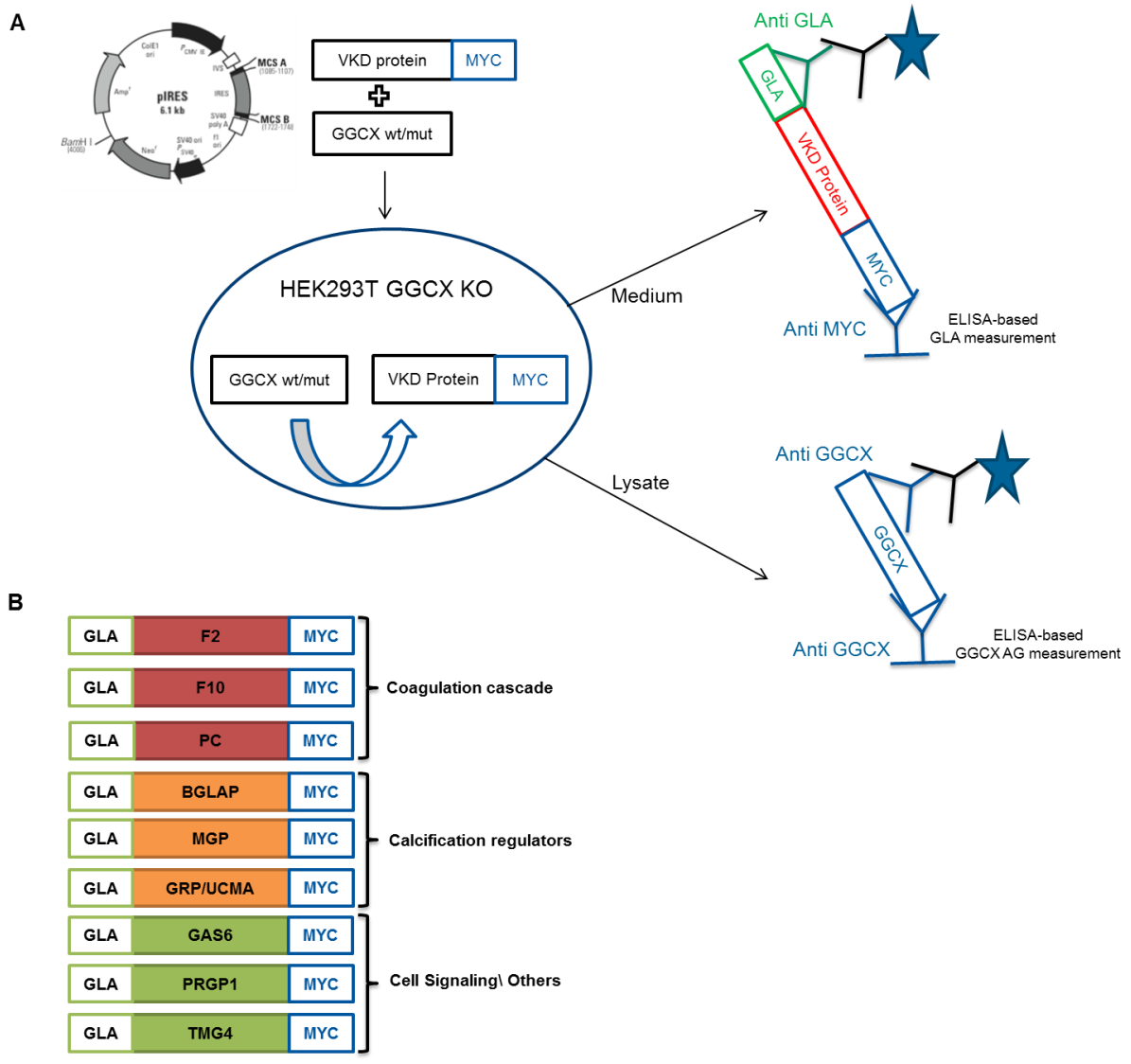

Figure 14: Assay for γ-carboxylation measurement of VKD proteins A. A myc tag was introduced at the C-terminus of VKD proteins and cloned into the multiple cloning site A (MCSA) of a bicistronic vector (pIRES). The cDNA of GGCX wt/mut was cloned into multiple cloning site B (MCSB). These vectors were transfected into a HEK293T *GGCX*$^{-/-}$ cell line. γ-carboxylation was measured by an ELISA where VKD proteins were captured by an anti-myc antibody and detected by a Gla-specific antibody.

Levels of γ-carboxylation were normalized to GGCX antigen level measured by another sandwich ELISA. **B,** In our study, γ-carboxylation level of nine different VKD proteins were measured.

4.2 Validation of dependence on vitamin K for γ-carboxylation in our assay

First, the bicistronic plasmids containing cDNAs of individual VKD protein and GGCX wt were expressed and the γ-carboxylation of VKD proteins was measured. The γ-carboxylation of these selected VKD proteins with respect to GGCX wt were increasing with increasing concentration of K_1 (0.1-100 µM) (Figure 15). This validated vitamin K dependent γ-carboxylation of VKD proteins in this cellular system.

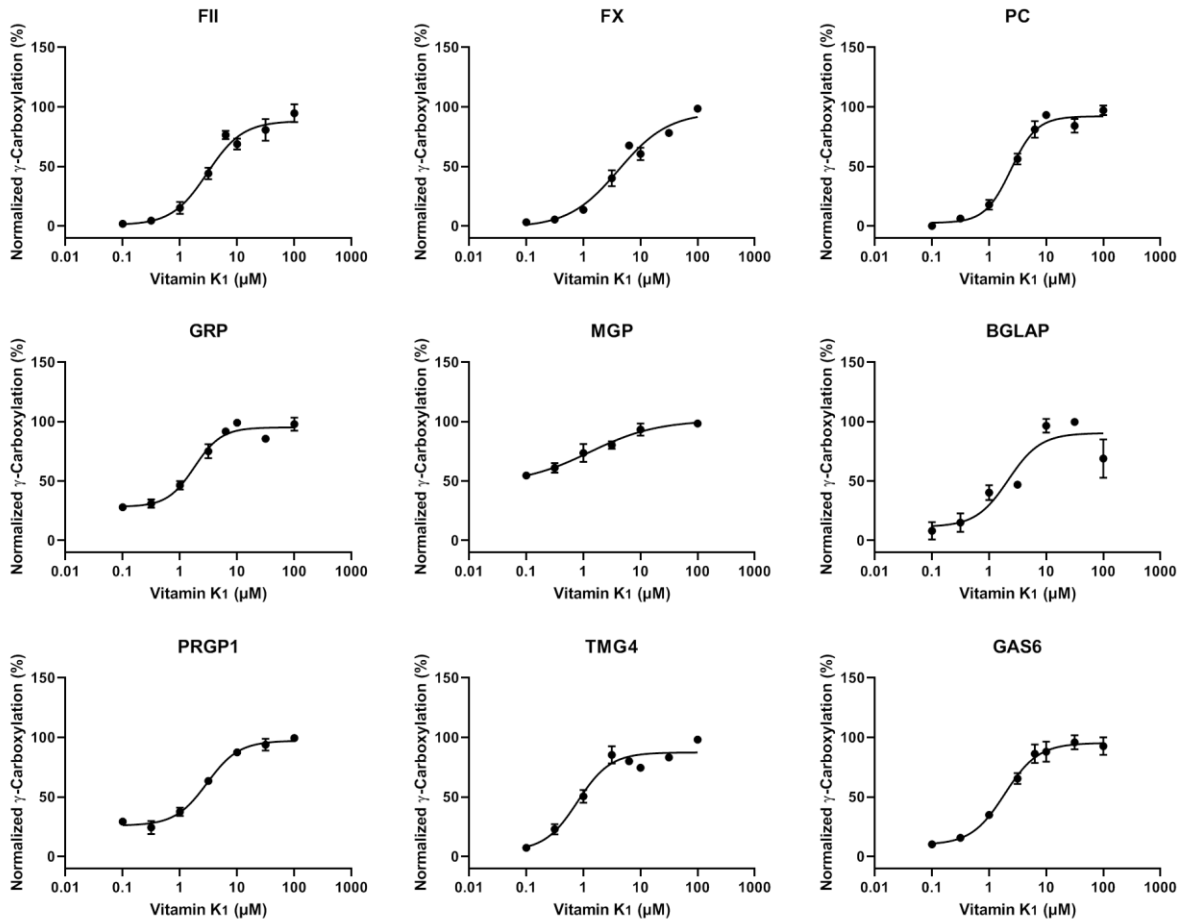

Figure 15: Determination of γ-carboxylation of VKD proteins by GGCX wt. γ-carboxylation dose-response curves of GGCX wt with respect to all VKD proteins - haemostatic proteins (FII, FX, PC) and non-haemostatic proteins (BGLAP, MGP, GRP, PRGP1, TMG4, and GAS6). The y-axis represents γ-carboxylation (%) that were normalized to wt. The x-axis display K_1 concentrations (0.1-100µM). Error bars depict SD of triplicate measurements of n=3 experiments.

After establishing the ELISA conditions and confirming the vitamin K dose dependence, 22 GGCX missense mutations were expressed which led to different types of dose response curves for both haemotstaic and non-haemostatic proteins as shown in the following section.

4.2.1 Characterization of GGCX mutations effect on γ-carboxylation of VKD haemostatic proteins

The curve patterns were categorised into four types under vitamin K treatment, where mutants compared to wt shows a. similar levels of γ-carboxylation (responder mutation) , b. higher levels of γ-carboxylation (high responder mutations) , c. lower levels of γ-carboxylation (low responders), and d. zero or nearly zero levels of γ-carboxylation (loss-of-function). These patterns of γ-carboxylation are shown in the following sections with respect to haemostatic proteins.

GGCX mutations responding to vitamin K similar to or higher than wt

There were seven GGCX mutations which showed similar γ-carboxylation for clotting factors as wt and were categorised as responder mutations GGCX:p.(W157R), GGCX:p.(R204C), GGCX:p.(V225M), GGCX:p.(S284P), GGCX:p.(R325Q), GGCX:p.(R476C), GGCX:p.(R476H). The exceptions were FX γ-carboxylation by GGCX:p.(R476C) which is increasing only to 12 % and PC γ-carboxylation by GGCX:p.(W157R) is increasing to 16.4 % only (Figure 16).

A

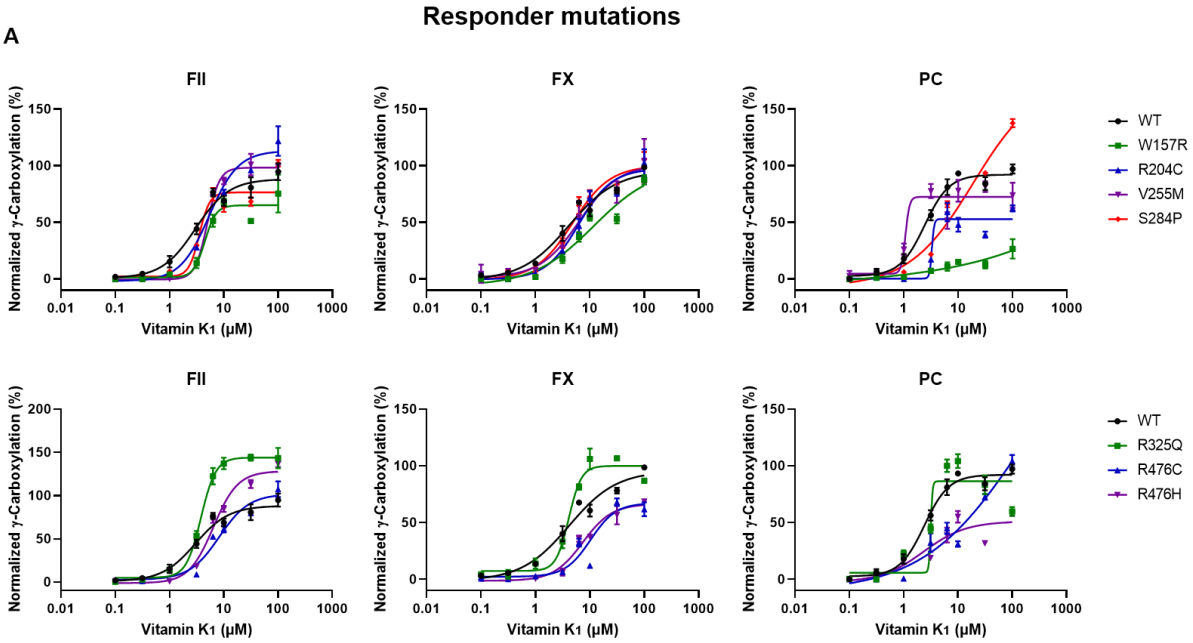

B

GGCX mutation	γ-carboxylated FII [%]		γ-carboxylated FX [%]		γ-carboxylated PC [%]	
	Low K (1 μM K_1)	High K (10μM K_1)	Low K (1μM K_1)	High K (10μM K_1)	Low K (1 μM K_1)	High K (10μM K_1)
W157R	25.4 %	93.1 %	13.1 %	97.2 %	7.4 %	16.4 %
R204C	20.1 %	105.1 %	41.9 %	120.8 %	0 %	49.9 %
V255M	0 %	119 %	49.4 %	130.9 %	144.1	87 %
S284P	30.3 %	84.1 %	55 %	123 %	37.5 %	128.6 %
R325Q	74.3 %	188.5 %	115.1 %	189.2 %	141.4 %	115.7 %
R476C	78.8 %	87.3 %	12.1 %	12 %	0 %	32.4 %
R476H	0 %	113.5 %	0 %	67.1 %	95.9 %	57.4 %

Figure 16: Dose-response curves of responder GGCX mutations on γ-carboxylation of haemostatic proteins measured by ELISA. **A,** The y-axis represents normalized γ-carboxylation (%) of FII, FX, and PC. The x-axis represents K_1 concentrations (0.1-100μM). In each figure dose response curve for GGCX wt is shown in black. Error bars depict SD of n=3 technical replicates of three experiments. **B,** The table shows the γ-carboxylation values of mutations at 1μM (low K) and 10μM (high K) K_1 of clotting factors normalized to wt values.

However, there are four responder mutations (GGCX:p.(I532T), GGCX:p.(G537A), GGCX:p.(W501S), GGCX:p.(W493C)) showing unusual high levels of γ-carboxylated clotting factors at low and high K_1 conditions when compared to wt (Figure 17). This indicates two possibilities that either these four mutations lead to gain-of-function of GGCX or it results to incomplete processivity leading to secretion of partially γ-carboxylated VKD clotting factors.

High responder mutations

A

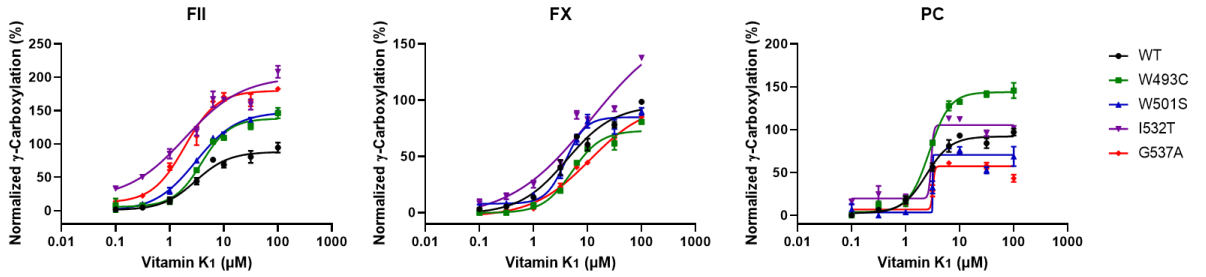

B

GGCX mutation	γ-carboxylated FII [%]		γ-carboxylated FX [%]		γ-carboxylated PC [%]	
	Low K (1 μM K_1)	High K (10μM K_1)	Low K (1μM K_1)	High K (10μM K_1)	Low K (1 μM K_1)	High K (10μM K_1)
W493C	61.9 %	150.2 %	34.3 %	101 %	121.7 %	138.1 %
W501S	143.8 %	159 %	106.2 %	139.4 %	24.0 %	78.9 %
I532T	450.8 %	228.9 %	191.6 %	147.8 %	127.2 %	116.9 %
G537A	349.4 %	234.6 %	25.7 %	79.5 %	79 %	73.5 %

Figure 17: Dose-response curves of high responder GGCX mutations on γ-carboxylation of haemostatic proteins measured by ELISA. **A,** The y-axis represents normalized γ-carboxylation (%) of FII, FX, and PC. The x-axis represents K_1 concentrations (0.1-100μM). In each figure dose response curve for GGCX wt is shown in black. Error bars depict SD of n=3 technical replicates of three experiments. **B,** The table shows the γ-carboxylation values of mutations at 1μM (low K) and 10μM (high K) K_1 of clotting factors normalized to wt values.

GGCX mutations showing low or zero response to vitamin K

Six mutations showed extremely reduced γ-carboxylation of clotting factors which was categorised as low responding mutation which were GGCX:p.(R83P), GGCX:p.(R83W), GGCX:p.(D153G), GGCX:p.(L394R), GGCX:p.(S300F), and GGCX:p.(H404P) (Figure 18).

Interestingly the mutation GGCX:p.(L394R) and GGCX:p.(H404P) lies in the known glutamate binding site in GGCX explaining their low activity whereas the structural implication of other low responding mutations are unknown.

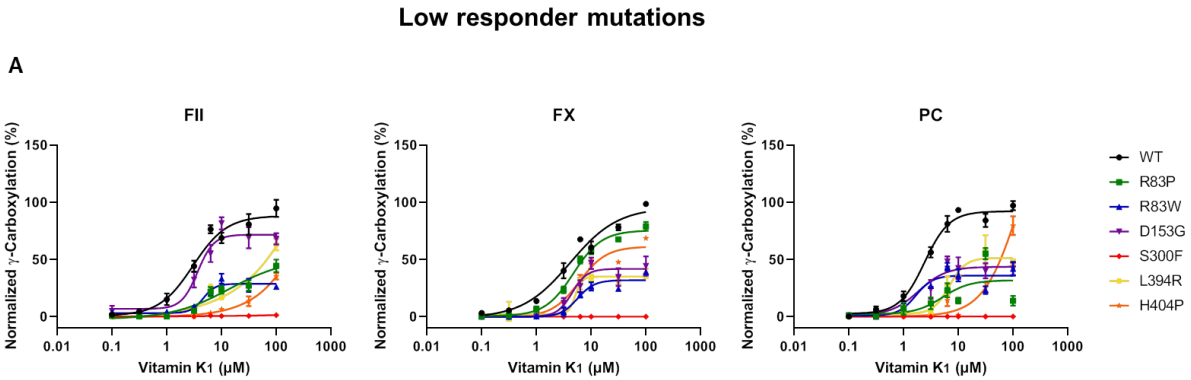

B

GGCX mutation	γ-carboxylated FII [%]		γ-carboxylated FX [%]		γ-carboxylated PC [%]	
	Low K (1 μM K_1)	High K (10μM K_1)	Low K (1μM K_1)	High K (10μM K_1)	Low K (1 μM K_1)	High K (10μM K_1)
D153G	68.7 %	101 %	0.2 %	66.8 %	106.8 %	44.2 %
R83W	23.1 %	42.3 %	0.5 %	50.9 %	64.1 %	40.9 %
R83P	0 %	32.4 %	55.4 %	102.9 %	25.4 %	13 %
L394R	0 %	22.7 %	0 %	57.9 %	55.5 %	37.3 %
S300F	0 %	1.1 %	0 %	0 %	0 %	0.2 %
H404P	0 %	8.9 %	8 %	85 %	0 %	0 %

Figure 18: Dose-response curves of low responder GGCX mutations on γ-carboxylation of haemostatic proteins measured by ELISA. **A,** The y-axis represents normalized γ-carboxylation (%) of FII, FX, and PC. The x-axis represents K_1 concentrations (0.1-100μM). In each figure dose response curve for GGCX wt is shown in black. Error bars depict SD of n=3 technical replicates of three experiments. **B,** The table shows the γ-carboxylation values of mutations at 1μM (low K) and 10μM (high K) K_1 of clotting factors normalized to wt values.

Two mutations GGCX:p.(F299S) and GGCX:p.(M174R) showed complete loss-of-function for all three haemostatic proteins (Figure 19) which indicated that it either affects structurally or functionally important residues. Thus, from this evaluation a hint of the structurally or functionally crucial residues was obtained.

A

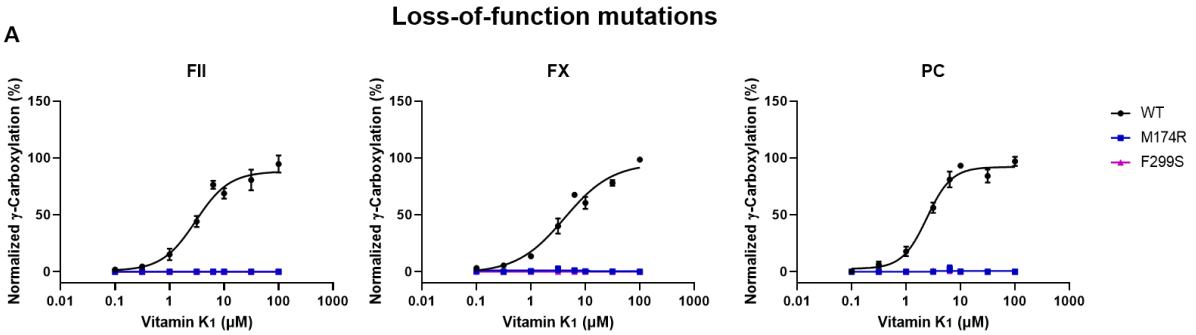

B

GGCX mutation	γ-carboxylated FII [%]		γ-carboxylated FX [%]		γ-carboxylated PC [%]	
	Low K (1 μM K_1)	High K (10μM K_1)	Low K (1μM K_1)	High K (10μM K_1)	Low K (1 μM K_1)	High K (10μM K_1)
M174R	0 %	0 %	0 %	0.3 %	0 %	0 %
F299S	0 %	0 %	0%	0%	0%	0%

Figure 19: Dose-response curves of loss-of-function GGCX mutations effect on γ-carboxylation of haemostatic proteins measured by ELISA. **A,** The y-axis represents normalized γ-carboxylation (%) of FII, FX, and PC. The x-axis represents K_1 concentrations (0.1-100μM). In each figure dose response curve for GGCX wt is shown in black. Error bars depict SD of n=3 technical replicates of three experiments. **B,** The table shows the γ-carboxylation values of mutations at 1μM (low K) and 10μM (high K) K_1 of clotting factors normalized to wt values.

4.2.2. FVII activity

To further validate whether the γ-carboxylated clotting factors recognized by ELISA were functional protein, FVII activity was measured by APTT assay. The FVII activity measurement showed similar results for responder mutation which showed increasing activity between 71-108 %. The low responder mutations resulted in FVII activity around 51-72 %. Compared to other low responders one mutation GGCX:p.(S300F) showed extremely reduced FVII activity of only 20 %. The two loss-of-function mutation GGCX:p.(F299S) and GGCX:p.(M174R) showed zero FVII activity reflecting the ELISA data (Figure 20).

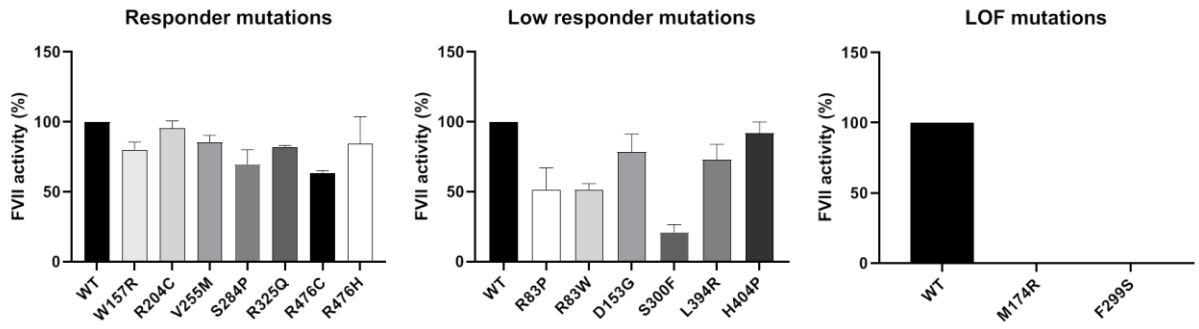

Figure 20: FVII activity measured with respect to responder, low responder and loss-of-function GGCX mutations. FVII activity measured in media from *GGCX*$^{-/-}$ HEK293T cells that were transfected with bicistronic vectors harboring cDNAs of *GGCX* wt/mut together with F7. Cells were treated with 10 µM K_1. Error bars depict SD of *n* = 3 experiments.

The FVII activity was measured at low (1 µM K) and high (10 µM) K_1 concentration for high responder mutations (GGCX:p.(I532T), GGCX:p.(G537A), GGCX:p.(W501S), GGCX:p.(W493C)) to validate the high γ-carboxylation shown by ELISA at both concentrations. The results showed high FVII activity for all high responding GGCX mutations at both low and high K concentration which justified the high γ-carboxylation measurement (Figure 21). This confirms that these GGCX mutations cause high γ-carboxylation also at low vitamin K concentration.

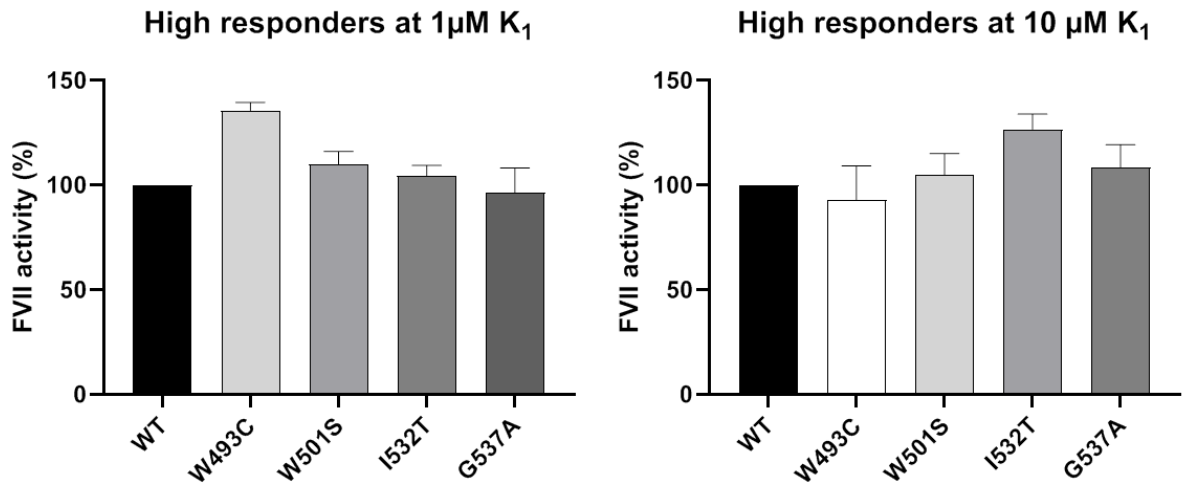

Figure 21: FVII activity measured with respect to high responder GGCX mutations. FVII activity measured in media from *GGCX*$^{-/-}$ HEK293T cells that were transfected with bicistronic vectors harboring cDNAs of *GGCX* wt/mut together with F7. Cells were treated with 1 µM or 10 µM K_1. Error bars depict SD of *n* = 3 experiments.

4.2.3. GGCX mutations effect on the antigen levels

GGCX antigen levels were measured for all mutation by ELISA. The immunogenic region of the antibodies used did not include any analyzed mutation. All analyzed GGCX mutations were expressed in HEK293T *GGCX*$^{-/-}$ cells. Mutation GGCX GGCX:p.(R83W), GGCX:p.(W157R), GGCX:p.(R204C), GGCX:p.(R476C), GGCX:p.(M174R), GGCX:p.(F299S), and GGCX:p.(G537A) showed lower antigens levels compared to wt whereas others showed expression similar to wt. Thus, showing none of the reported missense mutations was causing complete loss of protein expression (Figure 22).

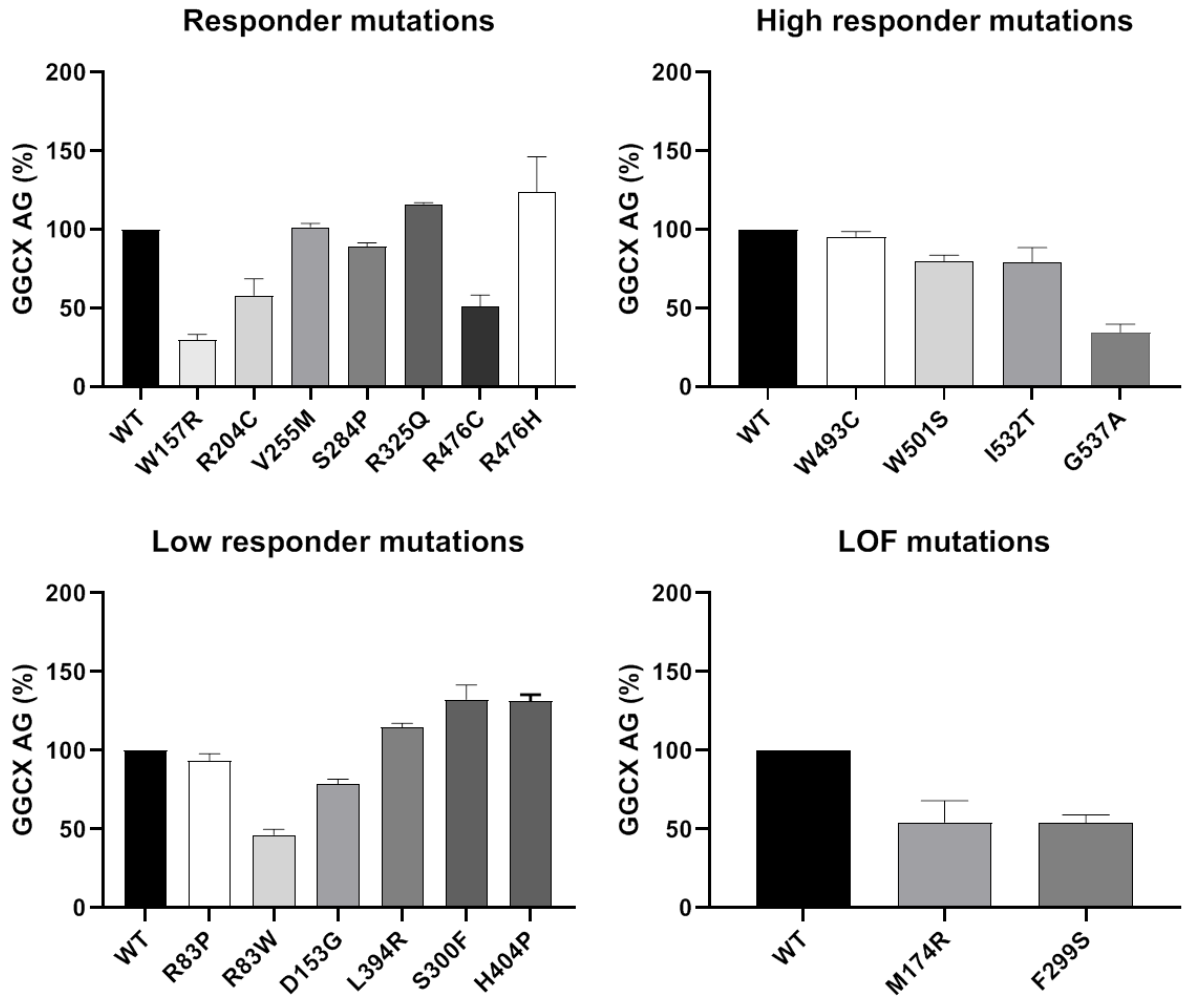

Figure 22: Antigen levels of GGCX mutations measured by ELISA. GGCX wt/mut were expressed in *GGCX*$^{-/-}$ HEK293T cells. Error bars depict SD of *n* = 3 technical replicates of *n* = 3 experiments.

4.2.4 Specific GGCX mutations causing differential effect on γ-carboxylation of VKD haemostatic proteins

Interestingly, selective mutations as f.e. GGCX:p.(R485P) showed different dose-responses amongst the coagulation factors FII, FX, and PC and hence FVII and FIX were included. GGCX:p.(R485P) γ-carboxylated FX, FVII and FIX similar to wt whereas FII is only γ-carboxylated to a maximum of 27.6 % when compared to wt at 10 µM K concentration (Figure 23). Another two mutations GGCX:p.(G558R) and GGCX:p.(T591K) showed also different effects on clotting factors as both did not γ-carboxylate FIX and FX, and showed extremely reduced γ-carboxylation for FVII (Figure 23). GGCX:p.(G558R) was γ-carboxylating FII like wt whereas GGCX:p.(T591K) showed reduced γ-carboxylation (Ghosh et al., *JTH* 2021) [101].

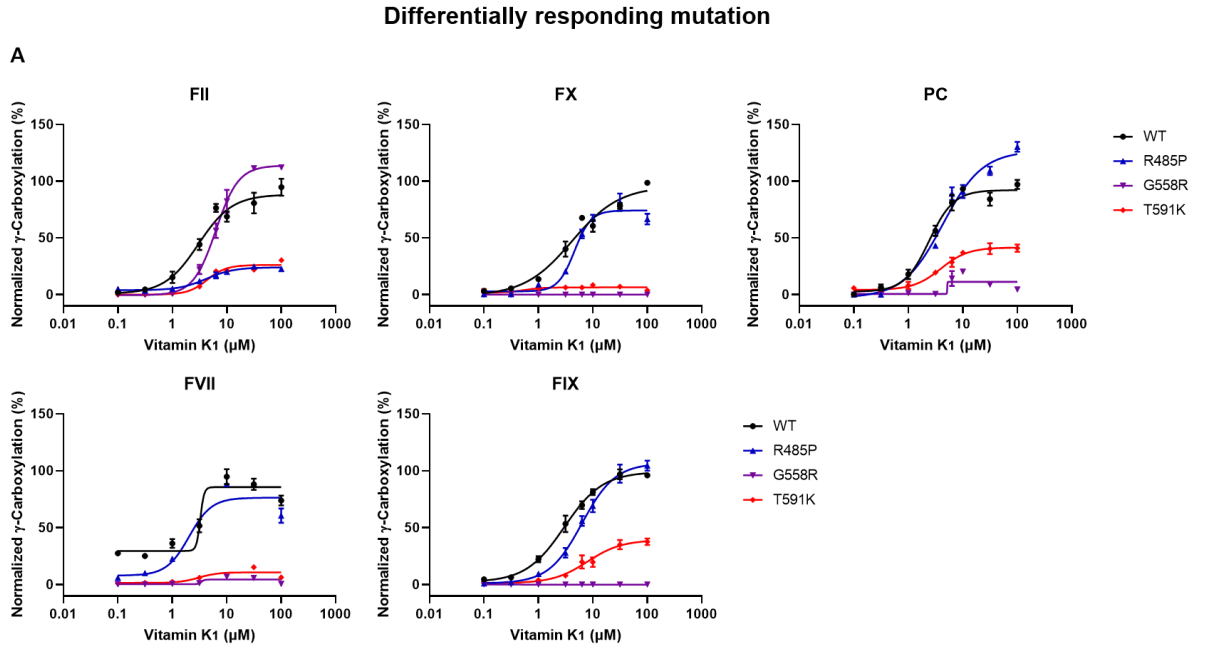

B

GGCX mutation	γ-carboxylated FII [%]		γ-carboxylated FX [%]		γ-carboxylated FVII [%]		γ-carboxylated FIX [%]		γ-carboxylated PC [%]	
	Low K (1 µM K_1)	High K (10µM K_1)	Low K (1µM K_1)	High K (10µM K_1)	Low K (1µM K_1)	High K (10µM K_1)	Low K (1µM K_1)	High K (10µM K_1)	Low K (1 µM K_1)	High K (10µM K_1)
R485P	28 %	27.6 %	57.2 %	117.9 %	64.7 %	88.4 %	40.6 %	80.1 %	124.6 %	94.7 %
G558R	1.7 %	113.2 %	0 %	0 %	1.6 %	6.5 %	0 %	0%	0 %	21.2 %
T591K	5.9 %	29.4 %	33.1 %	13.1 %	6.7 %	30.5 %	17 %	23.8 %	62.5 %	38.5 %

Figure 23: Dose-response curves of GGCX mutations showing different effects on γ-carboxylation of haemostatic proteins measured by ELISA. **A**, The y-axis represents normalized γ-carboxylation (%) of FII, FVII, FIX, FX, and PC. The x-axis represents K_1 concentrations (0.1-100µM). In each figure dose response curve for GGCX wt is shown in black. Error bars depict SD of n=3 technical replicates of three experiments. **B**, The table shows the γ-carboxylation values of mutations at 1µM (low K) and 10µM (high K) K_1 of clotting factors normalized to wt values.

FVII activity were reduced to 67.2 % and 17.9 % for R485P and G558R respectively whereas 0 % for T591K. So, these three mutants continued to show differential response also for FVII

activity (Figure 24A). However, the GGCX antigen levels for all three mutations were present thus indicating that these mutations are expressed but they selectively affect the γ-carboxylation of individual clotting factors (Figure 24B).

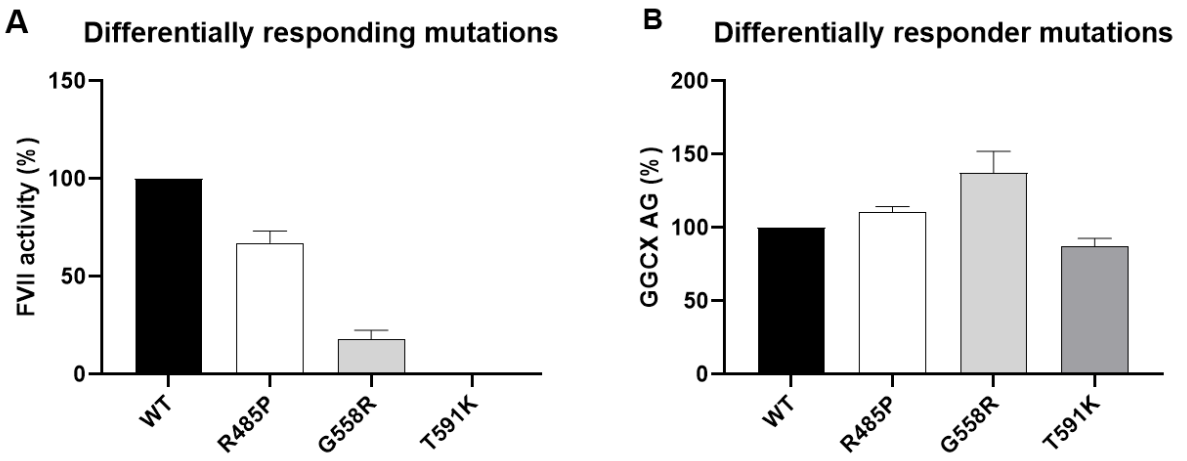

Figure 24: FVII activity and antigen levels of differentially responding GGCX mutations. A, FVII activity measured in media from *GGCX*$^{-/-}$ HEK293T cells that were transfected with bicistronic vectors harboring cDNAs of *GGCX* wt/mut together with F7. Cells were treated with 1 µM or 10 µM K_1. Error bars depict SD of *n* = 3 experiments. **B,** Antigen levels of corresponding GGCX mutations measured by ELISA. GGCX wt/mut were expressed in *GGCX*$^{-/-}$ HEK293T cells. Error bars depict SD of *n* = 3 technical replicates of *n* = 3 experiments.

To further examine the selected deficiency to γ-carboxylate FII, immunofluorescent (IF) staining was performed and verified that GGCX:p.(R485P) and FII were properly expressed but co-localized with a lower Pearson´s correlation coefficient when compared to wt GGCX (Figure 25A). In contrast, FX co-localizes with GGCX:p.(R485P) as wt GGCX, which is in line with the findings from ELISA showing that FX is properly γ-carboxylated comparable to wt (Figure 26). This demonstrates that GGCX:p.(R485P) selectively affects propeptide binding of FII, which reduces the binding to GGCX, thereby resulting in markedly reduced γ-carboxylation of FII only.

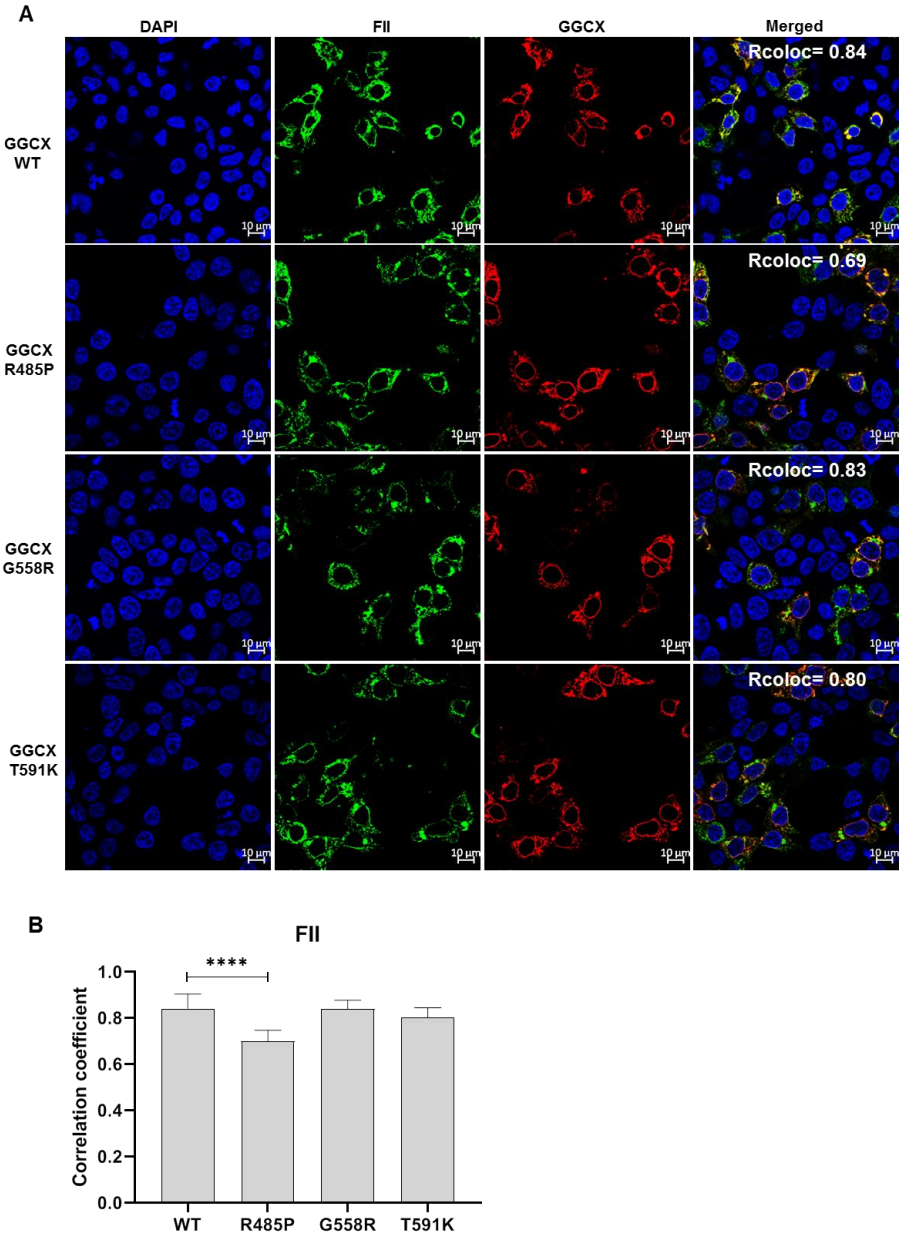

Figure 25: Immunofluorescent staining of FII. A, Immunofluorescent staining of FII that was co-expressed with selected GGCX mutations showing different effects on clotting factors in HEK293T *GGCX*$^{-/-}$ cells. Cells were treated with 10 µM K_1 after transfection. First panel represents Dapi counter stain followed by FII staining with Alexa Fluor 488 (green) and GGCX stained with Alexa Fluor 594 (red) and the merged picture. The Pearson´s correlation co-efficient is given as Rcoloc in the merged picture. Pearson's correlation coefficient >0.4 indicates co-localization and <0.4 is no co-localization. **B**, Mean Pearson´s correlation coefficient values for FII with GGCX wt/mut. Error bars depict SD of n=10 analyzed cells. Unpaired T-test shows statistically significant difference where **** signifies $p < 0.001$. Error bars depict SD of triplicate measurement of n=3 experiments.

For the other mutations GGCX:p.(G558R) and GGCX:p.(T591K), FII is uniformly expressed when co-transfected with these mutations but with a lower co-localization coefficient when compared to wt (Figure 26A). These results are in concordance with the observed lower levels of γ-carboxylated FII (Figure 24). IF staining and co-localization analysis was also performed for FX and confirmed for both mutations GGCX:p.(G558R) and GGCX:p.(T591K) that FX

accumulated within the cell in the presence of 10 µM K_1 and was not co-localizing with the GGCX mutants, whereas GGCX wt is highly co-localizing with FX (Figure 26). This reduced co-localization indicates that these mutants might drastically affect the binding of the VKD proteins with GGCX, hence leading to incomplete γ-carboxylation.

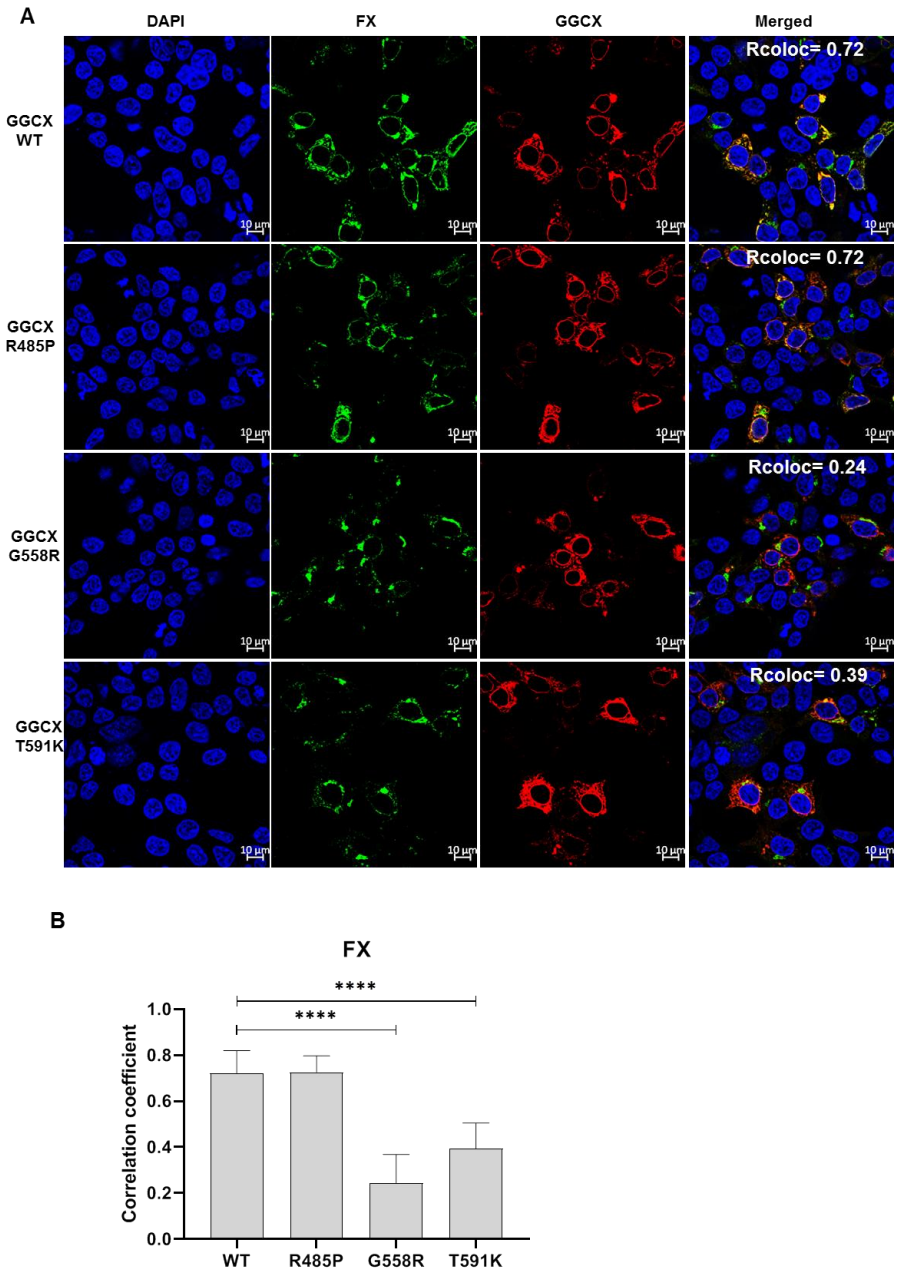

Figure 26: Immunofluorescent staining of FX. A, Immunofluorescent staining of FX that was co-expressed with selected GGCX mutations showing different effects on clotting factors in HEK293T *GGCX*$^{-/-}$ cells. Cells were treated with 10 µM K_1 after transfection. First panel represents Dapi counter stain followed by FX staining with Alexa Fluor 488 (green) and GGCX stained with Alexa Fluor 594 (red) and the merged picture. The Pearson´s correlation co-efficient is given as Rcoloc in the merged picture. Pearson's correlation coefficient >0.4 indicates co-localization and <0.4 is no co-localization. **B**, Mean Pearson´s correlation coefficient values for FX with GGCX wt/mut. Error bars depict SD of n=10

analyzed cells. Unpaired T-test shows statistically significant difference where **** signifies $p < 0.001$. Error bars depict SD of triplicate measurement of n=3 experiments.

4.3.1 Characterization of GGCX mutation on γ-carboxylation of non-hemostatic VKD proteins

To simplify the analysis of six non-haemostatic proteins, the GGCX mutations were grouped into three categories based on the patient's phenotype. As mentioned earlier the most prominent non-haemorrhagic phenotypes seen in VKCFD1 patients were skin, skeletal and cardiac abnormalities. Therefore, for genotype-phenotype correlation the mutations were grouped into these three categories (Table 7). Then the γ-carboxylation values for each non-haemostatic protein were compared with respect to the γ-carboxylation by mutations which did not cause the respective phenotype in the patient.

Table 7: The three groups of non- haemorrhagic phenotypes. The table represents three groups of non-haemostatic phenotypes- skin laxity, cardiac abnormalities and skeletal abnormalities

GGCX Mutant	Genotype	Non-haemostatic phenotype/s
R83W:Q374X (Li et al., 2009b)	**Compound heterozygous**	**Skin laxity**
G558R:F299S (Vanakker et al., 2007)	**Compound heterozygous**	**Skin laxity**
R476H:Wt (Vanakker et al., 2007)	**Heterozygous**	**Skin laxity**
V255M:S300F (Li et al., 2009a)	**Compound heterozygous**	**Skin laxity + Cardiac abnormalities**
G537A :Q374X (Vanakker et al., 2007)	**Compound heterozygous**	**Skin laxity + Cardiac abnormalities**
H404P:R485P (Watzka et al., 2014)	**Compound heterozygous**	**Skin laxity + Cardiac abnormalities**
R476C:Wt (Vanakker et al., 2007)	**Heterozygous**	**Skin laxity + Cardiac abnormalities**
W157R:D31N+T591K (Dargouth et al., 2006)	**Compound heterozygous**	**Cardiac abnormalities**
R83P:R83P (Watzka et al., 2014)	**Homozygous**	**Skeletal abnormalities + Cardiac abnormalities**
S284P:W315X (Watzka et al., 2014)	**Compound heterozygous**	**Skeletal abnormalities + Cardiac abnormalities**
D153G:R325Q+M174R (Tie et al., 2016)	**Compound heterozygous**	**Skeletal abnormalities**

In the following three sections, the results of γ-carboxylated GRP, MGP, BGLAP with respect to the corresponding non-haemostatic phenotypes are described in details.

4.3.2 Effect of GGCX mutations on γ-carboxylation of VKD proteins causing the skin phenotype

Seven VKCFD1 patients were reported with a severe PXE-like phenotype with skin hyper-laxity and skin folds [85,86,94]. Out of these, four patients were found to be compound heterozygous, where one allele has a loss-of-function or a nonsense mutation resulting into disability to γ-carboxylate VKD proteins by this allele. In these patients the other alleles harbor mutations GGCX:p.(R83W), GGCX:p.(V255M), GGCX:p.(G537A) or GGCX:p.(G558R) that exhibited levels between 18 – 32 % of γ-carboxylated GRP at 10 µM K_1 when compared to wt (Figure 27). Levels of γ-carboxylated MGP and BGLAP for the four above mutations were in between 10 % - 102 % and 15% - 156 % respectively (Figure 27).

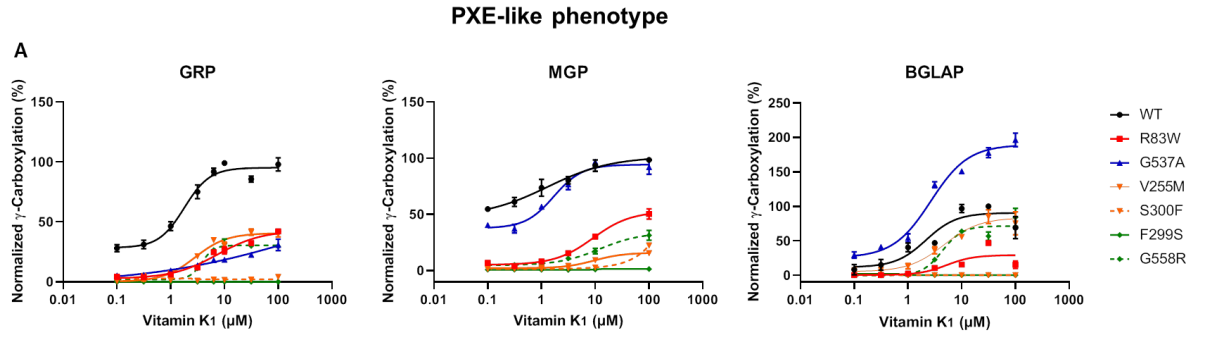

B

GGCX mutation	Age (Age of onset)	Genotype	Non-haemostatic phenotype/s	γ-carboxylated GRP ([%] at 10µM K_1)	γ-carboxylated MGP ([%] at 10µM K_1)	γ-carboxylated BGLAP ([%] at 10µM K_1)	Comments	VKORC1 c.-1639	Ref.
R83W Q374X	48 year (27 year)	CH	PXE-like phenotype	26.2 % -	31.7 % -	15.8 % -	Family heterozygous for R83W or Q374X did not developed skin phenotype		Li et al., 2009b
G537A Q374X	46 year, 44 year	CH	PXE-like phenotype+ Atherosclerosis	18.4 % -	102 % -	155.8 % -			Vanakker et al., 2007
V255M S300F	16 year	CH	PXE-like phenotype+ Cardiac abnormality	30.7 % 1.5 %	10.2 % 2.9 %	57.3 % 0 %			Li et al., 2009a
G558R F299S	40 year	CH	PXE-like phenotype	31.7 % 0 %	18.2 % 1 %	65.8 % 0 %			Vanakker et al., 2007

Figure 27: Dose response curves for γ-carboxylation of calcification regulators with respect to mutants causing skin phenotype measured by ELISA. **A**, The y-axis represents normalized γ-carboxylation (%) for GRP, MGP, and BGLAP. The x-axis represents K_1 concentrations (0.1-100µM). Error bars depict SD of triplicate measurement of n=3 experiments. In each figure dose-response curve for GGCX wt is depicted in black. Compound heterozygous mutants in one particular patient were represented by same color with each allele variant in solid and dotted line. **B**, The table shows the γ-carboxylation values for calcification regulators GRP, MGP, and BGLAP normalized to wt values with respect to GGCX mutations at 10µM K_1.

For one patient a mild skin phenotype was diagnosed, harboring mutations GGCX:p.(H404P);p.(R485P) [79]. Levels of γ-carboxylated GRP for these mutations were reduced to 34.8 % and 57.7 % respectively indicating that this patient with moderate ability to γ-carboxylate GRP developed a mild skin phenotype (Figure 28). GGCX:p.(H404P) γ-carboxylated MGP and BGLAP upto 8.9 % and 0.4 % whereas GGCX:p.(R485P) showed γ-carboxylation of 87.1 % and 47.7 % for MGP and BGLAP respectively.

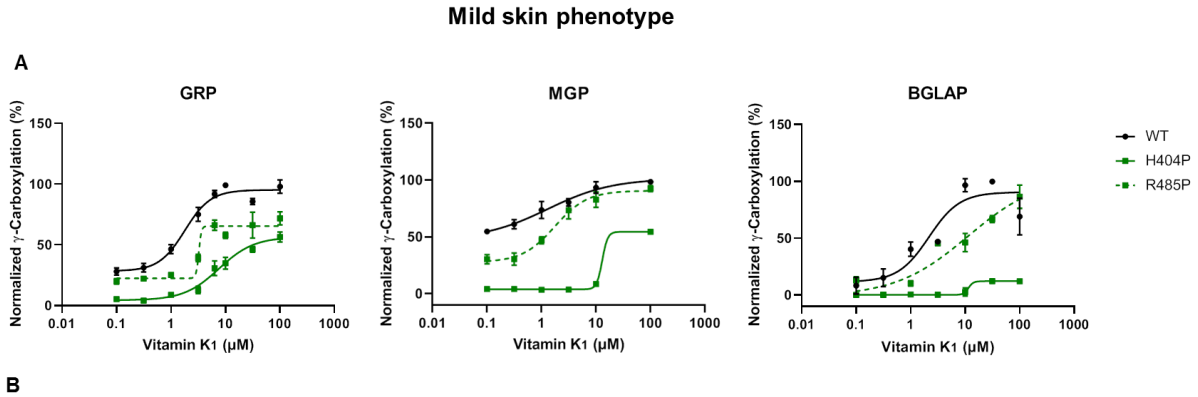

GGCX mutation	Age	Genotype	Non-haemostatic phenotype/s	γ-carboxylated GRP ([%] at 10μM K_1)	γ-carboxylated MGP ([%] at 10μM K_1)	γ-carboxylated BGLAP ([%] at 10μM K_1)	VKORC1 c.-1639	Ref.
H404P R485P	47 year	CH	Mild skin symptom + Calcified peripheral arteries	34.8 % 57.7 %	8.9 % 87.1 %	0.4 % 47.7 %	GG	Watzka et al., 2014

Figure 28: Dose response curves for γ-carboxylation of calcification regulators with respect to mutants causing mild skin phenotype measured by ELISA. **A**, The y-axis represents normalized γ-carboxylation (%) for GRP, MGP, and BGLAP. The x-axis represents K_1 concentrations (0.1-100μM). Error bars depict SD of triplicate measurement of n=3 experiments. In each figure dose-response curve for GGCX wt is depicted in black. Compound heterozygous mutants in one particular patient were represented by same color with each allele variant in solid and dotted line. **B**, The table shows the γ-carboxylation values for calcification regulators GRP, MGP, and BGLAP normalized to wt values with respect to GGCX mutations at 10μM K_1.

There are two patients who are heterozygous for GGCX:p.(R476C) or GGCX:p.(R476H) who have developed a PXE-like phenotype at the age of 3 or 18 years, respectively. In our assay these two mutations did not show markedly reduced γ-carboxylated GRP and the second allele was wt having 100 % γ-carboxylation ability (Figure 29). Although they had a functional second allele, the two patients had developed severe skin laxity which is not fitting with our data and with the reported late onset of skin laxity [37]. They also did not harbor any mutation in *ABCC6* or *VKORC1* gene indicating that the genotype should be re-evaluated for mutations in *GGCX* or some other gene by next generation sequencing.

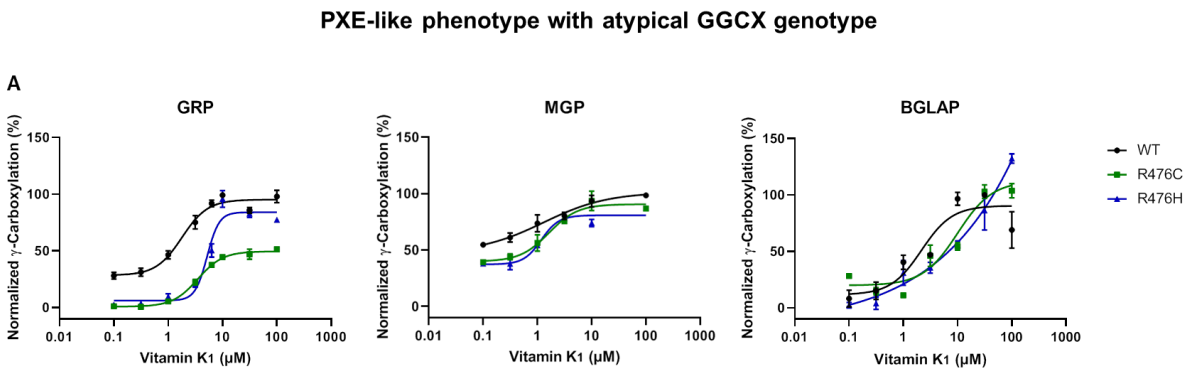

B

GGCX mutation	Age (Age of onset)	Genotype	Non-haemostatic phenotype/s	γ-carboxylated GRP ([%] at 10μM K_1)	γ-carboxylated MGP ([%] at 10μM K_1)	γ-carboxylated BGLAP ([%] at 10μM K_1)	Comments	VKORC1 c.-1639	Ref.
R476C WT	67 year (3 year)	HTZ	PXE-like phenotype + Atherosclerosis	41.7 % 100 %	93.5 % 100 %	56.2 % 100 %	Re-evaluation of genotype		Vanakker et al., 2007
R476H WT	32 year (18 year)	HTZ	PXE-like phenotype	95.7 % 100 %	77.9 % 100 %	57.1 % 100 %	Re-evaluation of genotype		Vanakker et al., 2007

Figure 29: Dose response curves for γ-carboxylation of calcification regulators with respect to mutants reported in patients with atypical genotype and causing skin phenotype measured by ELISA. **A**, The y-axis represents normalized γ-carboxylation (%) for GRP, MGP, and BGLAP. The x-axis represents K_1 concentrations (0.1-100μM). Error bars depict SD of triplicate measurement of n=3 experiments. In each figure dose-response curve for GGCX wt is depicted in black. **B**, The table shows the γ-carboxylation values for calcification regulators GRP, MGP, and BGLAP normalized to wt values with respect to GGCX mutations at 10μM K1.

Mutations GGCX:p.(R83P), GGCX:p.(L394R), GGCX:p.(W493C) and GGCX:p.(W501S) showed lower levels of γ-carboxylated GRP of around 2-33 % respectively (Figure 30). Three out of four mutations are reported in homozygous state in the patients who are currently infants so there is a possibility that they might develop skin hyper-laxity or mild skin phenotype in future due to biallelic reduction in γ-carboxylation of GRP. Another patient who is 1 year old was reported with mutation GGCX:p.(W493C) in compound heterozygous form in combination with a nonsense mutation. This will result into biallelic reduction in γ-carboxylation of GRP which might lead to skin hyper-laxity in future.

Expected to develop PXE-like phenotype

A

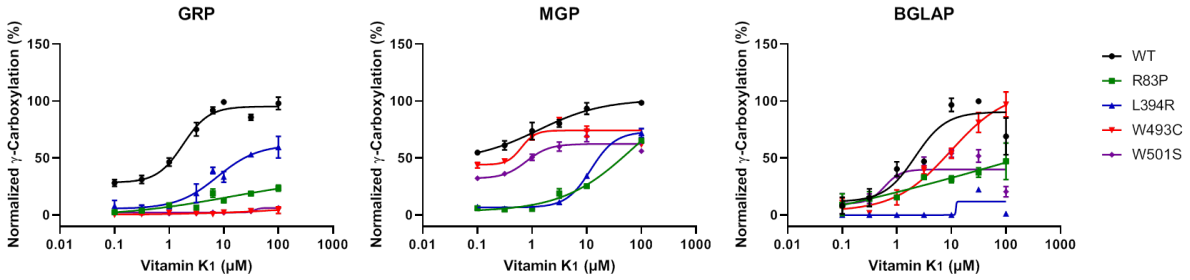

B

GGCX mutation	Age	Genotype	Non-haemostatic phenotype/s	γ-carboxylated GRP ([%] at 10μM K_1)	γ-carboxylated MGP ([%] at 10μM K_1)	γ-carboxylated BGLAP ([%] at 10μM K_1)	Comments	VKORC1 c.-1639	Ref.
R83P R83P	3 year	HMZ	Facial Dysmorphism + Septal defect	12.6 % 12.6 %	26.5 % 26.5 %	34 % 34 %	Expected to develop skin phenotype	AA	Watzka et al, 2014
L394R L394R	5 months, newborns	HMZ	-	33.3 % 33.3 %	36.1 % 36.1 %	0 % 0 %	Expected to develop mild skin phenotype		Brenner et al., 1998
W493C R704X	1 year	CH with nonsense	-	2.3 % -	81.5 % -	55.8 % -	Expected to develop mild skin phenotype		Darghouth et al., 2009
W501S W501S	7 days	HMZ	-	2 % 2 %	72.8 % 72.8 %	55.8 % 55.8 %	Expected to develop mild skin phenotype		Spronk et al., 2000

Figure 30: Dose response curves for γ-carboxylation of calcification regulators with respect to mutants expected to cause skin phenotype measured by ELISA. **A**, The y-axis represents normalized γ-carboxylation (%) for GRP, MGP, and BGLAP. The x-axis represents K_1 concentrations (0.1-100μM). Error bars depict SD of triplicate measurement of n=3 experiments. In each figure dose-response curve for GGCX wt is depicted in black. **B**, The table shows the patient data along with the γ-carboxylation of mutants expected to cause skin phenotype with respect to 100% wt γ-carboxylation at 10μM K_1.

MGP and BGLAP were excluded to be responsible for the skin phenotype since all types of dose-responses were detected (Figure 27).

4.3.3 Effect of GGCX mutations on γ-carboxylation of VKD proteins causing the skeletal phenotype

Three VKCFD1 patients were reported with facial dysmorphologies. A patient that is homozygous for GGCX:p.(R83P) developed midfacial hypoplasia [79]. This mutation showed markedly reduced levels of γ-carboxylated GRP, MGP, and BGLAP which was 13%, 26.5% and 34% respectively (Figure 31A and 31C). Additionally this patient was homozygous for VKORC1:c.-1639 AA polymorphism. VKORC1 is the enzyme which recycles vitamin K and generates its reduced form (vitamin K hydroquinone, KH_2) which is the substrate required for γ-carboxylation. Hence, mutations in *VKORC1* gene will influence γ-carboxylation efficiency. There was another patient who was reported to have a mutation in the same residue i.e. GGCX:p.(R83W) which was in compound heterozygous form where the other allele harbored a non-sense (Q374X) mutation. GGCX:p.(R83W) in our data showed only 31.7 % γ-carboxylated MGP but the patient was neither reported with any skeletal defects nor any mutation in VKORC1 gene.

A Keutel syndrome-like phenotype was described for a patient who is compound heterozygous for GGCX:p.(M174R+R325Q);p.(D153G) [88]. Strippling of fingers was observed along with facial dysmorphologies. For GGCX:p.(D153G) reduced levels of γ-carboxylated MGP around 38.3 % was detected whereas GRP and BGLAP showed higher γ-carboxylation of 93.5 % and 81.5 % respectively (Figure 31A and 31C). In the patient the other allele had GGCX:p.(M174R) along with GGCX:p.(R325Q) which will be not be functional as GGCX:p.(M174R) is a loss-of-function mutation which γ-carboxylated GRP, MGP, and BGLAP at 0.8 %, 1.2 % and 0 % respectively. This indicates that under γ-carboxylated MGP played a major role in developing skeletal phenotype for this patient.

There is another patient having a midfacial hypoplasia (GGCX:p.(S284P);p.(W315X)) [79], where level of γ-carboxylated MGP for GGCX:p.(S284P) was higher, around 100.2 % (Figure 31B and 31C). Notably, the mother reported a severe hyperemesis gravidarum with a weight loss of seven kg within the first trimester. Thus, indicating that the nutritional uptake of vitamin K during pregnancy might modulate the severity of those birth defects. Moreover this patient is also homozygous for the VKORC1:c.-1639 AA genotype.

Two patients out of three cases showing facial dysmorphologies had homozygous VKORC1:c.-1639 AA genotype which was reported with reduced mRNA expression and enzymatic availability [102].

Our results demonstrate that reduction of γ-carboxylated MGP along with additional factors such as mutations/polymorphism in VKORC1 gene or nutritional uptake during pregnancy are

lead cause of congenital defects like facial dysmorphologies in VKCFD1 patients (Figure 31). Low number of patients gives an additional hint that multiple critical factors have to be affected in an individual to develop congenital facial dysmorphologies.

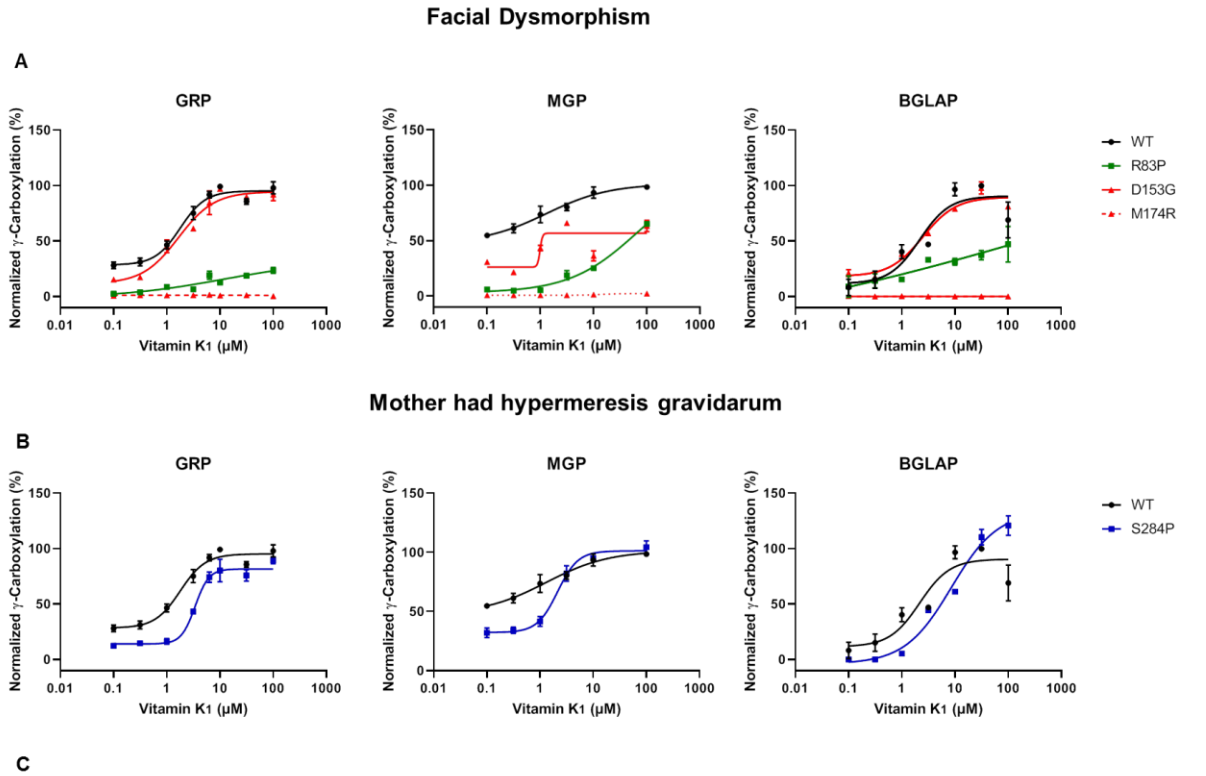

C

GGCX mutation	Age	Genotype	Non-haemostatic Phenotype/s	γ-carboxylated GRP ([%] at 10μM K_1)	γ-carboxylated MGP ([%] at 10μM K_1)	γ-carboxylated BGLAP ([%] at 10μM K_1)	Comments	VKORC1 c.-1639	Ref.
R83P R83P	3 year	HMZ	Facial Dysmorphism + Septal defect	12.6 % 12.6 %	26.5 % 26.5 %	34 % 34 %		AA	Watzka et al, 2014
D153G M174R+(R325Q)	4 months	CH	Keutel syndrome like phenotype	93.5 % 0.8 %	38.3 % 1.2 %	81.5 % 0 %			Tie et al., 2016
S284P W315X	13 year	CH	Midfacial hypoplasia + Septal defect	80.1% -	100.2 % -	63.2 % -	Mother had hyperemesis gravidarum	AA	Watzka et al, 2014

Figure 31: Dose response curves for γ-carboxylation of calcification regulators with respect to mutants causing facial hypoplasia measured by ELISA. **A-B**, The y-axis represents normalized γ-carboxylation (%) of GRP, MGP, and BGLAP. The x-axis represents K_1 concentrations (0.1-100μM). In each figure dose-response curve is depicted for GGCX wt (black). Compound heterozygous mutants in one particular patient were represented by same color with each allele variant in solid and dotted line. Error bars depict SD of triplicate measurement of n=3 experiments. **B,** The γ-carboxylation of GRP, MGP, and BGLAP with respect to the mutations reported in patient whose mother had hypermeresis gravidarum. **C**, Table shows patient data along with the γ-carboxylation values of mutants causing facial hypoplasia phenotype with respect to 100% wt γ-carboxylation at 10μM K_1.

There are also patients harboring mutations where level of γ-carboxylated MGP were reduced but did not show skeletal abnormalities (f.e. GGCX:p.(R83W), GGCX:p.(L394R); p.(L394R), or GGCX:p.(G558R), p.(F299S)) (Figure 32). This indicates that multiple factors like mutation or polymorphism in other gene or nutritional uptake have to be affected to develop skeletal defects.

A

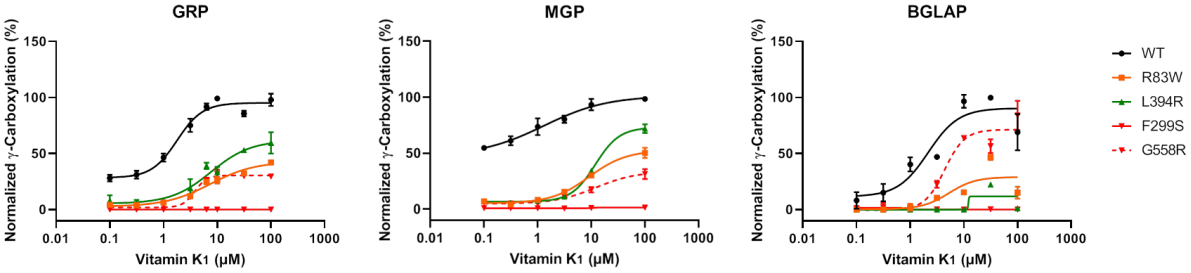

B

GGCX mutation	Age	Genotype	Non-haemostatic Phenotype/s	γ-carboxylated GRP ([%] at 10μM K_1)	γ-carboxylated MGP ([%] at 10μM K_1)	γ-carboxylated BGLAP ([%] at 10μM K_1)	Comments	VKORC1 c.-1639	Ref.
R83W Q374X	48 year (27 year)	CH	PXE-like phenotype	26.2 % -	31.7 % -	15.8 % -	Family heterozygous for R83W or Q374X did not developed skin phenotype		Li et al., 2009b
L394R L394R	5 months, newborns	HMZ	-	33.3 % 33.3 %	36.1 % 36.1 %	0 % 0 %	Expected to develop mild skin phenotype		Brenner et al., 1998
G558R F299S	40 year	CH	PXE-like phenotype	31.7 % 0 %	18.2 % 1 %	65.8 % 0 %			Vanakker et al., 2007

Figure 32: Dose response curves for γ-carboxylation of calcification regulators with respect to mutants causing showing reduced γ-carboxylation but no skeletal defects. **A**, The y-axis represents normalized γ-carboxylation (%) of GRP, MGP, and BGLAP. The x-axis represents K_1 concentrations (0.1-100μM). In each figure dose-response curve is depicted for GGCX wt (black). Compound heterozygous mutants in one particular patient were represented by same color with each allele variant in solid and dotted line. Error bars depict SD of triplicate measurement of n=3 experiments. **B**, Table with patient data along with the γ-carboxylation of mutants showing no facial defects with respect to 100% wt γ-carboxylation at 10μM K_1.

4.3.4 Effect of GGCX mutations on γ-carboxylation of VKD proteins showing cardiac phenotype

The cardiac phenotype in VKCFD1 patients summarizes several defects as septal closure abnormalities, persistent ductus arteriosus Botalli, congenital supravalvular pulmonary stenosis and peripheral artery stenosis or associated cardiac abnormalities [37].

Three patients with GGCX:p.(R83P);p.(R83P), GGCX:p.(S284P);p.(W315X), and GGCX:p.(W157R);p.(T591K) mutations have a congenital atrial septal defect. GGCX:p.(R83P) γ-carboxylates GRP, MGP and BGLAP around 12.6 %, 26.5 % and 34 % respectively (Figure 33). GGCX:p.(W157R) γ-carboxylates GRP, MGP and BGLAP around 44.1 %, 58 %, and 45.1 %. Mutation GGCX:p.(T591K) in the other allele γ-carboxylates 31.8 %, 23.8 %, and 0 % GRP, MGP and BGLAP respectively (Figure 33). The allele harboring GGCX:p.(T591K) also had a known rare polymorphism i.e. D31N that was showed to have 100 % activity [83].

GGCX:p.(S284P) showed higher levels of GRP, MGP, and BGLAP γ-carboxylation of 80.1 %, 100.2 % and 63.2 % respectively. GGCX:p.(S284P) was reported to be compound heterozygous where the other allele has a nonsense mutation (Figure 33). The mother of this patient was reported to have severe hyperemesis gravidarum with a weight loss of seven kg within the first trimester which might be the sole reason for developing septal defect [79]. As in our assay the allele with GGCX:p.(S284P) should be functional.

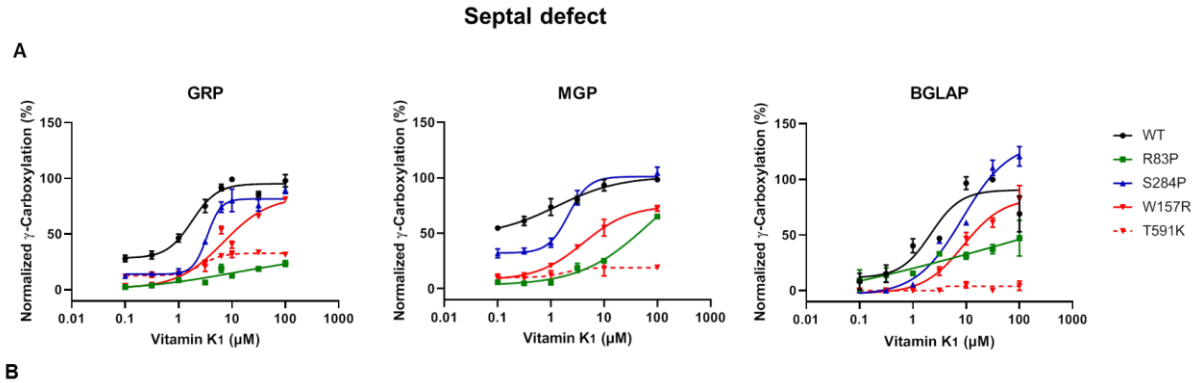

B

GGCX mutation	Age	Genotype	Non-haemostatic Phenotype/s	γ-carboxylated GRP ([%] at 10μM K_1)	γ-carboxylated MGP ([%] at 10μM K_1)	γ-carboxylated BGLAP ([%] at 10μM K_1)	Comments	VKORC1 c.-1639	Ref.
R83P R83P	3 year	HMZ	Facial Dysmorphism + Septal defect	12.6 % 12.6 %	26.5 % 26.5 %	34 % 34 %		AA	Watzka et al, 2014
S284P W315X	13 year	CH	Midfacial hypoplasia + Septal defect	80.1% -	100.2 % -	63.2 % -	Mother had hyperemesis gravidarum	AA	Watzka et al, 2014
W157R (D31N)+T591K	2 year	CH	Developmental delay + Septal Defect	44.1 % 31.8 %	58 % 23.8 %	45.1 % 0 %			Dargouth et al., 2006

Figure 33: Dose response curves for γ-carboxylation of calcification regulators with respect to mutants causing septal defects measured by ELISA. **A**, The y-axis represents normalized γ-carboxylation (%) of GRP, MGP, and BGLAP. The x-axis represents K_1 concentrations (0.1-100μM). In each figure dose-response curve is depicted for GGCX wt in black. Compound heterozygous mutants in one particular patient were represented by same color with each allele variant in solid and dotted line.

Error bars depict SD of triplicate measurement of n=3 experiments. **B**, Table with patient data along with the γ-carboxylation of mutants with respect to 100% wt γ-carboxylation at 10μM K_1.

Another four patients with mutations GGCX:p.(V255M);p.(S300F), GGCX:p.(H404P);p(R485P), GGCX:p.(R476C) and GGCX:p.(G537A);p.(Q374X) developed aged associated subclinical atherosclerosis. All these patients were harboring mutations that have reduced ability to γ-carboxylate GRP around 18-58 % (Figure 34). All types of dose-responses were detected for MGP and BGLAP (Figures 33 and 34). Therefore, this data suggest the role of GRP under-carboxylation in developing cardiac defects.

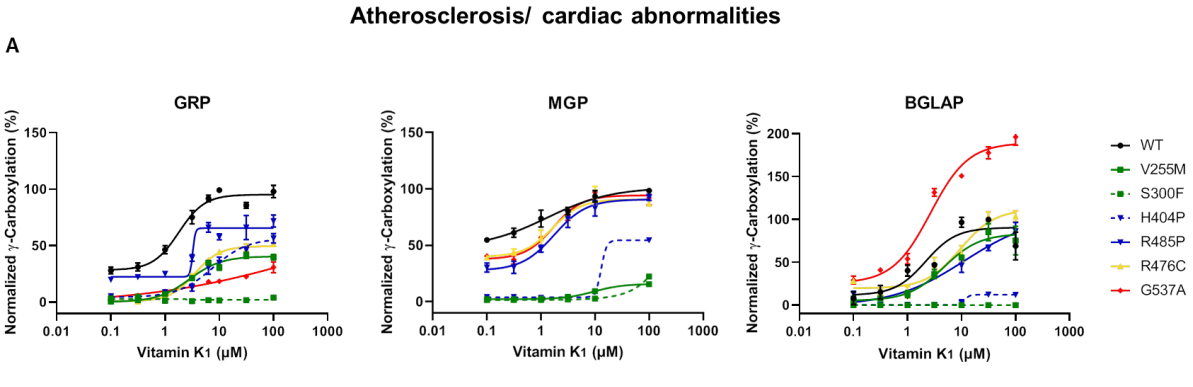

B

GGCX mutation	Age	Genotype	Non-haemostatic Phenotype/s	γ-carboxylated GRP ([%] at 10μM K_1)	γ-carboxylated MGP ([%] at 10μM K_1)	γ-carboxylated BGLAP ([%] at 10μM K_1)	VKORC1 c.-1639	Ref.
V255M S300F	16 year	CH	PXE-like phenotype+ Cardiac abnormality	30.7 % 1.5 %	10.2 % 2.9 %	57.3 % 0 %		Li et al., 2009a
H404P R485P	47 year	CH	Mild skin symptom + Calcified peripheral arteries	34.8 % 57.7 %	8.9 % 87.1 %	0.4 % 47.7 %	GG	Watzka et al, 2014
R476C WT	67 year	HTZ	PXE-like phenotype+ Atherosclerosis	41.7 % 100 %	93.5 % 100 %	56.2 % 100 %		Vanakker et al., 2007
G537A Q374X	46 year, 44 year	CH	PXE-like phenotype+ Atherosclerosis	18.4 % -	102 % -	155.8 % -		Vanakker et al., 2007

Figure 34: Dose response curves for γ-carboxylation of calcification regulators with respect to mutants causing subclinical atherosclerosis and cardiac abnormalities measured by ELISA. **A**, The y-axis represents normalized γ-carboxylation (%) of GRP, MGP, and BGLAP. The x-axis represents K_1 concentrations (0.1-100μM). In each figure dose-response curve is depicted for GGCX wt in black. Compound heterozygous mutants in one particular patient were represented by same color with each allele variant in solid and dotted line. Error bars depict SD of triplicate measurement of n=3 experiments. **B**, Table with patient data along with the γ-carboxylation of mutants normalized to 100% wt γ-carboxylation at 10μM K_1.

4.3.5 No effect of γ-carboxylation status of PRGP1, TMG4 and GAS6 on skin, skeletal and cardiac abnormalities

The influence of γ-carboxylation of PRGP1, TMG4 and GAS6 on the development of skin, skeletal and cardiac abnormalities was eliminated as all types of dose response curves were detected (Table 8). Therefore, it was eliminated to be one of the causative under-carboxylated protein for the above mentioned non-haemostatic phenotype.

Table 8: Effect of GGCX mutations on γ-carboxylation of PRGP1, TMG4 and GAS6 causing non-haemostatic phenotypes. The table shows the patient data along with the γ-carboxylation effect of mutations on PRGP1, TMG4 and GAS6 with respect to 100% wt γ-carboxylation at 100µM K_1 obtained from ELISA

GGCX Mutant	Genotype	Non-haemostatic phenotype/s	PRGP1 ([%] at 100µM K1))	TMG4 ([%] at 100µM K1))	GAS6 ([%] at 100µM K1))	Reference
R83W Q374X	Compound heterozygous	Skin laxity	176.9 % -	4.9 % -	138.5 % -	Li et al., 2009b
G558R F299S	Compound heterozygous	Skin laxity	0.3 % 0 %	50.6 % 0 %	5.3 % 1.6 %	Vanakker et al., 2007
R476H wt	Heterozygous	Skin laxity	170.2 % 100 %	137.3 % 100 %	112.7 % 100 %	Vanakker et al., 2007
V255M S300F	Compound heterozygous	Skin laxity + Cardiac abnormalities	151.7 % 0 %	111.5 % 3.5 %	153.1 % 2.7 %	Li et al., 2009a
G537A Q374X	Compound heterozygous	Skin laxity + Cardiac abnormalities	117.6 % -	108 % -	83.8 % -	Vanakker et al., 2007
H404P R485P	Compound heterozygous	Skin laxity + Cardiac abnormalities	72.7 % 118.2 %	120.7 % 91.1 %	51.7 % 61.8 %	Watzka et al., 2014
R476C wt	Heterozygous	Skin laxity + Cardiac abnormalities	91.1 % 100 %	95.7 % 100 %	87.8 % 100 %	Vanakker et al., 2007
W157R D31N+T591K	Compound heterozygous	Cardiac abnormalities	72.2 % 7.1 %	56.4 % 33 %	75.5 % 1.9 %	Dargouth et al., 2006
R83P R83P	Homozygous	Skeletal abnormalities + Cardiac abnormalities	218.1 % 218.1 %	47.1 % 47.1 %	119.8 % 119.8 %	Watzka et al., 2014
S284P W315X	Compound heterozygous	Skeletal abnormalities+ Cardiac abnormalities	101.4 % -	116.2 % -	96.2 % -	Watzka et al., 2014
D153G R325Q M174R	Compound heterozygous	Skeletal abnormalities	164.1 % 113.5 % 2 %	78.1 % 139.1 % 1.8 %	117.1 % 142.9 % 0 %	Tie et al., 2016

4.3.6 Effect of GGCX mutations on γ-carboxylation of BGLAP

All categories of dose-responses were detected and no correlation was found between decreased or increased levels of γ-carboxylated BGLAP and a reported VKCFD1 phenotype. However, mutations GGCX:p.(W157R);p.(T591K) was reported in one patient showing acute infection, developmental retardation and stunted growth, and ventricular septal closure defects. GGCX:p.(W157R) and GGCX:p.(T591K) showed 45 % and 0 % of γ-carboxylated BGLAP respectively (Figure 35).

GGCX:p.(L394R) was reported in a patient in homozygous state who did not show any non-haemostatic phenotype. Our data showed that GGCX:p.(L394R) has 0 % ability to γ-carboxylate BGLAP (Figure 35). The mutation was reported in four siblings where one was 5 months old and others were newborns [80]. Brenner et al. reported that there were no skeletal

abnormalities in these siblings [80]. However, there is a possibility that later these siblings will develop additional known or unknown phenotypes associated with calcification defects.

A

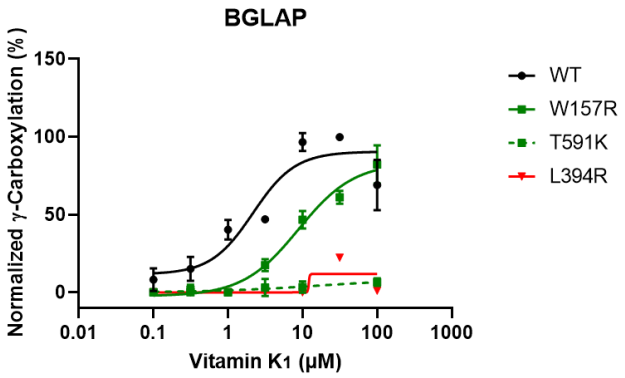

B

GGCX Mutant	Age	Genotype	Non-haemostatic Phenotype/s	BGLAP ([%] at 10μM K_1)	Comments	References
W157R (D31N)+T591K	2 year	Compound heterozygous	Developmental delay + Septal Defect	45.1 % 0 %	Expected higher bone mass	Dargouth et al., 2006
L394R L394R	5 months, newborns	Homozygous	-	0 % 0 %	Expected higher bone mass	Brenner et al., 1998

Figure 35: Dose response curves for γ-carboxylation of BGLAP with respect to mutants causing reduced γ-carboxylation measured by ELISA. **A,** The y-axis represents normalized γ-carboxylation (%) of BGLAP. The x-axis represents K_1 concentrations (0.1-100μM). In the figure dose-response curve is depicted in black for GGCX wt. Compound heterozygous mutants in one particular patient were represented by same color with each allele variant in solid and dotted line. Error bars depict SD of triplicate measurement of n=3 experiments. **B,** The table shows the patient data along with the γ-carboxylation of mutants showing loss-of-function for BGLAP with respect to 100% wt γ-carboxylation at 10 μM K_1.

4.4 Structural aspect of GGCX

4.4.1 hGGCX structural model characteristics

Since the crystal structure of GGCX is unknown and no homologue has been resolved structurally, an *in silico* model was generated using threading method (Figure 36). The model was subjected to a membrane embedded simulation which equilibrated around 15 ns. The production phase for the equilibrated model was run for another 15 ns and the final snapshot was selected for further analysis. In this definite equilibrated model, the majority of the C-terminal region from aa 420-758 localized towards the ER luminal side, which also includes the published propeptide binding site (aa 495-513) [47].

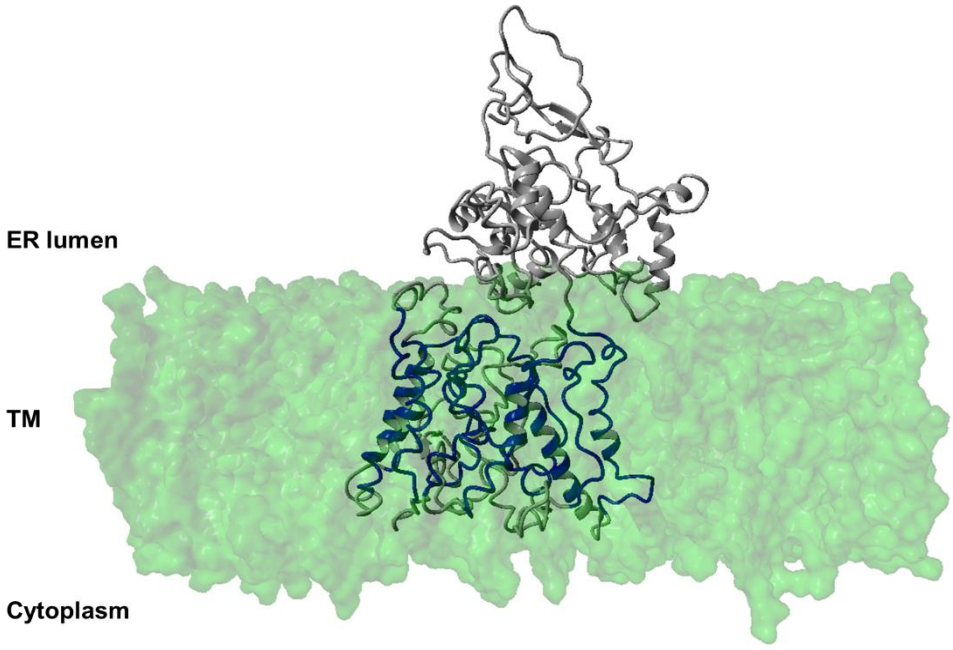

Figure 36: A snapshot of the simulated energy minimized GGCX protein represented in grey (ribbon style) that is embedded in a phosphatidylcholine bilayer membrane in green (molecular surface style) where the transmembrane region of the protein is marked in blue.

Our present *in silico* model has 10 transmembrane domains with four proper helices (aa 116-134, 240-262, 274-292, and 362-377) and two disordered regions (aa 95-115, 394-419). The transmembrane residues in the model are mentioned in the table 9.

Table 9: The table depicts transmembrane domain distribution

Transmembrane	Domain residues	Proper helices
TM1	60-80	
TM2	95-113	Disordered
TM3	114-135	116-134
TM4	137-155	
TM5	156-175	
TM6	199-219	
TM7	240-262	240-262
TM8	274-319	274-292
TM9	361-374	362-377
TM10	394-419	Disordered

The existence of significant disordered regions suggests that major conformational changes are likely to occur in the protein upon substrate binding. For example, the region of aa 385-420 that bears the glutamate binding site (aa 393-404) is highly disordered and therefore might reorient towards the luminal side after substrate binding like the propeptide.

All residues which were mutated and were investigated in the current thesis have been marked in the model to visualize their distribution (Figure 37). The GGCX residues R476, R485, W493, W501, I532, G537, G558, and T591 are all located towards the luminal side of the endoplasmic reticulum whereas R325 is located in the cytoplasmic domain. Luminal residues W493, R485, I532, G537 and G558 are in a close proximity to the propeptide binding domain and W501 is located within the propeptide binding site. Residues L394, H404 are located in the glutamate binding site which belongs to the disordered region in our model. Residues R83, M174, R204, V255M and S284P also belong to disorganized region. GGCX residues D153, W157, F299, and S300 are located towards the periphery of the membrane towards the luminal side.

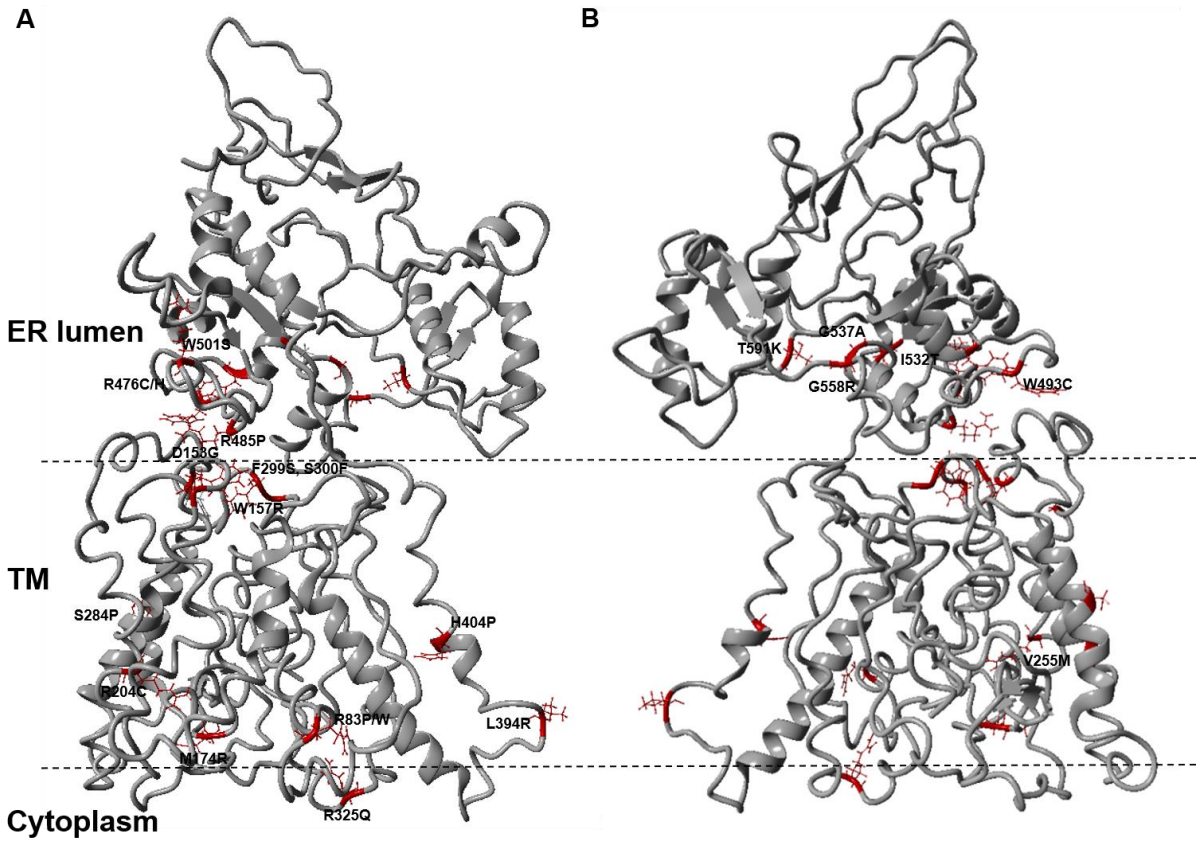

Figure 37: Mutation distribution in GGCX causing VKCFD1. A, The backbone of the GGCX structural model depicted in grey ribbon format. All GGCX mutations are marked in red and the side chain of these residues are represented in stick style. **B**, The spatially reverse orientation of image in **A**. The dotted line indicates the imaginary ER membrane. TM, transmembrane.

4.4.2 Identification of the Vitamin K Hydroquinone binding site in GGCX

Out of 22 *GGCX* missense mutations, two mutations showed loss-of-function GGCX:p.(M174R), GGCX:p.(F299S), and another mutation GGCX:p.(S300F) showed extremely reduced level of γ-carboxylation for all investigated VKD proteins (Figure 38 and figure 18 and 19 in page 49 and 50 respectively). This gave us a hint that these residues might affect the structure leading to protein degradation or affect other unknown functional binding site.

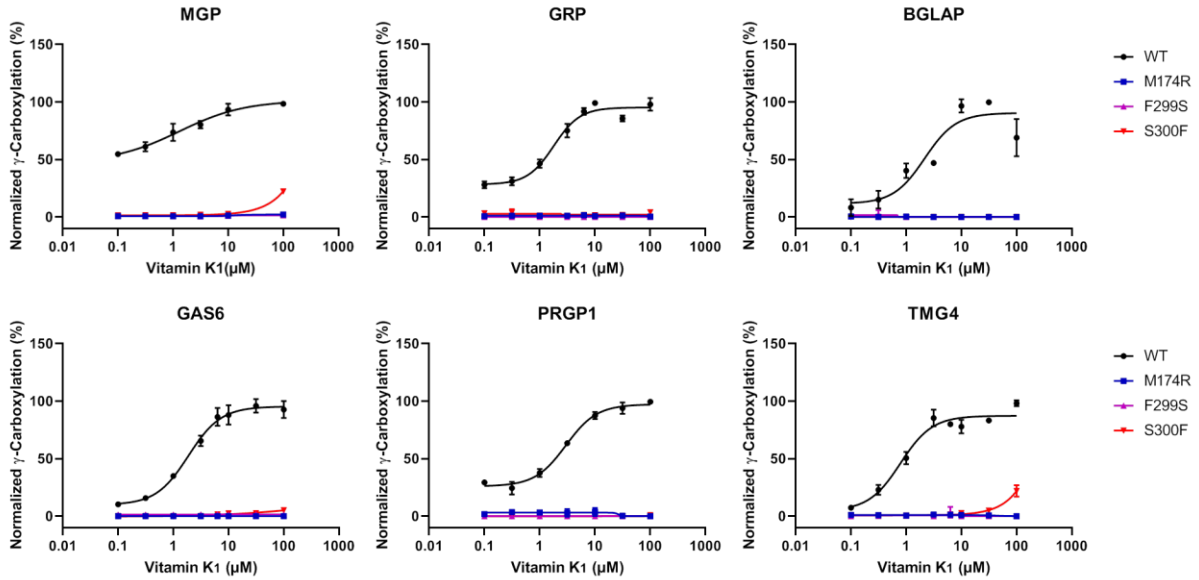

Figure 38: γ-carboxylation of VKD proteins with respect to loss-of-function and low responding mutations. The y-axis represents normalized γ-carboxylation of MGP, GRP, BGLAP, GAS6, PRGP1, and TMG4 (%). The x-axis represents K_1 concentrations (0.1-100µM). Error bar: SD, n=3 experiments.

Therefore, immunostaining was performed to check their expression and localization in the ER (Figure 39A). GGCX:p.(F299S) and GGCX:p.(S300F) are co-localizing with PDI in the ER similar to wt GGCX with a Pearson´s correlation coefficient of +0.74 and +0.76, respectively (Figure 39B). GGCX:p.(M174R) co-localizes to the ER with a significantly reduced Pearson correlation coefficient of +0.53 when compared to the coefficient of +0.73 for wt (Figure 39). Hence, the loss-of-function of GGCX:p.(M174R) is reflected by significant reduction in co-localization to the ER which is in concordance with a previous study who stated that this mutation leads to protein degradation [88].

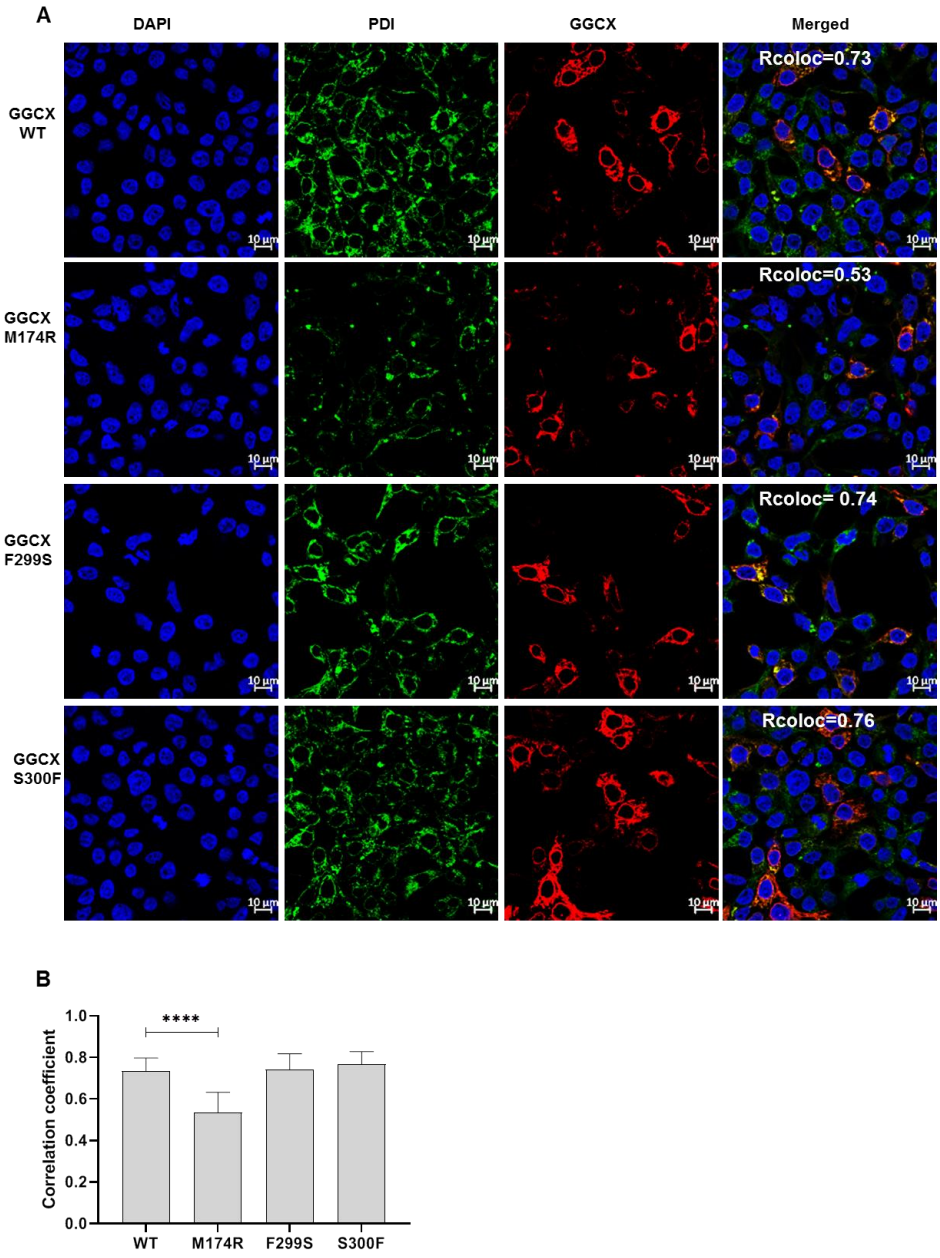

Figure 39: Immunostaining of loss-of-function and low responding GGCX mutations. A, The correlation coefficients Pearson of GGCX loss-of-function mutations with PDI. Unpaired T-test shows statistically significant difference where **** signifies p<0.001. Error bars depict SD of triplicate measurement of 3 experiments. **B**, Colocalization images of HEK293T *GGCX*$^{-/-}$ cells expressing GGCX wt, M174R, F299S, and S300F. First panel represents Dapi counter stain followed by PDI stained with Alexa Fluor 488, GGCX stained with Alexa Fluor 594 and merged.

Mutations GGCX:p.(W315X) and GGCX:p.(K218A) were generated which served as the negative and the positive control respectively, for immunofluorescent staining (Figure 40). IF staining for GGCX:p.(W315X), a natural stop mutation, did not show GGCX expression whereas mutation GGCX:p.(K218A) which is the known active site residue showed proper localization thus validating the antibodies.

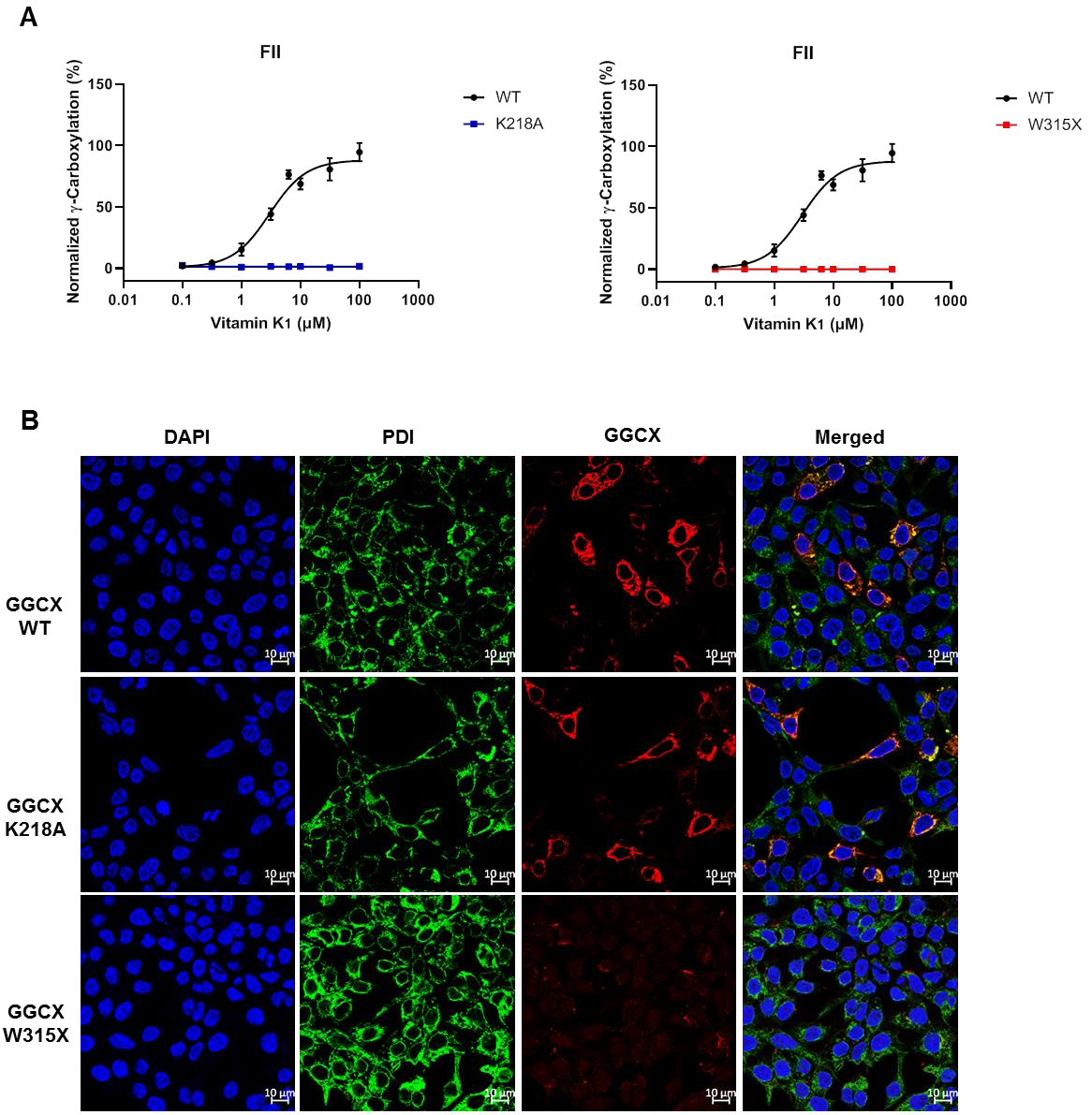

Figure 40: Immunostaining of GGCX mutations (positive and negative control). A, γ-carboxylation dose-responses of GGCX with respect to the active site variant K218A, and the nonsense mutation W315X for FII. **B**, Immunofluorescent staining of PDI and GGCX mutations K218A and W315X that were co-expressed in HEK293T *GGCX*$^{-/-}$ cells. First panel represents Dapi counter stain followed by PDI stained with Alexa Fluor 488 (green) and GGCX stained with Alexa Fluor 594 (red) and the merged picture. The exposure time used for the red filter was 80 psec for all GGCX mutations.

The loss-of-function for F299S and reduced γ-carboxylation ability of S300F along with proper localization in the ER indicated the role of these residues in functional binding rather than structural degradation.

4.4.3 GGCX mutations affecting the Vitamin K Hydroquinone binding site in GGCX

Previous *in vitro* studies and bioinformatics analysis have led to the identification of different functional domains like the propeptide and glutamate binding site as well as the active site of GGCX [43,47,48]. However, no knowledge exists regarding the KH_2 binding site. Therefore, we docked KH_2 onto the equilibrated GGCX model. The initial docking result showed 29 docking poses that were further analyzed (Figure 41).

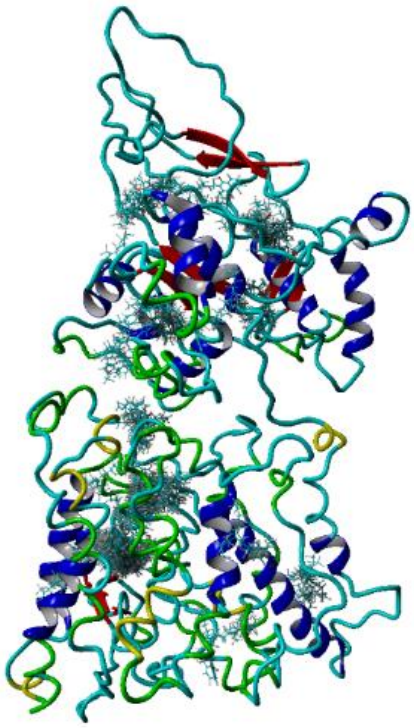

Figure 41: A snapshot of all 29 predicted KH_2 docking complexes shown in stick style.

The ones located in the cytoplasmic side and distant end of the C-terminus were eliminated as the probability of KH_2 binding in this position is minimal due to its hydrophobic nature of vitamin K hydroquinone. Interestingly, five complexes out of remaining nine docking poses belonged to a singular cluster. Then this docking poses were individually analyzed to check the orientation of the vitamin K hydroquinone molecule. Amongst these, docking pose 6 had the correct orientation of KH_2, where the head group of KH_2 is exposed to the exterior, available for interaction, and the hydrophilic tail group is inside the membrane (Figure 42A). This docking pose is also in close proximity to two catalytically important residues: H160 involved in Glu carbanion formation [103] and the active site K218 [43]. Therefore, this docking pose was the

complex of our choice for further evaluation. In the docked complex, KH_2 interacted with ten GGCX residues, amongst which S295 showed hydrogen bonding with KH_2 and residues F299 and Y345 showed both Pi-Pi and hydrophobic interaction with the KH_2 head group (Figure 42B). The involvement of a loss-of-function mutation in KH_2 binding further supported our complex of choice.

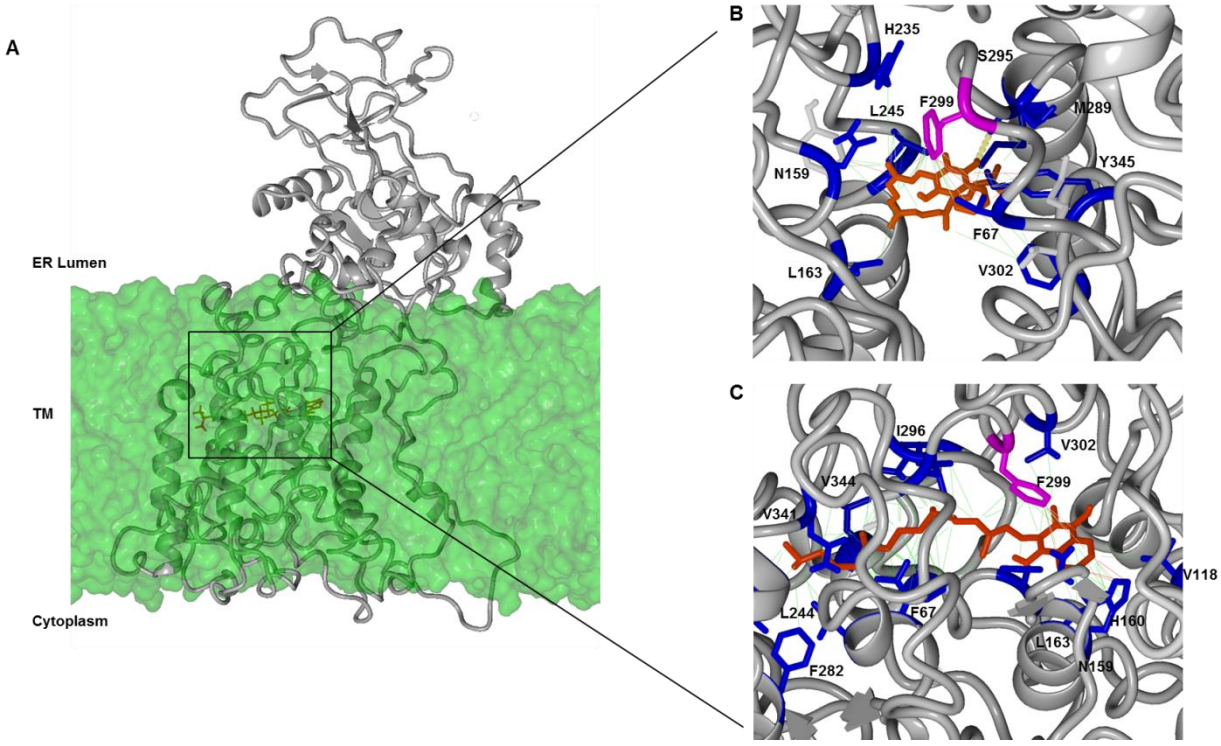

Figure 42: GGCX *in silico* model along with Vitamin K hydroquinone docking complex. **A**, A snapshot of the GGCX structural model (grey) embedded in membrane (green) with bound KH_2 (brown) (complex 6). Model is depicted in ribbon format whereas the membrane is depicted by its molecular surface and KH_2 is depicted in stick format. **B**, Close up view of the docking pose 6 (brown) with ten interacting residues (blue) and critical interacting residue F299 (purple). Interactions by Pi-Pi and hydrophobic binding with the head group of KH_2 are depicted by red and green lines respectively and one hydrogen bonding residue S295 depicted by yellow dotted line. The GGCX structural model is depicted in ribbon format while KH_2 and interacting residues are depicted in stick format. **C**, Close up view of the equilibrated docking complex. Visualization formats remain the same as in b.

Therefore, to further validate this binding site amino acids Y345 and S295 was mutated to alanine *in vitro* and determined their effect on γ-carboxylation of FII. Vitamin K_1 treatment for GGCX:p.(Y345A) and GGCX:p.(S295A) showed only negligible γ-carboxylation of FII thus further verifying that docking pose 6 is the closest model for KH_2 binding (Figure 43).

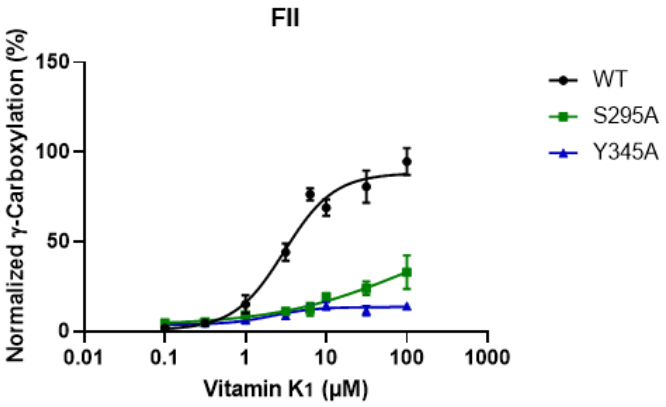

Figure 43: γ-carboxylation of VKD proteins with respect to mutants involved in KH_2 binding. The y-axis represents normalized γ-carboxylation of FII (%). The x-axis represents K_1 concentrations (0.1-100μM). Error bar: SD, n=3 experiments.

Hence this modeled complex was simulated for a total of 250 ns in order to equilibrate it and to study its thermal motion during the production phase. The interaction between F299 and the KH_2 head group was stable post equilibration of the docked complex as well as throughout the production phase (equilibration occurred around ~ 25 ns; therefore the equilibrated complex model was run for >200 ns in the production phase) (Figure 42C, 44). Residues Y345 and S295 were eliminated as direct binding residues post equilibration, but remained in close proximity to the binding site explaining the residual ability to γ-carboxylate the VKD proteins.

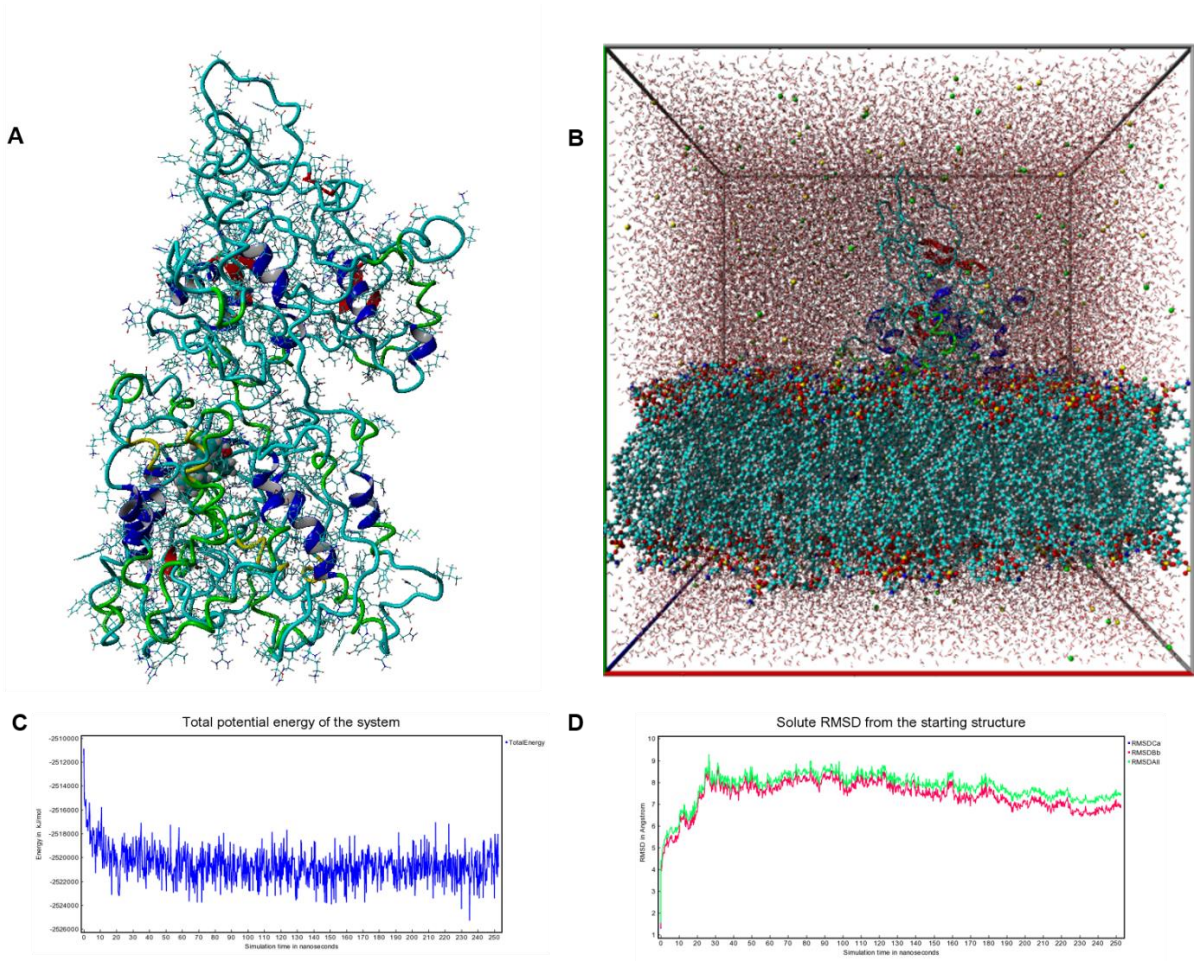

Figure 44: Simulation parameters of GGCX *in silico* model along with Vitamin K hydroquinone docking complex. A, A snapshot of the simulated vitamin K hydroquinone bound GGCX structural model shown in ribbon and ligand style. **B,** The membrane embedded GGCX-KH_2 complex model inside the simulation cell. **C,** Total potential energy of the system where y-axis shows energy in KJ/mol and x-axis shows simulation time in nanoseconds. **D,** Receptor movement RMSD of GGCX wt where y-axis shows energy in RMSD in Angstrom and x-axis shows simulation time in nanoseconds.

In our GGCX structural model F299 stably interacts with KH_2 by both hydrophobic and Pi-Pi interactions. Hence, mutation of this hydrophobic phenylalanine to a polar serine leads to complete disruption of the interaction with KH_2, thereby resulting in loss-of-function (Figure 38).

The involvement of one out of two loss-of-function mutation intrigued us to analyze the possibility of KH_2 binding with other loss-of-function mutations GGCX:p.(M174R) and mutation next to residue F299 i.e. GGCX:p.(S300F) which also showed reduced γ-carboxylation ability. So, these mutations were introduced in the GGCX *in silico* model to check its influence on the binding complex.

Although residue S300 is not present in our equilibrated modeled complex it might affect KH_2 binding owing to its proximity to the binding site. In the production phase, the simulation of a GGCX:p.(S300F) mutated docked complex showed high root mean square deviation (RMSD)

for receptor and ligand movement when compared to wt (all reported RMSDs are c-α backbone RMSDs; Figure 45). The amino acid change to phenylalanine might break the small helix that forms between residue 299-300 thereby creating disorder which disrupts the binding site. This also affects the spatial orientation of F299 with respect to the KH_2 head group, disrupting their Pi-Pi interaction which explains the loss-of-function for the GGCX:p.(S300F) mutation.

The production phase of another mutated docked complex GGCX:p.(M174R) also showed an increase in RMSD for receptor movement more than the ligand movement (Figure 45). Therefore, this mutation most likely alters the structural stability of GGCX more than it directly affects the KH_2 binding site. This is in concordance with the low correlation coefficient in IF staining (Figure 39)

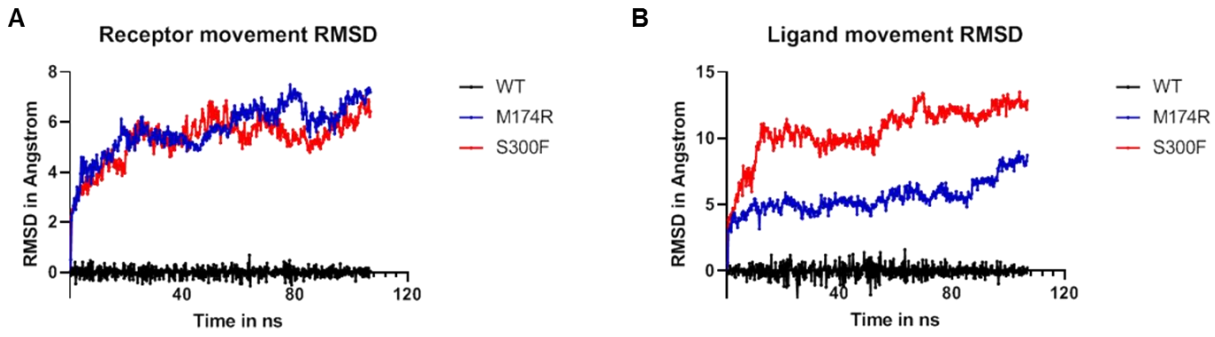

Figure 45: Receptor and ligand movement RMSD (c-α backbone) for GGCX wt (black), M174R (blue), and S300F (red). **A-B**, The y-axis represents RMSD and x-axis represents simulation time.

4.4.4 Mutations affecting the propeptide binding site

The propeptide binding site is another important domain in GGCX, which is crucial for substrate recognition and processing. It is known that propeptide binding takes place in 495-513 residues [47]. Therefore, some mutations, which consistently showed gain-of-function or differential γ-carboxylation for VKD proteins were analyzed further in the GGCX *in silico* structure.

GGCX:p.(W501S) exhibited a higher γ-carboxylation for most VKD proteins (Figure 46A). This mutation is the only known located within the propeptide binding site [81]. Two more mutations GGCX:p.(G537A) and GGCX:p.(I532T) that are in close proximity to W501 (10 Å and 16 Å respectively; distances measured based on c-alpha atoms) also exhibited a higher γ-carboxylation for most VKD proteins (Figure 47). These mutations might affect the flexibility of the disordered region between the propeptide binding site and the Glu binding site enabling faster catalysis of VKD proteins. However, W501S and G537A were not γ-carboxylating GRP to a high extent, which might be due to the selective effect on this particular protein only.

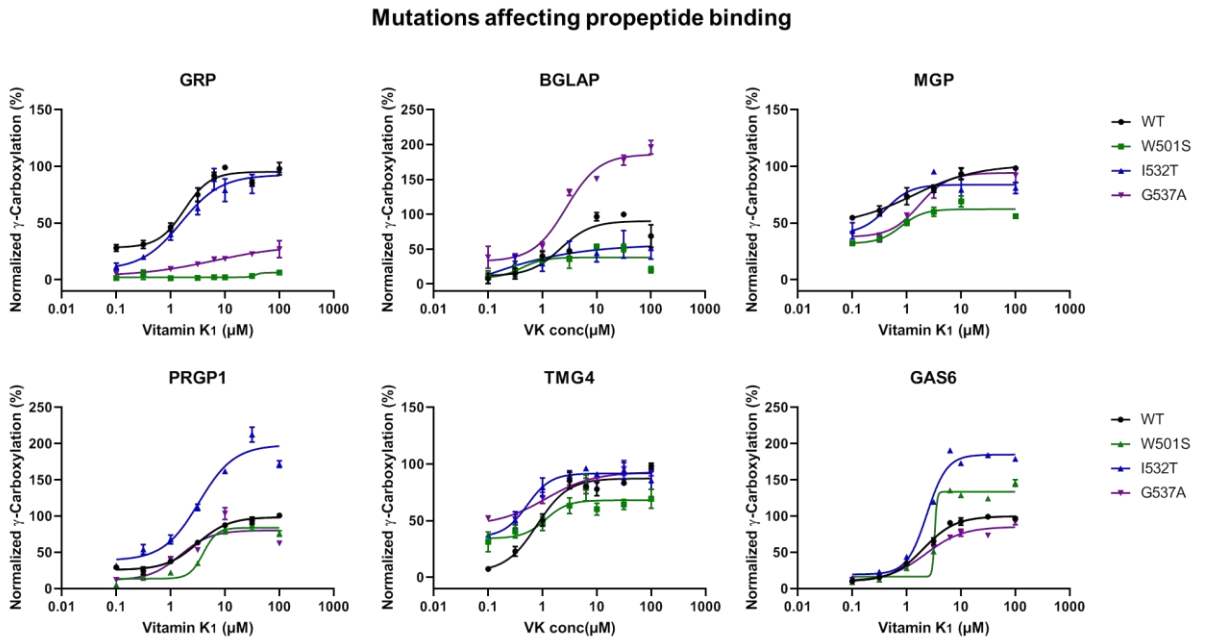

Figure 46: Mutations affecting propeptide binding site. A, γ-carboxylation of VKD proteins with respect to mutants affecting functional binding domain measured by ELISA. The y-axis represents normalized γ-carboxylation (%). The x-axis represents K_1 concentrations (0.1-100μM). In each figure dose-response curve is depicted for GGCX wt (black). Compound heterozygous mutants in one particular patient were represented by same color with each allele variant in solid and dotted line. Error bars depict SD of triplicate measurement of n=3 experiments.

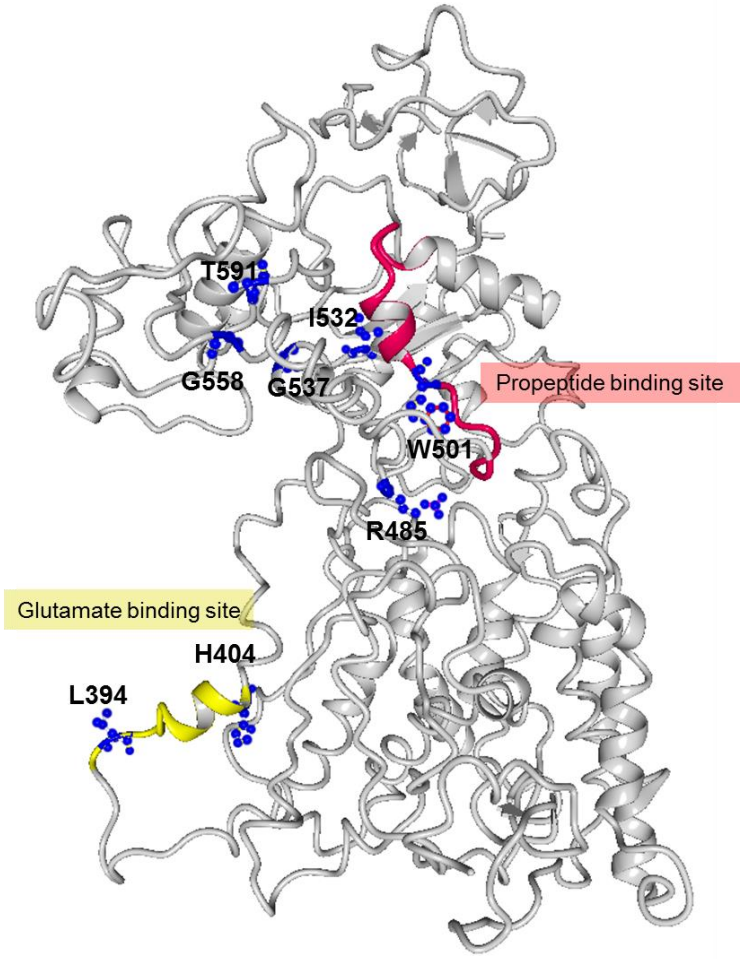

Figure 47: GGCX *in silico* model with marked functional binding sites and important residues. The GGCX structural model showing propeptide binding site (pink), glutamate binding site (yellow) and the mutant residues (blue). The backbone of the model is depicted in ribbon format while specific residues of interests are depicted in stick and ball format.

Then there are three mutations GGCX:p.(R485P), GGCX:p.(G558R), and GGCX:p.(T591K), which showed differential γ-carboxylation among different VKD proteins. Hence, this were also analyzed with respect to the *in silico* model.

According to our GGCX structural model, residues GGCX:G558 and GGCX:T591 are in close proximity to each other (9.3 Å) and to the propeptide binding site (˜20 Å). Their mutual proximity to the propeptide binding site could explain their similar behavior leading to loss-of-function for solely FX, PRGP1, and GAS6 when mutated (Figure 23, 47 and 48). Level of γ-carboxylated FII and PC are similarly reduced. Mutations GGCX:p.(G558R) and GGCX:p.(T591K), both do not co-localize with FX. FX seemed to accumulate within the cell demonstrating that propeptide binding of FX is abolished (Figure 26).

Residue R485 is in close proximity to the propeptide binding site (~14 Å) and therefore might negatively influence the binding of FII when mutated (Figure 25A).

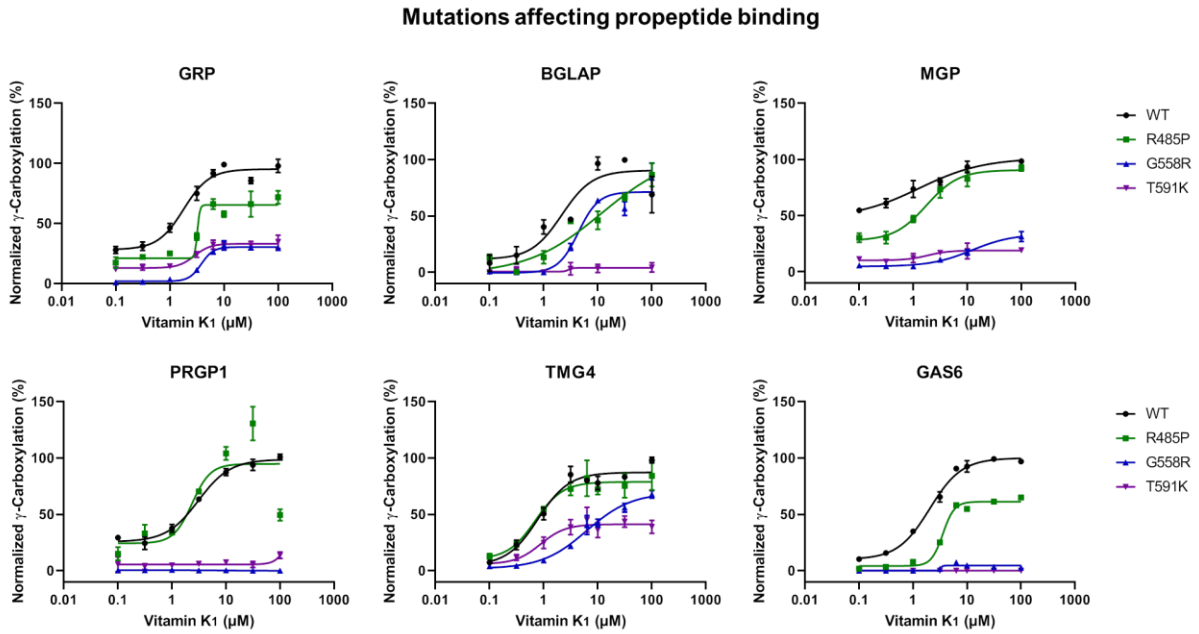

Figure 48: Mutations affecting propeptide binding site. γ-carboxylation of VKD proteins with respect to mutants affecting functional binding domain measured by ELISA. The y-axis represents normalized γ-carboxylation (%). The x-axis represents K_1 concentrations (0.1-100μM). In each figure dose-response curve is depicted for GGCX wt (black). Error bars depict SD of triplicate measurement of n=3 experiments.

4.4.5 Mutations affecting the glutamate binding site

Glutamate binding site (393-404 aa) is another functional region that is known [48,104,105]. GGCX:p.(H404P) and GGCX:p.(L394R) are located within the glutamate binding site. We observed for both mutations that most VKD proteins are not γ-carboxylated at low K_1 concentrations (0.1- 6.32 μM) and showed a sudden increase at 10μM K_1 indicating that the ability to γ-carboxylate proteins is affected (Figure 49). Both mutations are most likely disrupting a small helix, which is the only ordered region in the glutamate binding site that is surrounded by many disordered regions in our model, explaining their reduced ability to γ-carboxylate VKD proteins (Figure 47).

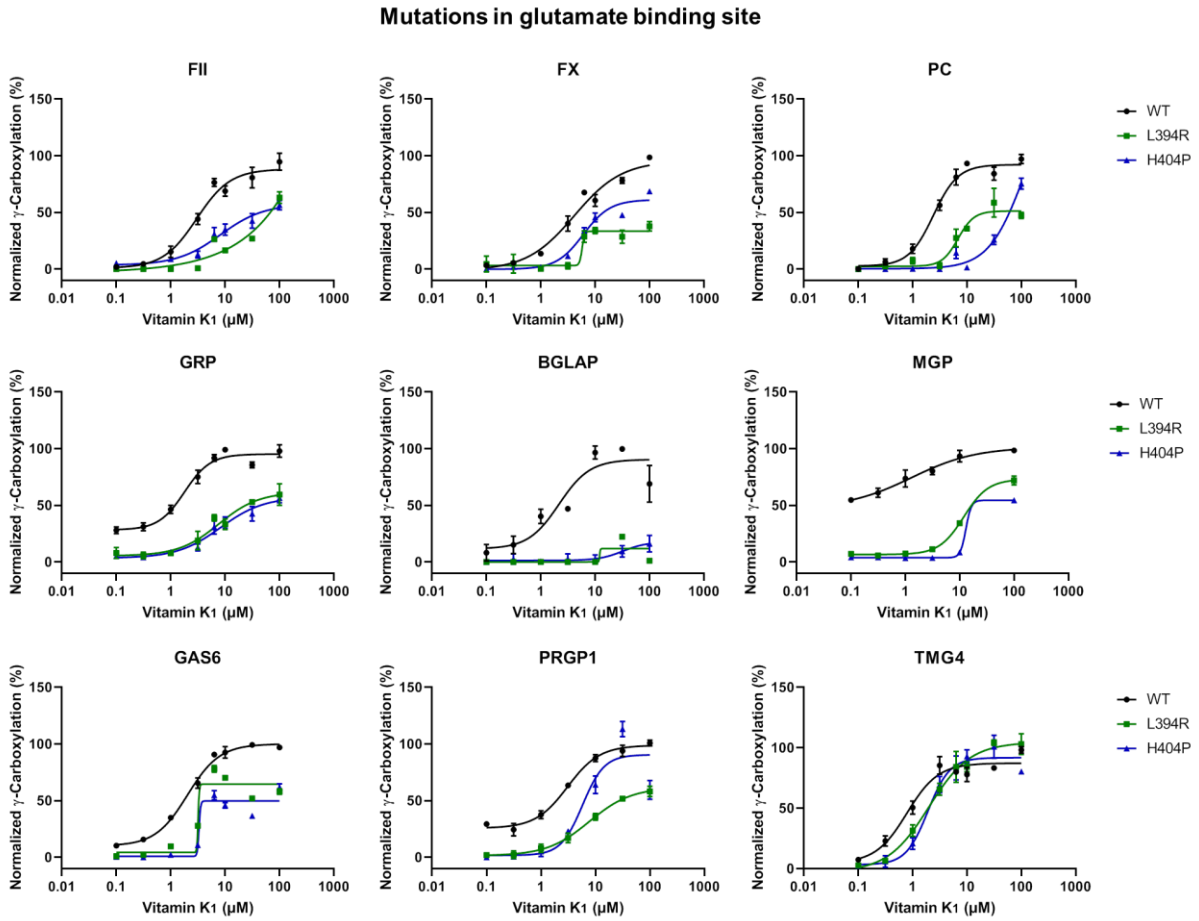

Figure 49: Mutations affecting glutamate binding site. A, γ-carboxylation of VKD proteins with respect to mutants affecting glutamate binding site measured by ELISA. The y-axis represents normalized γ-carboxylation (%). The x-axis represents K_1 concentrations (0.1-100μM). In each figure dose-response curve is depicted for GGCX wt (black). Compound heterozygous mutants in one particular patient were represented by same color with each allele variant in solid and dotted line. Error bars depict SD of triplicate measurement of n=3 experiments.

Altogether our *in silico* model in combination with *in vitro* data helped us to identify the vitamin K binding site and the residues affecting the propeptide binding explaining the differential effect GGCX mutations on VKD proteins.

5. Discussion

γ-Carboxylation is an essential post-translational modification that is required for regulation of the coagulation cascade, calcification, and cell signaling pathway. Mutations in the *GGCX* gene causes VKCFD1, where patients are diagnosed with haemostatic and non-haemostatic phenotypes.

In the first part of the thesis, *GGCX* mutations causing VKCFD1 were analyzed. Therefore, a HEK293T *GGCX*$^{-/-}$ cell line was generated by CRISPR/Cas9 gene editing technology, where GGCX wt/muts and VKD proteins were expressed and treated with different concentrations of vitamin K_1. The effects of 22 missense mutations on γ-carboxylation of 9 different VKD proteins were measured by ELISA. The data demonstrated how these mutations affect γ-carboxylation of clotting factors and non-haemostatic proteins and their response to vitamin K_1 treatment.

These data can be used to predict the clinical course of VKCFD1 patients and facilitate decisions on treatment with either vitamin K or Prothrombin complex concentrate (PCC), to correct the haemorrhagic phenotype. With respect to the non-haemorrhagic phenotype, the causative undercarboxylated VKD proteins were identified by correlating the γ-carboxylation status from our data with the existing patient phenotype. Personalized medication with γ-carboxylated VKD proteins to treat non-haemorrhagic phenotypes may represent a promising strategy in future.

In the second part of the thesis, a GGCX *in silico* model was generated to locate the heterogeneous distribution of these mutations. Based on the data obtained from the *in vitro* screening and mutation localization in the *in silico* model, vitamin K hydroquinone docking was performed. The vitamin K hydroquinone site was identified which showed that F299 is a major interacting residue.

5.1 The haemorrhagic phenotype: A defective allele is compensated by mutations that respond well to K treatment

Initially VKCFD1 patients were only diagnosed with bleeding phenotypes, which included large area of brain bleeds, spontaneous bruising, multiple hematomas in chest and thighs etc. This is caused due to the reduced γ-carboxylation of VKD clotting factors. A generalized treatment for correcting the bleeding phenotype is the oral administration of high dose of vitamin K (140 mg weekly or 20 mg daily). However, until now no study exists, which showed how these GGCX mutations effects γ-carboxylation of clotting factors both pre and post vitamin K treatment.

Almost all GGCX mutations showed reduced level of clotting factor activities upon low vitamin K_1 treatment [101] (Table 10). However, most of these mutations responded with increased γ-carboxylation at high vitamin K doses in our assay. Therefore, high dose of vitamin K supplementation is required, which will rescue the clotting factor activities. This is reflected by the elevation of γ-carboxylated clotting factor FII, FX, PC and FVII activity upon 10 µM vitamin K treatment for most mutations (Table 10). For example, mutations GGCX:p.(S284P), GGCX:p.(G537A), and GGCX:p.(W493C) are responding well to K_1 and results in higher or equal levels of γ-carboxylated FII, FX, and PC compared to wt. These mutations were reported to be compound heterozygous, where the other allele has a nonsense mutation (GGCX:p.(W315X), GGCX:p.(Q374X), or GGCX: p.(R704X)). Therefore, these patients can be treated with K_1 as they are in combination with a responder mutation. For example, the patient harboring GGCX:p.(S284P);(W315X) the clotting factor activity increased from 41% to 76% for FII and from 18% to 57% for FX after treatment with 70 mg/week of vitamin K [79]. This is in agreement with our data where GGCX:p.(S284P), γ-carboxylated FII and FX levels are increasing to 84 % and 123 % at 10 µM K_1 (Table 10). This demonstrates that only one allele has to respond to K_1 treatment in order to correct the bleeding phenotype. Mutation GGCX:p.(R204C);p.(R204C) reported in homozygous form showed increased levels of γ-carboxylated FII and FX to 105 % and 120 % at 10 µM vitamin K concentration. This is in accordance with the patient data who also showed increase up to 69 % and 71 % of FII and FX activity upon 12.5 mg/ day treatment. Hence, the data for other mutations will be useful for selected treatment of patients, where earlier post vitamin K treatment data is unavailable.

Out of all investigated mutations, two mutations i.e. GGCX:p.(F299S) and GGCX:p.(M174R) did not respond well to high K_1 treatment (10 µM K) . Thus, patients harboring one of these loss-of-function mutations must have a functional second allele that is sufficient for a viable phenotype. The loss-of-function mutation GGCX:p.(M174R) was reported in two patients. In one patient GGCX:p.(M174R) had an additional mutation GGCX:p.(R325Q) in the same allele, which was responding well in our data [88]. However, the allele harboring these two mutations

will not be functional as it harbors a loss-of-function GGCX:p.(M174R) mutation. In this patient GGCX:p.(D153G) was present in the other allele, which showed moderate increase in γ-carboxylation of FII, FX and PC. Therefore, the patient harboring these mutations who was treated with 20 mg /day of vitamin K showed reduced increase in clotting factor activity (Table 10). GGCX:p.(M174R) was also reported in another patient as compound heterozygous mutations where the other allele harbored GGCX:p.(I532T) [84]. GGCX:p.(I532T) showed higher γ-carboxylation of FII, FX, PC and also increased FVII activity, thus giving a viable phenotype. However, the post treatment data showed that the patient did not respond well to 10 mg/day K treatment, which was only given for three days. Therefore, higher dose of vitamin K treatment for longer use can be recommended. Immunofluorescent staining and *in silico* analysis indicates that GGCX:p.(M174R) leads to structural instability therefore showing zero γ-carboxylation. Therefore, this mutation will be always reported with a fully or partially responding mutation in order to achieve a viable phenotype.

GGCX:p.(F299S) is another loss-of-function mutation, which was reported to be compound heterozygous where the other allele harbors GGCX:p.(G558R) [94]. For GGCX:p.(F299S), the deficiency for selected clotting factors (FIX and FX) are not compensated by the other allele GGCX:p.(G558R) resulting in biallelic loss-of-function for FIX and FX. Although, *F10*$^{-/-}$ mice are lethal, it was shown by the Friuli mice that FX activities of 4-9% and antigen levels of 1-3% are sufficient to rescue lethality [106]. Since antigen levels of clotting factors are not affected in VKCFD1 patients it seems that very low FIX and FX activities are sufficient for a viable phenotype. However, in case of bleedings this patient should be treated with PCC since vitamin K administration will not increase activities for FIX and FX.

Therefore, patients harbouring a low responding mutations in compound heterozygous state with a loss-of-function (GGCX:p.(F299S), GGCX:p.(M174R)) or a nonsense mutation are difficult to treat with vitamin K and will result into severe haemostatic phenotypes. Thus, in case of bleedings or surgery, this patient should be treated with PCC since K_1 administration might not correct the bleeding phenotype. GGCX:p.(M174R) and GGCX:p.(F299S) will be never reported in homozygous form as it shows loss-of-function in γ-carboxylation for all VKD proteins, which will lead to embryonic lethality comparable to a *GGCX*$^{-/-}$ in mice [110].

Another mutation which showed extremely reduced levels is GGCX:p.(S300F) and was reported to be compound heterozygous where the other allele has GGCX:p.(V255M) [85]. In our assay, GGCX:p.(V255M) responded as wt around 87-130 % for FII, FX and PC γ-carboxylation (Table 10). Thus, for this genotypic combination the clotting factor activity can be normalized with vitamin K treatment and thereby reversing bleeding tendency.

Mutations (GGCX:p.(L394R), GGCX:p.(H404P)) showed reduced activity at high vitamin K. According to the literature these two residues are located within the glutamate binding site (aa 393-404) and hence the reduced γ-carboxylation activity is justified. The other known important

domain is the propeptide binding site and according to our *in silico* model three residues (GGCX:p.(R485P), GGCX:p.(G558R), GGCX:p.(T591K)) affects this domain thereby showing differential behavior. Therefore, mutations, which shows extreme differential reduction in γ-carboxylation of one particular clotting factor f.e. FX and is in combination with a loss-of-function or nonsense mutation, should also be directly treated with PCC. GGCX:p.(W501S) is another mutation located within the propeptide binding site which shows increasing response to vitamin K treatment. The patient showed 36 % of FII and 66 % FX activity at 5 mg /day of treatment. Since GGCX:p.(W501S) has the potential to increase γ-carboxylation hence the patient should be treated with higher dose of vitamin K.

Family members of VKCFD1 patients, where only one allele is deficient due to nonsense or loss-of-function mutations, exhibit normal clotting factor activities (Table 11). Contrary to this observation, only two patients were reported to be heterozygous i.e. GGCX:p.(R476C) or GGCX:p.(R476H) [94]. The genotype of these patients is not correlating to the overall data who showed extreme low levels of FII and FX activity (17–38 %). Therefore, the genotype of these two reported heterozygous VKCFD1 patients should be re-evaluated for the presence of additional mutations in *GGCX* or other potential genes. The recommendation of re-evaluation is also supported by the fact that heterozygous *GGCX*$^{+/-}$ mice develop normal blood coagulation (89% of FIX, 100% of FX and 98% of FII compared to WT mice), whereas *GGCX*$^{-/-}$ mice are intrauterine lethal [107]. This is also confirmed by our data where non-responding or extremely low responding mutations are always in combination with a responder mutation.

The similarity in structural domain distribution of clotting factors and differential effect of GGCX mutations on γ-carboxylation of clotting factors is fascinating. Hence, development of a native cellular model (iPSc) will be useful for understanding how γ-carboxylation is regulated or prioritized for different clotting factor and why GGCX has different affinity for clotting factors.

Table 10: γ-Carboxylation values and activities for clotting factors along with patients data. CH, compound heterozygous; HTZ, heterozygous; HMZ, homozygous; LOF, loss-of-function; NA, not available, - , not analysed

GGCX mutation	Genotype	γ-carboxylated FII [%]		γ-carboxylated FX [%]		γ-carboxylated PC [%]		FVII activity [%]	Reported patient´s data		
		Low K (1 µM K_1)	High K (10µM K_1)	Low K (1µM K_1)	High K (10µM K_1)	Low K (1 µM K_1)	High K (10µM K_1)	(at 10µM K_1)	FII activity (*K treatment)	FX activity (*K treatment)	Vitamin K administration
D153G M174R+(R325Q)	CH with LOF	68.7 % 0 %	101 % 0 %	0.2 % 0 %	66.8 % 0.3 %	106.8 % 0 %	44.2 % 0 %	58.6 % 0 %	26 % (*38 %)	13 % (*31 %)	20 mg/day
I532T M174R	CH with LOF	450.8 % 0 %	228.9 % 0 %	191.6 % 0 %	147.8 % 0.3 %	127.2 % 0 %	116.9 % 0 %	126.6 % 0 %	15-20 % (*20-24 %)	20-13 % (*18%)	10 mg/day for 3 days
G558R F299S	CH with LOF	1.7 % 0 %	113.2 % 0 %	0% 0%	0% 0%	0 % 0%	21.2 % 0%	17.9 % 0 %	NA	NA	NA
V255M S300F	CH with low responding	0 % 0 %	119 % 1 %	49.4 % 0 %	130.9 % 0 %	144.1 0 %	87 % 0.2 %	85.3 % 20.9 %	64 % (*NA)	33 % (*NA)	NA
R83W Q374X	CH with nonsense	23.1 % -	38 % -	0.5 % -	43.3 % -	64.1 % -	40.9 % -	51.5 % -	20 % (*NA)	20-22 % (*NA)	5 mg/day
S284P W315X	CH with nonsense	30.3 % -	84.1 % -	55 % -	123 % -	37.5 % -	128.6 % -	69.6 % -	41 % (*76 %)	18 % (*57 %)	10 mg/day
W493C R704X	CH with nonsense	61.9 % -	150.2 % -	34.3 % -	101 % -	121.7 % -	138.1 % -	92.9 % -	3 % (*72 %)	3 % (*62 %)	NA
G537A Q374X	CH with nonsense	349.4 % -	234.6 % -	25.7 % -	79.5 % -	79 % -	73.5 % -	108.5 % -	20 % (*NA)	20 % (*NA)	NA
R83P R83P	HMZ	0 % 0 %	29.2 % 29.2%	55.4 % 55.4 %	85.1 % 85.1 %	25.4 % 25.4 %	13 % 13 %	51.3 % 51.3 %	27 % (*61 %)	33 % (*67 %)	2.5 mg/day
R204C R204C	HMZ	20.1 % 20.1 %	105.1 % 105.1 %	41.9 % 41.9 %	120.8 % 120.8 %	0 % 0 %	49.9 % 49.9 %	107.9 % 107.9 %	NA (*51-69 %)	6-20 % (*51-71 %)	12.8 mg/day
L394R L394R	HMZ	0 % 0 %	20.5 % 20.5 %	0 % 0 %	49.3 % 49.3%	55.5 % 55.5 %	37.3 % 37.3 %	72.9 % 72.9 %	2-24 U/dL (*18-45 U/dL)	2-20 U/dL (*15-27 U/dL)	1.4 mg/day
W501S W501S	HMZ	143.8 % 143.8 %	159 % 159 %	106.2 % 106.2 %	139.4 % 139.4 %	24.0 % 24.0 %	78.9 % 78.9 %	104.8 % 104.8 %	4.8 % (*36 %)	<1 % (*66 %)	5 mg/day
R476H WT	HTZ	0 % 100 %	113.5 % 100 %	0 % 100 %	67.1 % 100 %	95.9 % 100 %	57.4 % 100 %	84.2 % 100 %	38 % (*NA)	20 % (*NA)	NA
R476C WT	HTZ	78.8 % 100 %	87.3 % 100 %	12.1 % 100 %	12 % 100 %	0 % 100 %	32.4 % 100 %	63.6 % 100 %	38 % (*NA)	17 % (*NA)	NA
H404P R485P	CH	0 % 28 %	8 % 27.6 %	8 % 57.2 %	72.5 % 117.9 %	0 % 124.6 %	0 % 94.7 %	91.9 % 67.2 %	35 % (*94 %)	13 % (*37 %)	15 mg/day
W157R (D31N)+T591K	CH	25.4 % 5.9 %	93.1 % 29.4 %	13.1 % 33.1 %	97.2 % 13.1 %	7.4 % 62.5 %	16.4 % 38.5 %	88.5 % 0 %	9 % (*NA)	5 % (*NA)	10 mg/day for 2 weeks

Table 11: γ-carboxylation values of GGCX mutations for haemostatic VKD proteins. The table summarizes the VKCFD1 patient data along with the data of the family members and the γ-carboxylation values of corresponding GGCX mutations analyzed at 10 µM of K1 treatment with respect to investigated VKD clotting proteins

GGCX mutation (Patient`s genotype)	Genotype	γ-carboxylated FII ([%] at 10µM K_1)	γ-carboxylated FX ([%] at 10µM K_1)	γ-carboxylated PC ([%] at 10µM K_1)	FVII activity ([%] at 10µM K_1)	Reported patient´s data			
						FII activity (*K treatment)	FX activity (*K treatment)	Vitamin K administration	Phenotype
V255M S300F	CH with low responding	119 % 1.1 %	130.9 % 0 %	87 % 0.2 %	85.3 % 20.9 %	64 % (*NA)	33 % (*NA)	NA	
V255M WT	Mother	119 % 100 %	130.9 % 100 %	87 % 100 %	85.3 % 100 %	Within normal range	Within normal range		Asymptomatic
WT S300F	Father & Brother	100 % 1.1 %	100 % 0 %	100 % 0.2 %	100 % 20.9 %	Within normal range	Within normal range		Asymptomatic
W157R (D31N)+T591K	CH	93.1 % 29.4 %	97.2 % 13.1 %	16.4 % 38.5 %	88.5 % 0 %	9 % (*NA)	5 % (*NA)	10 mg/day for 2 weeks	
(D31N)+T591K WT	Mother	29.4 % 100 %	13.1 % 100 %	38.5 % 100 %	0 % 100 %	119 %	82 %		Asymptomatic
WT W157R	Father	100 % 93.1 %	100 % 97.2 %	100 % 16.4 %	100 % 88.5 %	97 %	100 %		Asymptomatic
R83W Q374X	CH with nonsense	42.3 % -	50.9 % -	40.9 % -	51.5 % -	20 % (*NA)	20-22 % (*NA)	5 mg/day	
R83W WT	Mother	42.3 % 100%	50.9 % 100 %	40.9 % 100 %	51.5 % 100 %	100 %	98 %		Asymptomatic
WT Q374X	Father	100 % -	100 % -	100 % -	100 % -	140 %	90 %		Asymptomatic
L394R L394R	HMZ	22.7 % 22.7 %	57.9 % 57.9 %	37.3 % 37.3 %	72.9 % 72.9 %	2-24 U/dL (*18-45 U/dL)	2-20 U/dL (*15-27 U/dL)	1.4 mg/day	
L394R WT	Mother	22.7 % 100 %	57.9 % 100 %	37.3 % 100 %	72.9 % 100 %	116 U/dL	89 U/dL		Asymptomatic
WT L394R	Father	100 % 22.7 %	100 % 57.9 %	100 % 37.3 %	100 % 72.9 %	107 U/dL	84 U/dL		Asymptomatic
D153G M174R+(R325Q)	CH with nonsense	101 % 0 %	66.8 % 0.3 %	44.2 % 0 %	58.6 % 0 %	26 % (*38 %)	13 % (*31 %)	20 mg/day	
D153G R325Q	Mother	101 % 188.5 %	66.8 % 189.2 %	44.2 % 115.7 %	58.6 % 82.1. %	NA	NA		Asymptomatic
R325Q M174R+(R325Q)	Father & sister	188.5 % 0 %	189.2 % 0.3 %	115.7 % 0 %	82.1. % 0 %	NA	NA		Asymptomatic

5.2 Ectopic mineralization of skin, bone, and cardiac system in VKCFD1: Identification of causative VKD protein

Ectopic mineralization is the hallmark of many monogenic disorders including Pseudoxanthoma elasticum (PXE) [108–111] and Keutel syndrome [95]. The main feature of these disorders are mineral deposits mainly calcium hydroxyapatite in soft tissues like skin, blood vessels, and cardiac valves. This pathological condition arises from the imbalance in mineralization regulatory factors [95]. In 2007, Vanakker et al. reported six patients presented with excessive skin folds, who had mutations in GGCX gene [94].

Several other non-haemostatic phenotypes have been reported in VKCFD1 patients like septal defects or midfacial hypoplasia [79,88]. Unlike VKCFD1 bleeding phenotype, the treatment regime for non-haemostatic phenotype does not exist as majority of these defects are congenital. Therefore, identifying the causative VKD protein will pave the way for future personalized medicine.

The non-haemostatic phenotypes such as the skin hyper-laxity or cardiac or skeletal abnormalities are caused mainly due to misregulated calcification. Three out of all VKD proteins have a well-established role in mineralization regulation i.e. MGP, BGLAP, and GRP [112]. However, these studies do not report the influence of the γ-carboxylation status of the three proteins with respect to non-haemostatic phenotypes diagnosed in VKCFD1 patients. Thereby, analyzing the γ-carboxylation status of these calcification regulators with respect to *GGCX* mutations would lead to better understanding of this post-translational modification.

5.2.1 The skin phenotype is caused mainly by the reduction of γ-carboxylated GRP

Patients with genotypes GGCX:p.(R83W);(Q374X), GGCX:p.(V255M);(S300F), GGCX:p.(G537A);(Q374X), GGCX:p.(G558R);(F299S), developed extreme skin folds [85,86,94]. All these patients have one allele, which has either a non-sense or a mutation which shows reduced γ-carboxylation or loss-of-function. In our data it was seen that mutations in the other allele i.e. GGCX:p.(R83W), GGCX:p.(V255M), GGCX:p.(G537A), GGCX:p.(G558R) γ-carboxylates GRP in between 18-32 %. This indicates that the PXE-like phenotype seen in all patients is caused by the biallelic effect of GGCX mutations on γ-carboxylation of GRP (Table 12, red marking). These mutations causing skin laxity shows 10-102 % of γ-carboxylated MGP and 16-68 % γ-carboxylated BGLAP thereby eliminating these proteins as a causative protein for skin hyper-laxity. One patient with GGCX:p.(H404P);p.(R485P) developed a mild skin phenotype. GGCX:p.(H404P) and GGCX:p.(R485P) γ-carboxylated GRP up to 35 % and 58

%, respectively. Hence, both partially functional GGCX allele explains the mild skin phenotype seen in this patient.

Due to the reduced levels of γ-carboxylated GRP, we predict the development of a PXE-like phenotype for young patients with genotypes GGCX:p.(R83P);p.(R83P), and GGCX:p.(L394R); p.(L394R), GGCX:p.(W493C);(R704X) and GGCX:p.(W501S);p.(W501S) (Table 12, blue marking). The age of onset for skin hyper-laxity was reported to be around 18 years [37]. Therefore, early stage monitoring and vitamin K enriched diet might prevent or postpone the onset of skin laxity for these patients. However, until now it is unclear whether treatment with vitamin K will rescue development of skin folding and hyper-laxity.

The high number of patients with skin hyper-laxity and the biallelic reduction in GRP γ-carboxylation for all the corresponding GGCX mutations indicates a significant role of GRP in developing skin laxity. Furthermore, parents of these patients were asymptomatic who harbors mutations in a single allele as VKCFD1 is an autosomal recessive disorder indicating that the biallelic defect is required for developing skin hyper-laxity as well. But, there was one exception where the mother with genotype GGCX:p(V255M);(WT) developed skin folds at the age of 40. However she was reported with a known mutation in *ABCC6* gene (ABCC6:p.R1141X)[85] which explains the distinct skin folds. This mutation in *ABCC6* gene is reported in 30 % of patients with classic PXE phenotype in European population.

There were two patients from different families reported to have extreme skin laxity and were with heterozygous mutations GGCX:p(R476C) or GGCX:p(R476H) where the other allele was wt harboring 100 % ability to γ-carboxylate VKD proteins. This is not in accordance with remaining patients who are showing biallelic reduction in γ-carboxylation of GRP. This suggests that their genotype must be re-evaluated or next generation sequencing should be performed as there might be an additional mutation in another gene f.e. *GRP*.

Pathological calcification is a well-established phenomenon in soft tissues such as skin. Therefore, the knowledge of specific proteins leading to this ectopic calcification in skin will help elucidate a detailed pathway. Previous studies have reported deposition of un-carboxylated VKD proteins in microsomes of dermal and epidermal tissue under warfarin treatment [113] and also in the skin of patients with dermatomyositis and scleroderma [68]. Viegas et al. have showed the existence of GRP in sites of ectopic calcification and in epidermis and dermis. They also showed that GRP is highly expressed and accumulates in small blood vessels and capillaries that irrigate the skin and in fibroblasts of both papillary and reticular dermis in hair follicles and sebaceous glands [19]. However, the γ-carboxylation of GRP with respect to reported *GGCX* mutations causing skin hyper-laxity was not elucidated until now.

Therefore, the present finding indicates reduced γ-carboxylation of GRP is the lead cause of developing skin hyper-laxity in VKCFD1 patients.

Unfortunately, there is currently no treatment available but these patients might be medicated in future by the nanotechnology-based method of Viegas et al. where human γ-carboxylated GRP is loaded into extracellular vesicles [114]. This recent approach was invented to inhibit vascular calcification, which might have a high potential to treat skin ectopic calcification.

Table 12: Effect of GGCX mutations on γ-carboxylation of non-haemostatic proteins with respect mutations causing PXE-like phenotype in VKCFD1 patients. The patient data along with the ELISA results for γ-carboxylation of all analyzed non-haemostatic proteins with respect to 100% wt γ-carboxylation at 10 µM K_1. The red highlight represents the causative proteins for skin defects. The blue highlight represents the patients expected to develop skin hyper-laxity. The magenta highlight represents cases which should be re-evaluated

GGCX mutation	Age (Age of onset)	Genotype	Non-haemostatic phenotype/s	γ-carboxylated GRP ([%] at 10µM K_1)	γ-carboxylated MGP ([%] at 10µM K_1)	γ-carboxylated BGLAP ([%] at 10µM K_1)	γ-carboxylated PRGP1 ([%] at 10µM K_1)	γ-carboxylated TMG4 ([%] at 10µM K_1)	γ-carboxylated GAS6 ([%] at 10µM K_1)	Comments	VKORC1 c.-1639
R83W Q374X	48 year (27 year)	CH	PXE-like phenotype	26.2 % -	31.7 % -	15.8 % -	176.9 % -	4.9 % -	138.5 % -	Family heterozygous for R83W or Q374X did not developed skin phenotype	
G537A Q374X	46 year, 44 year	CH	PXE-like phenotype + Atherosclerosis	18.4 % -	102 % -	155.8 % -	117.6 % -	108 % -	83.8 % -		
V255M S300F	16 year	CH	PXE-like phenotype + Cardiac abnormality	30.7 % 1.5 %	10.2 % 2.9 %	57.3 % 0 %	151.7 % 0 %	111.5 % 3.5 %	153.1 % 2.7 %		
G558R F299S	40 year	CH	PXE-like phenotype	31.7 % 0 %	18.2 % 1 %	65.8 % 0 %	0.3 % 0 %	50.6 % 0 %	5.3 % 1.6 %		
H404P R485P	47 year	CH	Mild skin symptom + Calcified peripheral arteries	34.8 % 57.7 %	8.9 % 87.1 %	0.4 % 47.7 %	72.7 % 118.2 %	120.7 % 91.1 %	51.7 % 61.8 %		GG
R476C WT	67 year (3 year)	HTZ	PXE-like phenotype + Atherosclerosis	41.7 % 100 %	93.5 % 100 %	56.2 % 100 %	91.1 % 100 %	95.7 % 100 %	87.8 % 100 %	Re-evaluation of genotype	
R476H WT	32 year (18 year)	HTZ	PXE-like phenotype	95.7 % 100 %	77.9 % 100 %	57.1 % 100 %	170.2 % 100 %	137.3 % 100 %	112.7 % 100 %	Re-evaluation of genotype	
R83P R83P	3 year	HMZ	Facial Dysmorphism + Septal defect	12.6 % 12.6 %	26.5 % 26.5 %	34 % 34 %	218.1 % 218.1 %	47.1 % 47.1 %	119.8 % 119.8 %	Expected to develop skin phenotype	AA
L394R L394R	5 months, newborns	HMZ	-	33.3 % 33.3 %	36.1 % 36.1 %	0 % 0 %	38.6 % 38.6 %	105.9 % 105.9 %	79 % 79 %	Expected to develop skin phenotype	
W493C R704X	1 year	CH with nonsense	-	2.3 % -	81.5 % -	55.8 % -	103.5 % -	120.2 % -	137.2 % -	Expected to develop skin phenotype	
W501S W501S	7 days	HMZ	-	2 % 2 %	72.8 % 72.8 %	55.8 % 55.8 %	97.2 % 97.2 %	79.5 % 79.5 %	145.1 % 145.1 %	Expected to develop skin phenotype	

5.2.2 Keutel syndrome-like phenotype and facial dysmorphologies are caused by reduced γ-carboxylated MGP along with additional factors

Keutel syndrome (KS, MIM 245150) is an autosomal recessive disorder caused by mutations in *MGP* gene, which is characterized by abnormal cartilage calcification, peripheral pulmonary stenosis and midfacial hypoplasia [96]. Recently, it was reported that *Mgp*$^{-/-}$ mice causes the nasal septum to be abnormally mineralized and shortened and transgenic restoration of MGP expression in chondrocytes fully corrected the craniofacial anomalies [62]. And it is in concordance with our data that showed some mutations causing undercarboxylated MGP developed skeletal phenotype.

The skeletal phenotype seen in three VKCFD1 patients are midfacial hypoplasia and facial dysmorphisms, which are similar to Keutel syndrome. One patient with mutations GGCX:p.(M174R+R325Q);p.(D153G) developed Keutel syndrome-like phenotypes with short distal phalanges of the fingers. GGCX:p.(D153G) showed reduced ability to γ-carboxylate MGP only up to 38.3 % whereas GRP and BGLAP was γ-carboxylated up to 94 % and 82 % respectively (Table 13). The other allele has GGCX:p.(M174R+R325Q) is not functional as it harbors the loss-of-function mutation GGCX:p.(M174R). Therefore, it is clear that under γ-carboxylation of MGP is the lead cause of skeletal defect in this patient. The exclusion of GRP and BGLAP as a causative VKD protein for skeletal defects is in concordance with the reported GRP$^{-/-}$ and BGLAP$^{-/-}$ mice phenotype which did not report any skeletal abnormalities at birth [60,66].

Another patient with mutation GGCX:p.(R83P);p.(R83P) who developed facial dysmorphism also showed reduced levels of γ-carboxylated MGP around 26.5 %. Data from these two genotype-phenotype correlations indicates that MGP is a causative protein behind development of skeletal defects. However, this small number of patients makes it difficult to draw a strong conclusion.

The third patient with GGCX:p.(S284P);p.(W315X) also developed midfacial hypoplasia although levels are not that severely affected in this study. However, the hyperemesis gravidarum from the mother of the patient carrying GGCX:p.(S284P);p.(W315X) might had an influence on development of midfacial hypoplasia. The mother with hyperemesis gravidarum had a weight loss of seven kg within the first trimester [79], thus indicating that the nutritional uptake of vitamin K during pregnancy might modulate the severity of those birth defects.

Both patients with genotype GGCX:p.(S284P);p.(W315X) and GGCX:p.(R83P);p.(R83P) have the AA polymorphism in VKORC1 promoter. Previous studies have shown that this polymorphism in VKORC1 gene influences the mRNA expression [102]. Therefore, the deficiency

in the availability of KH_2 as a cofactor of GGCX effects γ-carboxylation of the non-haemostatic proteins giving rise to congenital defects. Furthermore, the prominent phenotype of warfarin embryopathy is skeletal abnormalities[115] including midfacial hypoplasia which further indicates the importance of homeostasis of vitamin K cycle and the availability KH_2 co-factor for γ-carboxylation.

Furthermore, other mutations f.e. GGCX:p.(R83W), GGCX:p.(L394R); p.(L394R), or GGCX:p.(G558R), p.(F299S) which showed reduced γ-carboxylated MGP did not develop skeletal defects (Table 13). Therefore, concluding that reduced levels of γ-carboxylated MGP is not exclusive for causing skeletal abnormalities in VKCFD1 patients. Multiple factors such as nutrition during pregnancy and availability of the vitamin K hydroquinone as cofactor plays a strong role in the development of congenital defects as skeletal abnormalities.

Altogether, it was found that GRP plays a fundamental role in the development of PXE-like phenotype. Reduced levels of MGP were seen for mutations causing skeletal anomalies together with additional factors. And these phenotypes are caused due to biallelic defects for γ-carboxylating GRP or MGP as the family members with mutation in one allele only did not develop such phenotypes (Table 14).

Table 13: Effect of GGCX mutations on γ-carboxylation of non-haemostatic proteins. The patient data along with the ELISA results for γ-carboxylation of all analyzed non-haemostatic proteins with respect to 100% wt γ-carboxylation at 10 µM K_1. The red highlight represents the causative proteins for skeletal defects

GGCX mutation	Age	Genotype	Non-haemostatic Phenotype/s	γ-carboxylated GRP ([%] at 10µM K_1)	γ-carboxylated MGP ([%] at 10µM K_1)	γ-carboxylated BGLAP ([%] at 10µM K_1)	γ-carboxylated PRGP1 ([%] at 10µM K_1)	γ-carboxylated TMG4 ([%] at 10µM K_1)	γ-carboxylated GAS6 ([%] at 10µM K_1)	VKORC1 c.-1639
R83P R83P	3 year	HMZ	Facial Dysmorphism + Septal defect	12.6 % 12.6 %	26.5 % 26.5 %	34 % 34 %	218.1 % 218.1 %	47.1 % 47.1 %	119.8 % 119.8 %	AA
D153G M174R+(R325Q)	4 months	CH	Keutel syndrome like phenotype	93.5 % 0.8 %	38.3 % 1.2 %	81.5 % 0 %	164.1 % 2 %	78.1 % 1.8 %	117.1 % 0 %	
S284P W315X	13 year	CH	Midfacial hypoplasia + Septal defect	80.1% -	100.2 % -	63.2 % -	101.4 % -	116.2 % -	96.2 % -	AA
L394R L394R	5 months, newborns	HMZ	-	33.3 % 33.3 %	36.1 % 36.1 %	0 % 0 %	38.6 % 38.6 %	105.9 % 105.9 %	79 % 79 %	
G558R F299S	40 year	CH	PXE-like phenotype	31.7 % 0 %	18.2 % 1 %	65.8 % 0 %	0.3 % 0 %	50.6 % 0 %	5.3 % 1.6 %	
R83W Q374X	48 year	CH	PXE-like phenotype	26.2 % -	31.7 % -	15.8 % -	176.9 % -	4.9 % -	138.5 % -	

Table 14: γ-carboxylation values of GGCX mutations for non-haemostatic VKD proteins. The table summarizes the VKCFD1 patient data along with the data of the family members and the γ-carboxylation values of corresponding GGCX mutations analyzed at 10 µM of K_1 treatment with respect to investigated VKD clotting proteins

GGCX mutation	Genotype	γ-carboxylated GRP ([%] at 10µM K_1)	γ-carboxylated MGP ([%] at 10µM K_1)	Non-haemostatic Phenotype/s
V255M S300F	CH with low responding	30.7 % 1.5 %	10.2 % 2.9 %	PXE-like phenotype + Cardiac abnormality
V255M WT	Mother	30.7 % 100 %	10.2 % 100 %	Distinct skin folds (ABCC6:p.R1141X)
WT S300F	Father	100 % 1.5 %	100 % 2.9 %	Asymptomatic
W157R (D31N)+T591K	CH	44.1 % 31.8 %	58 % 23.8 %	Developmental delay + Septal Defect
(D31N)+T591K WT	Mother	31.8 % 100 %	23.6 % 100 %	Asymptomatic
WT W157R	Father	100 % 44.1 %	100 % 58 %	Asymptomatic
R83W Q374X	CH with nonsense	26.2 % -	31.7 % -	PXE-like phenotype
R83W WT	Mother	26.2 % 100 %	31.7 % 100 %	Asymptomatic
WT Q374X	Father	100 % -	100 % -	Asymptomatic
L394R L394R	HMZ	33.3 % 33.3 %	36.1 % 36.1 %	-
L394R WT	Mother	33.3 % 100 %	36.1 % 100 %	Asymptomatic
WT L394R	Father	100 % 33.3 %	100 % 36.1 %	Asymptomatic
R83P R83P	HMZ	12.6 % 12.6 %	26.5 % 26.5 %	Facial Dysmorphism + Septal defect
R83P WT	Mother	12.6 % 100 %	26.5 % 100 %	Asymptomatic
WT R83P	Father	100 % 12.6 %	100 % 26.5 %	Asymptomatic
D153G R325Q M174R	CH with LOF	93.5 % 44.4 % 0.8 %	38.3 % 97.3 % 1.2 %	Keutel syndrome like phenotype
D153G R325Q	Mother	93.5 % 44.4 %	38.3 % 97.3 %	Asymptomatic
R325Q (R325Q)+M174R	Father	44.4 % 0.8 %	97.3 % 1.2 %	Asymptomatic
G558R F299S	CH with LOF	31.7 % 0 %	18.2 % 1 %	PXE-like phenotype
NA	Mother	31.7 % or 0 %	18.2 % or 1 %	Asymptomatic
NA	Father	31.7 % or 0 %	18.2 % or 1 %	Asymptomatic
G537A Q374X	CH with non-sense	18.4 % -	102 % -	PXE-like phenotype + Atherosclerosis
NA	Mother	18.4 % or -	102 % or -	NA
NA	Father	18.4 % or -	102 % or -	NA

5.2.3 Cardiac abnormalities and the impact of γ-carboxylated GRP

Three patients with mutations GGCX:p.(R83P);p.(R83P), GGCX:p.(S284P);p.(W315X), and GGCX:p.(W157R);p(T591K) out of seven patients with a cardiac phenotype had congenital atrial septal defect. Remaining four patients with mutants GGCX:p.(V255M);(S300F), GGCX:p.(H404P);(R485P), GGCX:p.(R476C);(wt) and GGCX:p.(G537A);(Q374X) developed slightly calcified arteries or subclinical atherosclerosis. It is observed in our data that the ability to γ-carboxylate GRP is reduced for mutations that were reported in patients with a cardiac phenotype (Table 15). Together with the knowledge that *Mgp*$^{-/-}$ mice[116] die due to extensive arterial calcification it was anticipated that MGP is affected in these patients, too. But there is a possibility that reduced levels of γ-carboxylated GRP indirectly effects MGP γ-carboxylation and downstream signaling of vascular calcification.

Previous studies have shown that MGP and fetuin complex is an active inhibitory system involved in vascular calcification [117]. Fetuin A is a circulating inhibitor of ectopic calcification produced in the liver. Viegas et al. showed by immunoprecipitation studies that GRP is associated with MGP-fetuin inhibitory complex. They also reported that GRP and MGP are present in non-calcifying extracellular vesicles originating from aortic fragments [21]. Thus, the low amount of γ-carboxylated GRP by GGCX mutations in VKCFD1 patients might negatively regulate the quantity of γ-carboxylated MGP within the tissue leading to cardiac defects.

We further realized that not all patients carrying mutations causing reduced level of γ-carboxylated GRP develop cardiac abnormalities like septal defects. Therefore, we assume that maternal transfer of K_1 during pregnancy, even though it´s low [118] , may modulate the severity of cardiac birth defects as for the patient harboring GGCX:p.(S284P);p.(W315X) whose mother had hyperemesis gravidarum. There is also a possibility that these patients with mutations showing reduced γ-carboxylated GRP will develop later in life subclinical atherosclerosis. Moreover, lifestyle and malnutrition might influence the development of age-related cardiac defects as calcified arteries. There is also a possibility that another VKD protein which is unknown or was not included in the study is the causative protein for cardiac defects. Therefore, further work needs to be done for deeper elucidation of the cardiac defect development.

Table 15: Effect of GGCX mutations on γ-carboxylation of non-haemostatic proteins with respect mutations causing cardiac phenotype in VKCFD1 patients. The patient data along with the ELISA results for γ-carboxylation of all analyzed non-haemostatic proteins with respect to 100% wt γ-carboxylation at 10µM K_1

GGCX mutation	Age	Genotype	Non-haemostatic Phenotype/s	γ-carboxylated GRP ([%] at 10µM K_1)	γ-carboxylated MGP ([%] at 10µM K_1)	γ-carboxylated BGLAP ([%] at 10µM K_1)	γ-carboxylated PRGP1 ([%] at 10µM K_1)	γ-carboxylated TMG4 ([%] at 10µM K_1)	γ-carboxylated GAS6 ([%] at 10µM K_1)	VKORC1 c.-1639
R83P R83P	3 year	HMZ	Facial Dysmorphism + Septal defect	12.6 % 12.6 %	26.5 % 26.5 %	34 % 34 %	218.1 % 218.1 %	47.1 % 47.1 %	119.8 % 119.8 %	AA
S284P W315X	13 year	CH	Midfacial hypoplasia + Septal defect	80.1% -	100.2 % -	63.2 % -	101.4 % -	116.2 % -	96.2 % -	AA
W157R (D31N)+T591K	2 year	CH	Developmental delay + Septal Defect	44.1 % 31.8 %	58 % 23.8 %	45.1 % 0 %	72.2 % 3.6 %	56.4 % 40.9 %	75.5 % 0 %	
V255M S300F	16 year	CH	PXE-like phenotype + Cardiac abnormality	30.7 % 1.5 %	10.2 % 2.9 %	57.3 % 0 %	151.7 % 0 %	111.5 % 3.5 %	153.1 % 2.7 %	
H404P R485P	47 year	CH	Mild skin symptom + Calcified peripheral arteries	34.8 % 57.7 %	8.9 % 87.1 %	0.4 % 47.7 %	72.7 % 118.2 %	120.7 % 91.1 %	51.7 % 61.8 %	GG
R476C WT	67 year	HTZ	PXE-like phenotype + Atherosclerosis	41.7 % 100 %	93.5 % 100 %	56.2 % 100 %	91.1 % 100 %	95.7 % 100 %	87.8 % 100 %	
G537A Q374X	46 year, 44 year	CH	PXE-like phenotype + Atherosclerosis	18.4 % -	102 % -	155.8 % -	117.6 % -	108 % -	83.8 % -	

5.2.4 Effect of undercarboxylated BGLAP on VKCFD1 phenotype

BGLAP is another calcification regulator known to be highly expressed in bone especially in mature osteoblasts and early hypertrophic chondrocytes.

The patients harboring mutations GGCX:p.(R83P);p.(R83P) who developed skeletal defects showed lower levels of BGLAP. Mutations GGCX:p.(L394R) and GGCX:p.(W501S) showed reduced ability to γ-carboxylate BGLAP and was reported in homozygous form in patients who did not develop midfacial hypoplasia or facial dysmorphism. Thereby, BGLAP can be eliminated to be the sole causative protein for developing skeletal defects. However, from our data it can be predicted that patient harboring these mutations might develop in future higher bone density as the *Bglap*$^{-/-}$ mouse [60] was normal at birth but develop higher bone density after six months.

5.2.5 No correlation between under-carboxylated GAS6 with VKCFD1 phenotype

The correlation of the existing knowledge of GAS6 function with these phenotypes is difficult. GAS6 is known to be expressed in endothelial cells, macrophages, bone marrow stromal cells, and vascular smooth muscle cells (VSMc) [69,75,119]. GAS6 binds via the N-terminal Gla-domain to phosphatidylserine residues in the nearby cell surface upon stress, apoptosis and cell activation. This binding helps for remodeling of endothelial cells, innate immunity regulation, VSMc homeostasis etc [69,75,120] . Although earlier studies indicate the role of GAS6 in VSMc but our data showed all types of dose response curves for γ-carboxylation with respect to mutations causing cardiac phenotype in VKCFD1 patients.

According to our data, two mutations GGCX:p.(G558R) and GGCX:p.(T591K) showed zero γ-carboxylation for GAS6 other than three non-responding mutations. The zero γ-carboxylation levels of GAS6 by GGCX:p.(T591K) may be the cause of acute infection in this patient as the existing literature indicates strongly the role of GAS6/TAM signaling on preserving immune homeostasis [69]. GAS6, a ligand for TAM receptors mainly functions by downregulating interleukin-6, interferon-γ, TNF-α etc and plays an anti-inflammatory role by regulating the immune homeostasis [69]. However, the other allele having GGCX:p.(W157R) responds well to vitamin K treatment and thus should prevent acute infection once treated. However, data from only one patient is difficult for genotype-phenotype correlation and this hypothesis should be further investigated.

With respect to knockout mice data, it is reported that *Gas6*$^{-/-}$ mice have normal development and are phenotypically normal. But they are protected from thrombosis and vary in platelet aggregation compared to the wt. Another study showed that GAS6 inhibition prevents liver inflammation and hepatic fibrosis [121]. This indicates that patients harboring *GGCX* mutations that leads to undercarboxylated GAS6 might be protected from developing thrombosis and liver inflammation.

5.2.6 The proline rich gla proteins might be involved in developmental retardation

One patient with genotype GGCX:p.(W157R);p.(T591K+D31N) was reported with developmental delay along with a septal defect. Both of these mutations showed reduced ability to γ-carboxylate both PRGP1 and TMG4 (Table 8). But since the brother has the same genotype who did not develop any developmental delay indicates that some other factor might be involved for the index patient [83].

A previous study, reported a patient with typical phenotypes of WAGR syndrome (Wilms tumor, aniridia, genitourinary malformation and mental retardation) had 8.6 Mb chromosomal deletion (11p13), which includes the TMG4 gene [122]. This indicates that transmembrane Gla proteins can be a candidate gene for causing developmental delay. But more patient reports are needed to confirm this correlation.

Compared to the other VKD proteins, very few studies exist for PRGPs and TMGs cellular function where they identified interacting proteins of TMG4, which include membrane-associated guanylate kinase-related (MAGI-1, 3) and Yes-associated protein (YAP) [78]. These proteins are involved in hippo pathway, which is an evolutionary conserved signaling pathway having role in organ size control and development [123]. Therefore, biallelic *GGCX* mutations affecting γ-carboxylation of proline rich or transmembrane Gla proteins, which has developmental function is rare or lethal. Hence, there is a possibility that these VKD transmembrane proteins have a significant contribution for warfarin embryopathy.

5.3 Influence of VKORC1 polymorphism in VKCFD1 patients

The promoter polymorphism of VKORC1 may modulate the severity of the VKCFD1 phenotype since VKORC1 is generating the substrate required for γ-carboxylation. The VKORC1:c.-1639 AA genotype is associated with 50% reduction of VKORC1 mRNA and enzymatic activity for each allele, whereas the GG genotype results into 100% mRNA and activity levels [102]. Patients

with GGCX:p.(R83P);p.(R83P) and GGCX:p.(S284P);p.(W315X) have the AA polymorphism in VKORC1:c.-1639 gene. Although this polymorphism has no impact on haemostasis within normal population it could influence VKCFD1 phenotypes due to reduced availability of KH_2. For example, patient with GGCX:p.(S284P);p.(W315X) is homozygous for the VKORC1:c.-1639 AA genotype that is associated with 50% reduction of VKORC1 mRNA and enzymatic activity for each allele [79,102]. Therefore, this reduced enzymatic activity might be the reason for development of midfacial hypoplasia and septal defects as GGCX:p.(S284P) responded moderately to vitamin K_1 treatment. There are three patients reported with the same GGCX genotype GGCX:p.(R204C); p.(R204C), who had either the VKORC1:c.-1639 GA or GG genotype. According to a previous study the patient with the GA polymorphism had lower levels of clotting factor activity compared to the one with the GG genotype, although both patients are siblings and were under similar vitamin K treatment. The VKORC1:c.-1639 GA polymorphism was reported to have 50 % mRNA and reduced enzymatic activity [79,102]. This indicates that the VKORC1:c.-1639 promotor polymorphism most likely has an effect on the development and severity of VKCFD1 phenotypes.

Reider et al. showed that different haplotypes regulate the mRNA expression and protein synthesis of the VKORC1 complex [102]. The presence of these haplotypes might influence the development of both haemostatic and non-haemostatic phenotypes in VKCFD1 patients and their response to vitamin K treatment. Therefore, polymorphisms in VKORC1 should be always analyzed for determining the amount of effective vitamin K therapeutics.

5.4 Identification of the vitamin K binding site in GGCX

Since the crystal structure of GGCX is unknown, the determination of specific functional binding residues in GGCX has been challenging. However, *in vitro* studies and bioinformatics analysis have led to the identification of the propeptide binding site (395-404), Gla binding site (495-513) and the active site (K218).

Our analysis showed two GGCX:p.(M174R) and GGCX:p.(F299S) mutations had loss-of-function of γ-carboxylase activity and mutation GGCX:p.(S300F) showed extremely reduced γ-carboxylation activity for all VKD proteins. These three residues are not located in other known functionally important domains. GGCX:p.(M174R) have been previously characterized by Tie et al., where they also showed the reason for its non-functionality is protein misfolding and degradation [88]. This data in is concordance with our data where we have seen that the co-localization coefficient of GGCX:p.(M174R) with the ER is lesser than GGCX:wt to the ER.

The remaining loss-of-function mutation GGCX:p.(F299S) have not been characterized yet. This intrigued us to generate a GGCX *in silico* model to visualize the localization of these residues. In the GGCX *in silico* model F299 residue were located towards the periphery of the membrane in the luminal side. The membrane localization and the hydrophobic nature of vitamin K hydroquinone further provided a hint that F299 residue might be involved in vitamin K binding site, which is unknown until now. Hence, *in silico* docking of vitamin K hydroquinone was performed on GGCX which confirmed that F299 is directly located in the vitamin K binding site whereas consecutive residue S300 also effects the KH_2 binding when mutated but is not directly located in the binding site.

The closer location of the propeptide binding site, the active site (K218) and the presently reported vitamin K binding site (~22 Å distance between K218 and F299) in our model indicates there must be a conformational change upon substrate binding (Figure 50). Therefore, it can be proposed that once the propeptide of the VKD proteins are binding to the propeptide binding site of GGCX, there is a conformational change which brings the bound vitamin K (via F299) closer to the active site (K218). This initiates the formation of a strong base (K^-) for abstracting the hydrogen from Glu starting the process of γ-carboxylation. This is also supported by the high number of disordered regions present in our model (f.e. 95-115 and 394-419 aa). Therefore, these disordered regions undergo conformational change since the spatial assembly of the multiple active sites contributing to γ-carboxylation is essential for GGCX catalytic efficiency.

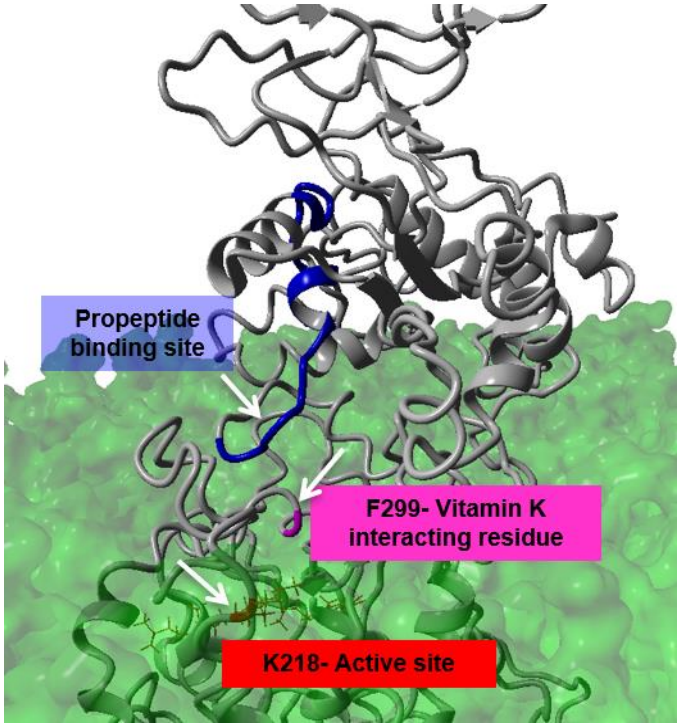

Figure 50: Functional binding sites in GGCX. GGCX protein represented in grey (ribbon style) that is embedded in a phosphatidylcholine bilayer membrane in green (molecular surface style). Propeptide binding site is marked in blue, active site in red and presently reported vitamin K interacting residue in magenta.

5.5 Conclusion

Finally, to conclude this study, *GGCX* missense mutations were characterized causing VKCFD1 with respect to their ability to γ-carboxylate haemostatic and non-hemostatic VKD proteins (Figure 51). Our study highlights the physiological importance of GGCX to γ-carboxylate VKD proteins in several tissues and pathways. This data will help to predict the clinical course, to treat patients with VKCFD1 bleeding phenotype more efficiently by using either vitamin K or PCC.

With respect to the non-haemostatic phenotype, the role of under-carboxylated GRP was identified contributing to the development of skin hyper-laxity. Moreover, the interplay between the calcification regulators MGP along with additional factors leads to skeletal abnormalities. This information will help in future to generate personalized medicine for treating non-haemostatic phenotypes maybe with γ-carboxylated VKD proteins. With structural point of view, an important KH_2 binding residue i.e. F299 was identified for the first time that directly interacts with the KH_2 head group. Altogether this study helps to understand the response of

mutated GGCX to vitamin K treatment and identified causative under-carboxylated VKD protein responsible for developing non-haemostatic phenotypes in VKCFD1 patients.

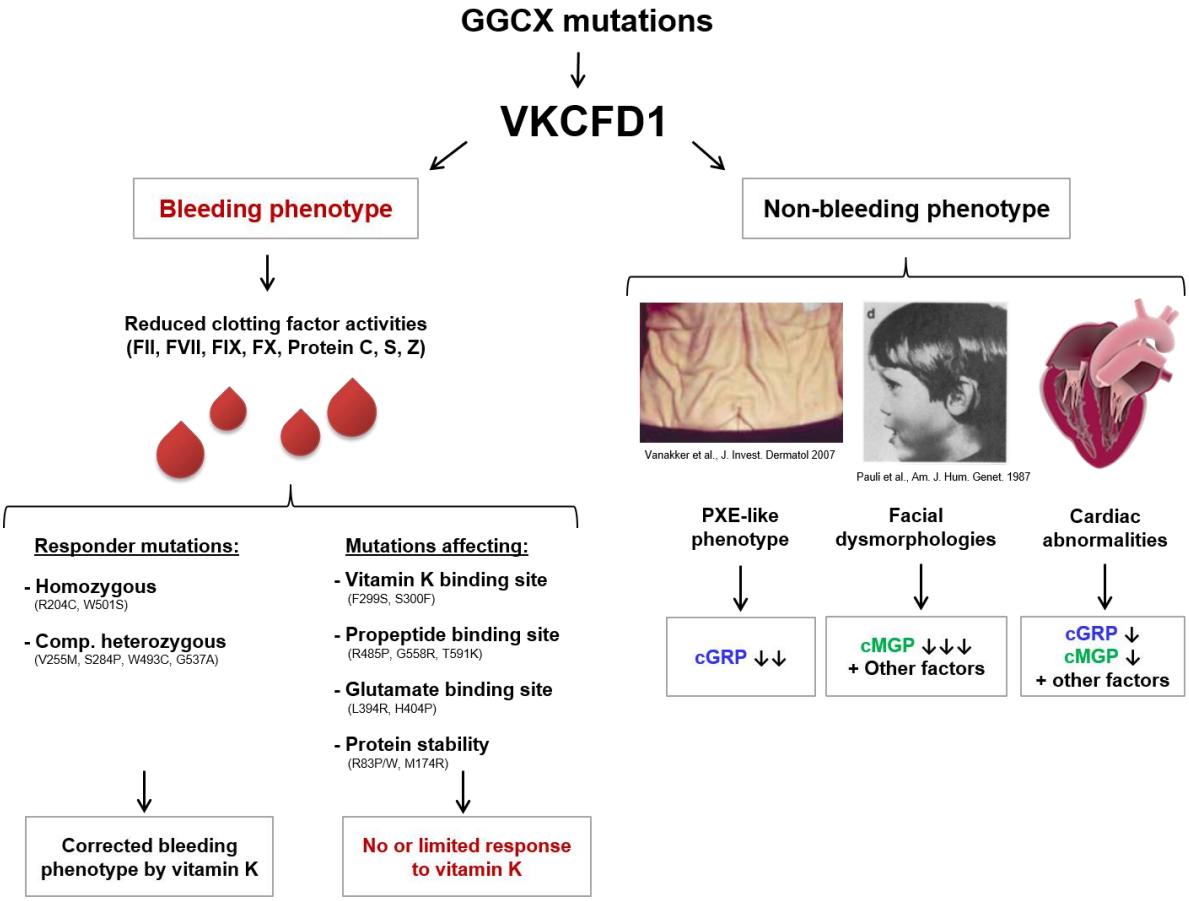

Figure 51: Summary of the main findings from the thesis. VKCFD1 patients are caused due to mutations in GGCX gene where patients are diagnosed with bleeding and non-bleeding phenotypes. GGCX mutations were analysed in this study and was categorized in responder and non-responder for vitamin K treatment for correcting bleeding phenotype. Mutations effecting functional binding regions like the vitamin K, propeptide or glutamate binding site will show limited response to vitamin K. Causative proteins were identified for calcification related non-bleeding phenotype i.e. PXE-like phenotype, facial dysmorphologies or cardiac abnormalities.

5.6 Future prospects

Due to the lack of crystal structure, our GGCX *in silico* model will help to unveil crucial residues of γ-carboxylation. Hence, strengthening the model further with biophysical experiments as f.e. atomic force microscopy will help to understand the distribution of transmembrane domains and the process of conformational change upon substrate binding.

The differential effect of GGCX mutations on VKD proteins gave us a hint that GGCX interacts with individual propeptides in a different way. Hence, individual docking of all 15 VKD propeptides to GGCX and validation of this binding by *in vitro* studies will be interesting.

Our data also demonstrated that γ-carboxylated GRP and MGP plays a major role in inhibition of calcification to maintain normal tissue homeostasis. But the mechanism of how these γ-carboxylated proteins interacts with each other and inhibits calcification remains to be elucidated.

Further new and more native cellular models as f.e. induced pluripotent stem (iPS) cells from VKCFD1 patients will be useful to study γ-carboxylation levels endogenously in the respective differentiated cell type f.e. haemostatic proteins in hepatocyte-like cells and non-haemostatic proteins in osteoblasts or fibroblasts.

List of figures

List of tables

Appendix

List of Primer

Mutagenesis primers	Sequence 5´→ 3´
R83W-GGCX-F	GACATTCCCCAGGAGTGGGGGCTCAGCTCT
R83W-GGCX-R	AGAGCTGAGCCCCCACTCCTGGGGAATGTC
R83P-GGCX-F	GACATTCCCCAGGAGCCGGGGCTCAGCTCTCTG
R83P-GGCX-R	CAGAGAGCTGAGCCCCGGCTCCTGGGGAATGTC
D153G-GGCX-F2	TACTGGTATGTGTTTCTCCTGGGCAAGACATCA
D153G-GGCX-R2	TGATGTCTTGCCCAGGAGAAACACATACCAGTA
W157R-GGCX-F	CTGGACAAGACATCACGGAACAACCACTCC
W157R-GGCX-R	GGAGTGGTTGTTCCGTGATGTCTTGTCCAG
M174R-GGCX-FSU	TTGGCCTTTCAGCTAACATTCAGGGATGCAAAC
M174R-GGCX-RSU	GTTTGCATCCCTGAATGTTAGCTGAAAGGCCAA
R204C-GGCX-F	TATGCAGTGCTCTGTGGCCAGATCTTCATT
R204C-GGCX-R	AATGAAGATCTGGCCACAGAGCACTGCATA
G215D-GGCX-F	TGTACTTCATTGCGGATGTG AAAAAGCTGGA
G215D-GGCX-R	TCCAGCTTTTTCACATCCGCAATGAAGTACA
K218A-GGCX-F	TACTTCATTGCGGGTGTGAAAGCGCTGGATGCAGACTGGGTT
K218A-GGCX-R	AACCCAGTCTGCATCCAGCGCTTTCACACCCGCAATGAAGT
H235N-GGCX-F	GAATAT TTGTCCCGGAACTGGCTCTTCAGTCC
H235N-GGCX-R	GGACTGAAGAGCCAGTTCCGGGACAAATATTC
V255M-GGCX-F	AGCCTGCTGGTCATGCACTGGGGTGGGCTG
V255M-GGCX-R	CAGCCCACCCCAGTGCATGACCAGCAGGCT
S284P-GGCX-F	GGACTGTTCTTTGTGCCCTACTTCCACTGCA
S284P-GGCX-R	TGCAGTGGAAGTAGGGCACAAAGAACAGTCC
F299S-GGCX-FSU2	CAGCTTTTCAGCATTGGTATGTCCTCCTACGTC
F299S-GGCX-RSU2	GACGTAGGAGGACATACCAATGCTGAAAAGCTG
S300F-GGCX-F	AGCATTGGTATGTTCTTCTACGTCATGCTG
S300F-GGCX-R	CAGCATGACGTAGAAGAACATACCAATGCT
R325Q-GGCX-F	TGTCCTACTGCCCCCAAAGGTTGCAACAACT
R325Q-GGCX-R	AGTTGTTGCAACCTTTGGGGGCAGTAGGACA
Y345A-GGCX-F	AGTGTTTCCTGTGTGGCTAAGAGGAGCCGGGGC
Y345A-GGCX-R	GCCCCGGCTCCTCTTAGCCACACAGGAAACACT
L394R-GGCX-FSU	TATAACAACTGGACAAATGGGCGGTATGGCTAT
L394R-GGCX-RSU	ATAGCCATACCGCCCATTTGTCCAGTTGTTATA
H404P-GGCX-FSU	TATTCCTGGGACATGATGGTGCCCTCCCGCTCC
H404P-GGCX-RSU	GGAGCGGGAGGGCACCATCATGTCCCAGGAATA
R476C-GGCX-F	GTCTCCATCAATGACTGCTTCCAGCAGAGG
R476C-GGCX-R	CCTCTGCTGGAAGCAGTCATTGATGGAGAC
R476H-GGCX-F	GTCTCCATCAATGACCACTTCCAGCAGAGG
R476H-GGCX-R	CCTCTGCTGGAAGTGGTCATTGATGGAGAC
W493S-GGCX-F2	GTGGACATCGTGCAGGCCGCTTCG TCACCCTTT
W493S-GGCX-R2	AAAGGGTGACGAAGCGGCCTGCACGATGTCCAC
R485P-GGCX-Fsu	CAGCAGAGGATTTTTGACCCTCCTGTGGACATC
R485P-GGCX-Rsu	GATGTCCACAGGAGGGTCAAAAATCCTCTGCTG
W501S-GGCX-FNEW	TTTCAGCGCACATCCTCG GTGCAACCACTCTT
W501S-GGCX-RNEW	AAGAGTGGTTGCACCGAGGATGTGCGCTGAAA
I532T-GGCX-FSU	AACCACACTGAG GTGGTCTTCACTGCAGATTT
I532T-GGCX-RSU	AAATCTGCAGTGAAGACCACCTCAGTGTGGTT

A533E-GGCX-F	**AGGTGGTCTTCATTGAAGATTTCCCTGGACT**
A533E-GGCX-R	**AGTCCAGGGAAATCTTCAATGAAGACCACCT**
G537A-GGCX-FSu	**GTCTTCATTGCAGATTTCCCTGCACTGCACTTG**
G537A-GGCX-RSu	**CAAGTGCAGTGCAGGGAAATCTGCAATGAAGAC**
G558R-GGCX-FSU	**CACTAGCATCCAGCTGCTGCAGCGGGAAGTGAC**
G558R-GGCX-RSU	**GTCACTTCCCGCTGCAGCAGCTGGATGCTAGTG**
T591K-GGCX-F	**CATAAGGTGTATAAGACATCACCTAGCCCT**
T591K-GGCX-R	**AGGGCTAGGTGATGTCTTATACACCTTATG**

Cloning primers	**Sequence 5´ → 3**
FII-Prop-F	**TACTTAAT ACGACTCACTATAGGCTAGCCT ATGGCGC ACGTCCGAGG**
FIIw/ostop_myc-R	**TCACAGATCCTCTTCTGAGATGAGTTTTTGTTCctctccaaactgatc aatg**
MSCA-F10-Myc-F	**cataacgtcctctccattaaagGAACAAAAACTCATCTCA GA**
F10-end-w/ostop-R	**ctttaatggagaggacgtta**
PC-end-w/ostop-R	**aggtgcccagctcttctggg**
MSCA-PC-Myc-F	**gaagccccccagaagagctgggcacctGAACAAAAACTCATCTCAGA**
PCw/ostop-Myc-R	**TCACAGATCCTCTTCTGAGATGAGTTTTTGTTCaggtgcccagctctt ctggg**
MGP-Prop-F	**TACTTAAT ACGACTCACTATAGGCTAGC CT AT GAAGAGCCTG ATCCTTCTTG**
MGPw/ostopmycR	**TCGTCACAGATCCTCTTCTGAGATGAGTTTTTGTTCtttggtccctcg gcgcttcc**
BGLA- Prop-F	**TACTTAAT ACGACTCACTATAGGCTAGC CT ATGAGAGC CCTCACACTC**
BGLAw/ostopmycR	**TCGTCACAGATCCTCTTCTGAGATGAGTTTTTGTTCgaccgggccg tagaagcgcc**
Gas6-end-w/ostop-R	**ggctgcggcgggctccacgg**
MSCA-GAS6-Myc-F	**tgccccccgtggagcccgccgcagccGAACAAAAACTCATCTCAGA**
Gas6-endw/ostop_myc-R	**TCACAGATCCTCTTCTGAGATGAGTTTTTGTTCggctgcggcgggct ccacg**
PRGP1-end-w/ostop-R	**tttgatggtggtgaccacag**
MSCA-PRGP1-Myc-F	**tgcctgtggtcaccaccatcaaaGAACAAAAACTCATCTCAGA**
PRGP1w/ostop-Myc-R	**TCGTCACAGATCCTCTTCTGAGATGAGTTTTTGTTCtttgatggtggt gaccacag**
MCSA-PRRG2-F	**TACTTAATACGACTCACTATAGGCTAGCCTATGAGGGGCCACC CCTCTC**
MCSA-PRRG2MYC-R	**TCACAGATCCTCTTCTGAGATGAGTTTTTGTTCGTGAGGCCTCC TGAGGCTG**
MCSA-PRRG3MYC-F	**TACTTAATACGACTCACTATAGGCTAGCCTATGGCAGTGTTTCT GGAGG**
MCSA-PRRG3MYC-R	**TCACAGATCCTCTTCTGAGATGAGTTTTTGTTCCTTGTCAGCGC CAGGGTTG**
MCSA-PRRG4MYC-F	**TACTTAATACGACTCACTATAGGCTAGCCTATGTTTACGCTTCT GGTTC**
MCSA-PRRG4MYC-R	**TCACAGATCCTCTTCTGAGATGAGTTTTTGTTCGTGAGATGGG AGAGACATA**
FII-SQ-F2	**TTCTGTGCTGGTTACAAGCC**
FII-SQ-F4	**TATTGTGAGG AGGCCGTGGA**
FII-SQ-Start-F	**ATGGCGC ACGTCCGAGGCTT**

FII-SQ-N1F	**CCTGAAATCA ACTCCACTAC**
FII-SQ-N1R	**TCAGGGACACACTGCTCCAA**
FII-SQ-N2F	**CAAGCACCAG GACTTCAACT**
FII-SQ-N3F	**ATCGACGGGC GCATTGTGGA**
FII-SQ-N3R	**TTCGCTCGTACCTGGTGCGG**
FII-SQ-N4F	**ACAACTGGCG GGAGAACCTG**
FX-SQ-F1	**AGCGTGACTG GGCCGAGTCC**
FX-SQ-F2	**CACCAAGCAG GAGGATGCCT**
FX-SQ-F3	**AAGATGGCGA CCAGTGTGAG**
FX-SQ-F4	**TCGACCTGCT TGACTTCAAC**
FX-SQ-New1F	**AAGGCCTGCA TTCCCACAGG**
FX-SQ-New2F	**GTTCTACATC CTAACGGCAG**
FX-SQ-NewR	**GTTCTGGGTGATGATGAAGC**
FX-SQ-NewendF	**C TACACCAAGG TCACCGCCT**
PC-SQ-F2	**CATCCTCGGG GACCGGCAGG**
PC-SQ-F3	**GACGGCATCG GCAGCTTCAG**
PC-SQ-F4	**AAGC TGGCCTGCGG GGCAGT**
MGP-SQ-F1	**CAGGAGAAAT GCAAATACCT**
BGLA-SQ-F1	**CGAGGTAGTG AAGAGACCCA**
Gas6-SQ-F1	**GTAGACTATC ACTCCACGAA**
Gas6-SQ-F2	**AGCTGCAGGA GAGGCTGGCC**
Gas6-SQ-F3	**TAGACTGCAT CAACAAGTAT**
Gas6-SQ-F4	**CCGAGATGTG GACGAGTGTC**
Gas6-SQ-F5	**CGCTACAACG GTGTCGGCCG**
Gas6-SQ-F6	**GAGAAGACAC CACCATCCAG**
Gas6-SQ-R1	**ACGCACTCCCTCTCCAGGTG**
PRGP1-SQ-F1	**GTTAATCTTT GGCCTCTTCA**
PRGP1-SQ-R1	**GTTGCGCTTTTGTGTAGGTG**
PRGP1-SQ-F2	**AGATTCCGTC TCTACTCGCC**
PRRG2-SQ-Start-F	**ATGAGGGGCCACCCCTCTC**
PRRG2-SQ-F1	**CTGAGTAGCCATACCCGGAT**
PRRG2-SQ-R1	**ATCCGGGTATGGCTACTCAG**
PRRG2-SQ-F2	**AGAGCTACATCTACAATGGC**
PRRG2-SQ-F3	**AGTCCTTTGAACCCTCTGGG**
PRRG2-SQ-F4	**ACCTATGAGCAGGCGCTGGC**
PRRG3-SQ-Start-F	**ATGGCAGTGTTTCTGGAGG**
PRRG3-SQ-F1	**CTGCAGCTACGAGGAGGTCA**
PRRG3-SQ-R1	**TGACCTCCTCGTAGCTGCAG**
PRRG3-SQ-F2	**GAACCGGTACCTAGCCAGTC**
PRRG3-SQ-F3	**CCTACGAGGAGGTGACTGCG**
PRRG3-SQ-F4	**GGCCAGCGTGTCTTACAGTGA**
PRRG4-SQ-Start-F	**ATGTTTACGCTTCTGGTTC**
PRRG4-SQ-F1	**GATTTGATCTGGAGCTCTTC**
PRRG4-SQ-R1	**GAAGAGCTCCAGATCAAATC**
PRRG4-SQ-F2	**GACTGGATTAATTGCTGCTGG**
PRRG4-SQ-F3	**GAACAGGCAGTGGCGCTGACC**
PRRG4-SQ-F4	**CCACCATATCCTGGGCACAC**

pIRES

Plasmid used for expression of *VKD proteins* and *GGCX* and its variants in different HEK293T cell lines. Vector information taken from www.clontech.com visited on 19-Jan-2018 (PR852529; published 20 May, 2008).

pIRES Vector Information PT3266-5

Cat. No. 631605

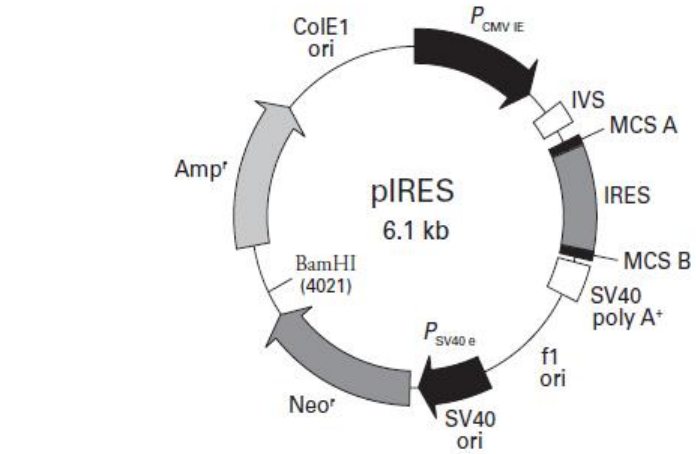

MCS A

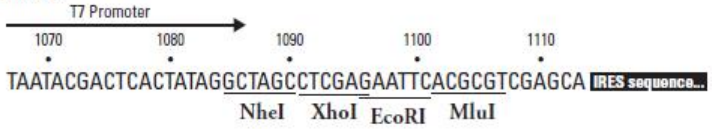

MCS B

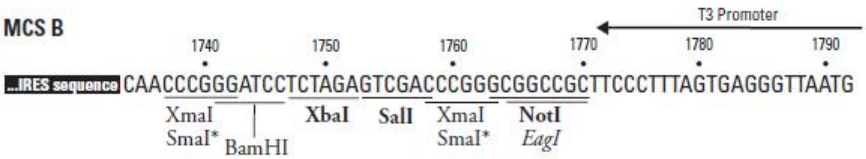

pIRES Vector Map and Multiple Cloning Sites (MCS). Unique restriction sites are in bold. The XmaI/SmaI sites can be treated as unique sites for cloning purposes.

References

1. Berkner, K. L. The vitamin K-dependent carboxylase. *The Journal of nutrition* **130,** 1877–1880; 10.1093/jn/130.8.1877 (2000).

2. Rishavy, M. A. & Berkner, K. L. Vitamin K oxygenation, glutamate carboxylation, and processivity: defining the three critical facets of catalysis by the vitamin K-dependent carboxylase. *Advances in nutrition (Bethesda, Md.)* **3,** 135–148; 10.3945/an.111.001719 (2012).

3. Vermeer, C. Gamma-carboxyglutamate-containing proteins and the vitamin K-dependent carboxylase. *The Biochemical journal* **266,** 625–636; 10.1042/bj2660625 (1990).

4. Wu, S. M., Cheung, W. F., Frazier, D. & Stafford, D. W. Cloning and expression of the cDNA for human gamma-glutamyl carboxylase. *Science (New York, N.Y.)* **254,** 1634–1636; 10.1126/science.1749935 (1991).

5. Azuma, K. *et al.* Liver-specific γ-glutamyl carboxylase-deficient mice display bleeding diathesis and short life span. *PloS one* **9,** e88643; 10.1371/journal.pone.0088643 (2014).

6. Degen, S. J., MacGillivray, R. T. & Davie, E. W. Characterization of the complementary deoxyribonucleic acid and gene coding for human prothrombin. *Biochemistry* **22,** 2087–2097; 10.1021/bi00278a008 (1983).

7. Kurachi, K. & Davie, E. W. Isolation and characterization of a cDNA coding for human factor IX. *Proceedings of the National Academy of Sciences of the United States of America* **79,** 6461–6464; 10.1073/pnas.79.21.6461 (1982).

8. Foster, D. & Davie, E. W. Characterization of a cDNA coding for human protein C. *Proceedings of the National Academy of Sciences of the United States of America* **81,** 4766–4770; 10.1073/pnas.81.15.4766 (1984).

9. Ichinose, A. *et al.* Amino acid sequence of human protein Z, a vitamin K-dependent plasma glycoprotein. *Biochemical and biophysical research communications* **172,** 1139–1144; 10.1016/0006-291x(90)91566-b (1990).

10. Leytus, S. P., Foster, D. C., Kurachi, K. & Davie, E. W. Gene for human factor X: a blood coagulation factor whose gene organization is essentially identical with that of factor IX and protein C. *Biochemistry* **25,** 5098–5102; 10.1021/bi00366a018 (1986).

11. Lundwall, A. *et al.* Isolation and sequence of the cDNA for human protein S, a regulator of blood coagulation. *Proceedings of the National Academy of Sciences of the United States of America* **83,** 6716–6720; 10.1073/pnas.83.18.6716 (1986).

12. Stenflo, J., Fernlund, P., Egan, W. & Roepstorff, P. Vitamin K dependent modifications of glutamic acid residues in prothrombin. *Proceedings of the National Academy of Sciences of the United States of America* **71,** 2730–2733; 10.1073/pnas.71.7.2730 (1974).

13. Nelsestuen, G. L. Enhancement of vitamin-K-dependent protein function by modification of the gamma-carboxyglutamic acid domain: studies of protein C and factor VII. *Trends in cardiovascular medicine* **9,** 162–167; 10.1016/s1050-1738(99)00024-9 (1999).

14. Metz, M. de *et al.* Partial purification of bovine liver vitamin K-dependent carboxylase by immunospecific adsorption onto antifactor X. *FEBS letters* **123,** 215–218; 10.1016/0014-5793(81)80290-6 (1981).

15. Poser, J. W., Esch, F. S., Ling, N. C. & Price, P. A. Isolation and sequence of the vitamin K-dependent protein from human bone. Undercarboxylation of the first glutamic acid residue. *The Journal of biological chemistry* **255,** 8685–8691 (1980).

16. Kulman, J. D., Harris, J. E., Haldeman, B. A. & Davie, E. W. Primary structure and tissue distribution of two novel proline-rich gamma-carboxyglutamic acid proteins. *Proceedings of the National Academy of Sciences of the United States of America* **94,** 9058–9062; 10.1073/pnas.94.17.9058 (1997).

17. Kulman, J. D., Harris, J. E., Xie, L. & Davie, E. W. Identification of two novel transmembrane gamma-carboxyglutamic acid proteins expressed broadly in fetal and adult tissues. *Proceedings of the National Academy of Sciences of the United States of America* **98,** 1370–1375; 10.1073/pnas.98.4.1370 (2001).

18. Manfioletti, G., Brancolini, C., Avanzi, G. & Schneider, C. The protein encoded by a growth arrest-specific gene (gas6) is a new member of the vitamin K-dependent proteins related to protein S, a negative coregulator in the blood coagulation cascade. *Molecular and cellular biology* **13,** 4976–4985; 10.1128/mcb.13.8.4976 (1993).

19. Viegas, C. S. B. *et al.* Gla-rich protein is a novel vitamin K-dependent protein present in serum that accumulates at sites of pathological calcifications. *The American journal of pathology* **175,** 2288–2298; 10.2353/ajpath.2009.090474 (2009).

20. Price, P. A., Fraser, J. D. & Metz-Virca, G. Molecular cloning of matrix Gla protein: implications for substrate recognition by the vitamin K-dependent gamma-carboxylase. *Proceedings of the National Academy of Sciences of the United States of America* **84,** 8335–8339; 10.1073/pnas.84.23.8335 (1987).

21. Gla-Rich Protein Acts as a Calcification Inhibitor in the Human Cardiovascular System.

22. Ferron, M. & Lacombe, J. Regulation of energy metabolism by the skeleton: osteocalcin and beyond. *Archives of biochemistry and biophysics* **561,** 137–146; 10.1016/j.abb.2014.05.022 (2014).

23. Lee, N. K. *et al.* Endocrine regulation of energy metabolism by the skeleton. *Cell* **130,** 456–469; 10.1016/j.cell.2007.05.047 (2007).

24. Gundberg, C. M., Lian, J. B. & Booth, S. L. Vitamin K-dependent carboxylation of osteocalcin: friend or foe? *Advances in nutrition (Bethesda, Md.)* **3,** 149–157; 10.3945/an.112.001834 (2012).

25. Schurgers, L. J., Cranenburg, E. C. M. & Vermeer, C. Matrix Gla-protein: the calcification inhibitor in need of vitamin K. *Thrombosis and haemostasis* **100,** 593–603 (2008).

26. Pan, L. C. & Price, P. A. The propeptide of rat bone gamma-carboxyglutamic acid protein shares homology with other vitamin K-dependent protein precursors. *Proceedings of the National Academy of Sciences of the United States of America* **82,** 6109–6113; 10.1073/pnas.82.18.6109 (1985).

27. Shiba, S. *et al.* γ-Glutamyl carboxylase in osteoblasts regulates glucose metabolism in mice. *Biochemical and biophysical research communications* **453,** 350–355; 10.1016/j.bbrc.2014.09.091 (2014).

28. Bordoloi, J., Dihingia, A., Kalita, J. & Manna, P. Implication of a novel vitamin K dependent protein, GRP/Ucma in the pathophysiological conditions associated with vascular and soft tissue calcification, osteoarthritis, inflammation, and carcinoma. *International journal of biological macromolecules* **113,** 309–316; 10.1016/j.ijbiomac.2018.02.150 (2018).

29. Willems, B. A. *et al.* Ucma/GRP inhibits phosphate-induced vascular smooth muscle cell calcification via SMAD-dependent BMP signalling. *Scientific reports* **8,** 4961; 10.1038/s41598-018-23353-y (2018).

30. Larson, A. E., Friedman, P. A. & Suttie, J. W. Vitamin K-dependent carboxylase. Stoichiometry of carboxylation and vitamin K 2,3-epoxide formation. *The Journal of biological chemistry* **256,** 11032–11035 (1981).

31. Oldenburg, J., Bevans, C. G., Müller, C. R. & Watzka, M. Vitamin K epoxide reductase complex subunit 1 (VKORC1): the key protein of the vitamin K cycle. *Antioxidants & redox signaling* **8,** 347–353; 10.1089/ars.2006.8.347 (2006).

32. Czogalla, K. J. *et al.* Warfarin and vitamin K compete for binding to Phe55 in human VKOR. *Nature structural & molecular biology* **24,** 77–85; 10.1038/nsmb.3338 (2017).

33. Czogalla, K. J., Biswas, A., Rost, S., Watzka, M. & Oldenburg, J. The Arg98Trp mutation in human VKORC1 causing VKCFD2 disrupts a di-arginine-based ER retention motif. *Blood* **124,** 1354–1362; 10.1182/blood-2013-12-545988 (2014).

34. Czogalla, K. J. *et al.* Human VKORC1 mutations cause variable degrees of 4-hydroxycoumarin resistance and affect putative warfarin binding interfaces. *Blood* **122,** 2743–2750; 10.1182/blood-2013-05-501692 (2013).

35. Wu, S. M. *et al.* Genomic sequence and transcription start site for the human gamma-glutamyl carboxylase. *Blood* **89,** 4058–4062 (1997).

36. Kuo, W. L., Stafford, D. W., Cruces, J., Gray, J. & Solera, J. Chromosomal localization of the gamma-glutamyl carboxylase gene at 2p12. *Genomics* **25,** 746–748; 10.1016/0888-7543(95)80024-g (1995).

37. De Vilder, Eva Y G, Debacker, J. & Vanakker, O. M. GGCX-Associated Phenotypes: An Overview in Search of Genotype-Phenotype Correlations, 2017 Jan 25.

38. Tie, J., Wu, S. M., Jin, D., Nicchitta, C. V. & Stafford, D. W. A topological study of the human gamma-glutamyl carboxylase. *Blood* **96,** 973–978 (2000).

39. Canfield, L. M., Sinsky, T. A. & Suttie, J. W. Vitamin K-dependent carboxylase: purification of the rat liver microsomal enzyme. *Archives of biochemistry and biophysics* **202,** 515–524; 10.1016/0003-9861(80)90457-9 (1980).

40. Rishavy, M. A. & Berkner, K. L. Insight into the coupling mechanism of the vitamin K-dependent carboxylase: mutation of histidine 160 disrupts glutamic acid carbanion

formation and efficient coupling of vitamin K epoxidation to glutamic acid carboxylation. *Biochemistry* **47,** 9836–9846; 10.1021/bi800296r (2008).

41. Dowd, P., Hershline, R., Ham, S. W. & Naganathan, S. Vitamin K and energy transduction: a base strength amplification mechanism. *Science (New York, N.Y.)* **269,** 1684–1691; 10.1126/science.7569894 (1995).

42. Berkner, K. L. The vitamin K-dependent carboxylase. *Annual review of nutrition* **25,** 127–149; 10.1146/annurev.nutr.25.050304.092713 (2005).

43. Rishavy, M. A. *et al.* Bronsted analysis reveals Lys218 as the carboxylase active site base that deprotonates vitamin K hydroquinone to initiate vitamin K-dependent protein carboxylation. *Biochemistry* **45,** 13239–13248; 10.1021/bi0609523 (2006).

44. Rishavy, M. A. *et al.* A new model for vitamin K-dependent carboxylation: the catalytic base that deprotonates vitamin K hydroquinone is not Cys but an activated amine. *Proceedings of the National Academy of Sciences of the United States of America* **101,** 13732–13737; 10.1073/pnas.0404989101 (2004).

45. Rishavy, M. A. & Berkner, K. L. Insight into the coupling mechanism of the vitamin K-dependent carboxylase: mutation of histidine 160 disrupts glutamic acid carbanion formation and efficient coupling of vitamin K epoxidation to glutamic acid carboxylation. *Biochemistry* **47,** 9836–9846; 10.1021/bi800296r (2008).

46. Berkner, K. L. & Runge, K. W. The physiology of vitamin K nutriture and vitamin K-dependent protein function in atherosclerosis. *Journal of thrombosis and haemostasis : JTH* **2,** 2118–2132; 10.1111/j.1538-7836.2004.00968.x (2004).

47. Parker, C. H. *et al.* A conformational investigation of propeptide binding to the integral membrane protein gamma-glutamyl carboxylase using nanodisc hydrogen exchange mass spectrometry. *Biochemistry* **53,** 1511–1520; 10.1021/bi401536m (2014).

48. Mutucumarana, V. P. *et al.* Expression and characterization of the naturally occurring mutation L394R in human gamma-glutamyl carboxylase. *The Journal of biological chemistry* **275,** 32572–32577; 10.1074/jbc.M006808200 (2000).

49. Willems, B. A. G., Vermeer, C., Reutelingsperger, C. P. M. & Schurgers, L. J. The realm of vitamin K dependent proteins: shifting from coagulation toward calcification. *Molecular nutrition & food research* **58,** 1620–1635; 10.1002/mnfr.201300743 (2014).

50. Higgins-Gruber, S. L. *et al.* Effect of vitamin K-dependent protein precursor propeptide, vitamin K hydroquinone, and glutamate substrate binding on the structure and function of {gamma}-glutamyl carboxylase. *The Journal of biological chemistry* **285,** 31502–31508; 10.1074/jbc.M110.143297 (2010).

51. Johari, V. & Loke, C. Brief overview of the coagulation cascade. *Disease-a-month : DM* **58,** 421–423; 10.1016/j.disamonth.2012.04.004 (2012).

52. Roberts, H. R. & Lozier, J. N. New perspectives on the coagulation cascade. *Hospital practice (Office ed.)* **27,** 97-105, 109-12; 10.1080/21548331.1992.11705345 (1992).

53. Schenone, M., Furie, B. C. & Furie, B. The blood coagulation cascade. *Current opinion in hematology* **11,** 272–277; 10.1097/01.moh.0000130308.37353.d4 (2004).

54. Davie, E. W., Fujikawa, K. & Kisiel, W. The coagulation cascade: initiation, maintenance, and regulation. *Biochemistry* **30,** 10363–10370; 10.1021/bi00107a001 (1991).

55. Shantsila, E. & Lip, G. Y. H. Non-Vitamin K Antagonist Oral Anticoagulants: A Concise Guide. Adis, 2016.

56. Stenflo, J. Contributions of Gla and EGF-like domains to the function of vitamin K-dependent coagulation factors. *Critical reviews in eukaryotic gene expression* **9,** 59–88 (1999).

57. Nelsestuen, G. L., Shah, A. M. & Harvey, S. B. Vitamin K-dependent proteins. *Vitamins and hormones* **58,** 355–389; 10.1016/s0083-6729(00)58031-5 (2000).

58. Hoang, Q. Q., Sicheri, F., Howard, A. J. & Yang, D. S. C. Bone recognition mechanism of porcine osteocalcin from crystal structure. *Nature* **425,** 977–980; 10.1038/nature02079 (2003).

59. Katagiri, T. & Takahashi, N. Regulatory mechanisms of osteoblast and osteoclast differentiation. *Oral diseases* **8,** 147–159; 10.1034/j.1601-0825.2002.01829.x (2002).

60. Ducy, P. *et al.* Increased bone formation in osteocalcin-deficient mice. *Nature* **382,** 448–452; 10.1038/382448a0 (1996).

61. Karsenty, G. & Ferron, M. The contribution of bone to whole-organism physiology. *Nature* **481,** 314–320; 10.1038/nature10763 (2012).

62. Marulanda, J. *et al.* Matrix Gla protein deficiency impairs nasal septum growth, causing midface hypoplasia. *The Journal of biological chemistry* **292,** 11400–11412; 10.1074/jbc.M116.769802 (2017).

63. Shanahan, C. M., Weissberg, P. L. & Metcalfe, J. C. Isolation of gene markers of differentiated and proliferating vascular smooth muscle cells. *Circulation research* **73,** 193–204; 10.1161/01.res.73.1.193 (1993).

64. Shanahan, C. M., Cary, N. R., Metcalfe, J. C. & Weissberg, P. L. High expression of genes for calcification-regulating proteins in human atherosclerotic plaques. *The Journal of clinical investigation* **93,** 2393–2402; 10.1172/JCI117246 (1994).

65. Murshed, M., Schinke, T., McKee, M. D. & Karsenty, G. Extracellular matrix mineralization is regulated locally; different roles of two gla-containing proteins. *The Journal of cell biology* **165,** 625–630; 10.1083/jcb.200402046 (2004).

66. Eitzinger, N. *et al.* Ucma is not necessary for normal development of the mouse skeleton. *Bone* **50,** 670–680; 10.1016/j.bone.2011.11.017 (2012).

67. Lian, J. B., Boivin, G., Patterson-Allen, P., Grynpas, M. & Walzer, C. Calcergy and calciphylaxis: timed appearance of gamma-carboxyglutamic acid and osteocalcin in mineral deposits. *Calcified tissue international* **35,** 555–561; 10.1007/BF02405093 (1983).

68. Lian, J. B., Skinner, M., Glimcher, M. J. & Gallop, P. The presence of gamma-carboxyglutamic acid in the proteins associated with ectopic calcification. *Biochemical*

and biophysical research communications **73,** 349–355; 10.1016/0006-291x(76)90714-2 (1976).

69. Law, L. A., Graham, D. K., Di Paola, J. & Branchford, B. R. GAS6/TAM Pathway Signaling in Hemostasis and Thrombosis. *Frontiers in medicine* **5,** 137; 10.3389/fmed.2018.00137 (2018).

70. Hasanbasic, I., Rajotte, I. & Blostein, M. The role of gamma-carboxylation in the anti-apoptotic function of gas6. *Journal of thrombosis and haemostasis : JTH* **3,** 2790–2797; 10.1111/j.1538-7836.2005.01662.x (2005).

71. Tutusaus, A. *et al.* A Functional Role of GAS6/TAM in Nonalcoholic Steatohepatitis Progression Implicates AXL as Therapeutic Target. *Cellular and molecular gastroenterology and hepatology* **9,** 349–368; 10.1016/j.jcmgh.2019.10.010 (2020).

72. Novitskiy, S. V. *et al.* Gas6/MerTK signaling is negatively regulated by NF-κB and supports lung carcinogenesis. *Oncotarget* **10,** 7031–7042; 10.18632/oncotarget.27345 (2019).

73. Salmi, L. *et al.* Gas6/TAM Axis in Sepsis: Time to Consider Its Potential Role as a Therapeutic Target. *Disease markers* **2019,** 6156493; 10.1155/2019/6156493 (2019).

74. Bárcena, C. *et al.* Gas6/Axl pathway is activated in chronic liver disease and its targeting reduces fibrosis via hepatic stellate cell inactivation. *Journal of hepatology* **63,** 670–678; 10.1016/j.jhep.2015.04.013 (2015).

75. Laurance, S., Lemarié, C. A. & Blostein, M. D. Growth arrest-specific gene 6 (gas6) and vascular hemostasis. *Advances in nutrition (Bethesda, Md.)* **3,** 196–203; 10.3945/an.111.001826 (2012).

76. Fernández-Fernández, L., Bellido-Martín, L. & García de Frutos, P. Growth arrest-specific gene 6 (GAS6). An outline of its role in haemostasis and inflammation. *Thrombosis and haemostasis* **100,** 604–610; 10.1160/th08-04-0253 (2008).

77. Angelillo-Scherrer, A. *et al.* Deficiency or inhibition of Gas6 causes platelet dysfunction and protects mice against thrombosis. *Nat Med* **7,** 215–221; 10.1038/84667 (2001).

78. Yazicioglu, M. N. *et al.* Cellular localization and characterization of cytosolic binding partners for Gla domain-containing proteins PRRG4 and PRRG2. *The Journal of biological chemistry* **288,** 25908–25914; 10.1074/jbc.M113.484683 (2013).

79. Watzka, M. *et al.* Bleeding and non-bleeding phenotypes in patients with GGCX gene mutations. *Thrombosis research* **134,** 856–865; 10.1016/j.thromres.2014.07.004 (2014).

80. Brenner, B. *et al.* A missense mutation in gamma-glutamyl carboxylase gene causes combined deficiency of all vitamin K-dependent blood coagulation factors. *Blood* **92,** 4554–4559 (1998).

81. Spronk, H. M., Farah, R. A., Buchanan, G. R., Vermeer, C. & Soute, B. A. Novel mutation in the gamma-glutamyl carboxylase gene resulting in congenital combined deficiency of all vitamin K-dependent blood coagulation factors. *Blood* **96,** 3650–3652 (2000).

82. Darghouth, D. *et al.* Compound Heterozygosity of a W493C Substitution and R704/Premature Stop Codon within the γ-Glutamyl Carboxylase in Combined Vitamin K-Dependent Coagulation Factor Deficiency in a French Family. *Blood* **114,** 1302; 10.1182/blood.V114.22.1302.1302 (2009).

83. Darghouth, D. *et al.* Compound heterozygosity of novel missense mutations in the gamma-glutamyl-carboxylase gene causes hereditary combined vitamin K-dependent coagulation factor deficiency. *Blood* **108,** 1925–1931; 10.1182/blood-2005-12-010660 (2006).

84. Lunghi, B. *et al.* Novel phenotype and γ-glutamyl carboxylase mutations in combined deficiency of vitamin K-dependent coagulation factors. *Haemophilia : the official journal of the World Federation of Hemophilia* **17,** 822–824; 10.1111/j.1365-2516.2011.02524.x (2011).

85. Li, Q. *et al.* Mutations in the GGCX and ABCC6 genes in a family with pseudoxanthoma elasticum-like phenotypes. *The Journal of investigative dermatology* **129,** 553–563; 10.1038/jid.2008.271 (2009).

86. Li, Q. *et al.* Co-existent pseudoxanthoma elasticum and vitamin K-dependent coagulation factor deficiency: compound heterozygosity for mutations in the GGCX gene. *The American journal of pathology* **174,** 534–540; 10.2353/ajpath.2009.080865 (2009).

87. Rost, S. *et al.* Compound heterozygous mutations in the gamma-glutamyl carboxylase gene cause combined deficiency of all vitamin K-dependent blood coagulation factors. *British journal of haematology* **126,** 546–549; 10.1111/j.1365-2141.2004.05071.x (2004).

88. Tie, J.-K. *et al.* Characterization of vitamin K-dependent carboxylase mutations that cause bleeding and nonbleeding disorders. *Blood* **127,** 1847–1855; 10.1182/blood-2015-10-677633 (2016).

89. Goldsmith, G. H., JR, Pence, R. E., Ratnoff, O. D., Adelstein, D. J. & Furie, B. Studies on a family with combined functional deficiencies of vitamin K-dependent coagulation factors. *The Journal of clinical investigation* **69,** 1253–1260; 10.1172/jci110564 (1982).

90. Soute, B. A. M. *et al.* Characteristics of recombinant W501S mutated human gamma-glutamyl carboxylase. *Journal of thrombosis and haemostasis : JTH* **2,** 597–604; 10.1111/j.1538-7836.2004.00686.x (2004).

91. Napolitano, M., Mariani, G. & Lapecorella, M. Hereditary combined deficiency of the vitamin K-dependent clotting factors. *Orphanet journal of rare diseases* **5,** 21; 10.1186/1750-1172-5-21 (2010).

92. Rishavy, M. A., Hallgren, K. W., Zhang, H., Runge, K. W. & Berkner, K. L. Exon 2 skipping eliminates γ-glutamyl carboxylase activity, indicating a partial splicing defect in a patient with vitamin K clotting factor deficiency. *Journal of thrombosis and haemostasis : JTH* **17,** 1053–1063; 10.1111/jth.14456 (2019).

93. Rost, S. *et al.* Founder mutation Arg485Pro led to recurrent compound heterozygous GGCX genotypes in two German patients with VKCFD type 1. *Blood coagulation & fibrinolysis : an international journal in haemostasis and thrombosis* **17,** 503–507; 10.1097/01.mbc.0000240927.88177.d1 (2006).

94. Vanakker, O. M. *et al.* Pseudoxanthoma elasticum-like phenotype with cutis laxa and multiple coagulation factor deficiency represents a separate genetic entity. *The Journal of investigative dermatology* **127,** 581–587; 10.1038/sj.jid.5700610 (2007).

95. Nollet, L., van Gils, M., Verschuere, S. & Vanakker, O. The Role of Vitamin K and Its Related Compounds in Mendelian and Acquired Ectopic Mineralization Disorders. *International journal of molecular sciences* **20**; 10.3390/ijms20092142 (2019).

96. Munroe, P. B. *et al.* Mutations in the gene encoding the human matrix Gla protein cause Keutel syndrome. *Nature genetics* **21,** 142–144; 10.1038/5102 (1999).

97. Land, H. & Humble, M. S. YASARA: A Tool to Obtain Structural Guidance in Biocatalytic Investigations. *Methods in molecular biology (Clifton, N.J.)* **1685,** 43–67; 10.1007/978-1-4939-7366-8_4 (2018).

98. Roy, A., Kucukural, A. & Zhang, Y. I-TASSER: a unified platform for automated protein structure and function prediction. *Nature protocols* **5,** 725–738; 10.1038/nprot.2010.5 (2010).

99. Yan, Y., Di Zhang, Zhou, P., Li, B. & Huang, S.-Y. HDOCK: a web server for protein-protein and protein-DNA/RNA docking based on a hybrid strategy. *Nucleic acids research* **45,** W365-W373; 10.1093/nar/gkx407 (2017).

100. Schmid-Burgk, J. L., Höning, K., Ebert, T. S. & Hornung, V. CRISPaint allows modular base-specific gene tagging using a ligase-4-dependent mechanism. *Nature communications* **7,** 12338; 10.1038/ncomms12338 (2016).

101. Ghosh, S. *et al.* GGCX mutations show different responses to vitamin K thereby determining the severity of the hemorrhagic phenotype in VKCFD1 patients. *Journal of thrombosis and haemostasis : JTH*; 10.1111/jth.15238 (2021).

102. Rieder, M. J. *et al.* Effect of VKORC1 haplotypes on transcriptional regulation and warfarin dose. *The New England journal of medicine* **352,** 2285–2293; 10.1056/NEJMoa044503 (2005).

103. Rishavy, M. A., Hallgren, K. W. & Berkner, K. L. The vitamin K-dependent carboxylase generates gamma-carboxylated glutamates by using CO2 to facilitate glutamate deprotonation in a concerted mechanism that drives catalysis. *The Journal of biological chemistry* **286,** 44821–44832; 10.1074/jbc.M111.249177 (2011).

104. Mutucumarana, V. P., Acher, F., Straight, D. L., Jin, D.-Y. & Stafford, D. W. A conserved region of human vitamin K-dependent carboxylase between residues 393 and 404 is important for its interaction with the glutamate substrate. *The Journal of biological chemistry* **278,** 46488–46493; 10.1074/jbc.M307707200 (2003).

105. Tie, J.-K. & Stafford, D. W. Structural and functional insights into enzymes of the vitamin K cycle. *Journal of thrombosis and haemostasis : JTH* **14,** 236–247; 10.1111/jth.13217 (2016).

106. Tai, S. J. *et al.* A viable mouse model of factor X deficiency provides evidence for maternal transfer of factor X. *Journal of thrombosis and haemostasis : JTH* **6,** 339–345; 10.1111/j.1538-7836.2007.02849.x (2008).

107. Zhu, A. *et al.* Fatal hemorrhage in mice lacking gamma-glutamyl carboxylase. *Blood* **109,** 5270–5275; 10.1182/blood-2006-12-064188 (2007).

108. Kariminejad, A. *et al.* Retinitis pigmentosa, cutis laxa, and pseudoxanthoma elasticum-like skin manifestations associated with GGCX mutations. *The Journal of investigative dermatology* **134,** 2331–2338; 10.1038/jid.2014.191 (2014).

109. Marconi, B. *et al.* Pseudoxanthoma elasticum and skin: Clinical manifestations, histopathology, pathomechanism, perspectives of treatment. *Intractable & rare diseases research* **4,** 113–122; 10.5582/irdr.2015.01014 (2015).

110. Germain, D. P. Pseudoxanthoma elasticum. *Orphanet journal of rare diseases* **12,** 85; 10.1186/s13023-017-0639-8 (2017).

111. Bleeding and non-bleeding phenotypes in patients Bleeding and non-bleeding phenotypes in patients with GGCX gene mutations.

112. Azuma, K. *et al.* Osteoblast-Specific γ-Glutamyl Carboxylase-Deficient Mice Display Enhanced Bone Formation With Aberrant Mineralization. *Journal of bone and mineral research : the official journal of the American Society for Bone and Mineral Research* **30,** 1245–1254; 10.1002/jbmr.2463 (2015).

113. de Boer-van den Berg, M A, Verstijnen, C. P. & Vermeer, C. Vitamin K-dependent carboxylase in skin. *The Journal of investigative dermatology* **87,** 377–380; 10.1111/1523-1747.ep12524848 (1986).

114. Viegas, C. *et al.* Use of an innovative system and nanotechnology-based strategy for therapeutic applications of Gla-rich protein (GRP). *Annals of Medicine* **51,** 38; 10.1080/07853890.2018.1561804 (2019).

115. Songmen, S., Panta, O. B., Paudel, S. S. & Ghimire, R. K. Chondrodysplasia Punctata: A Case Report of Fetal Warfarin Syndrome. *J Nepal Health Res Counc* **15,** 81–84; 10.3126/jnhrc.v15i1.18026 (2017).

116. Luo, G. *et al.* Spontaneous calcification of arteries and cartilage in mice lacking matrix GLA protein. *Nature* **386,** 78–81; 10.1038/386078a0 (1997).

117. Viegas, C. S. B. *et al.* Gla-rich protein acts as a calcification inhibitor in the human cardiovascular system. *Arteriosclerosis, thrombosis, and vascular biology* **35,** 399–408; 10.1161/ATVBAHA.114.304823 (2015).

118. Mandelbrot, L. *et al.* Placental transfer of vitamin K1 and its implications in fetal hemostasis. *Thrombosis and haemostasis* **60,** 39–43 (1988).

119. Nakamura, Y. S. *et al.* Tyro 3 receptor tyrosine kinase and its ligand, Gas6, stimulate the function of osteoclasts. *Stem cells (Dayton, Ohio)* **16,** 229–238; 10.1002/stem.160229 (1998).

120. Stenhoff, J., Dahlback, B. & Hafizi, S. Vitamin K-dependent Gas6 activates ERK kinase and stimulates growth of cardiac fibroblasts. *Biochemical and biophysical research communications* **319,** 871–878; 10.1016/j.bbrc.2004.05.070 (2004).

121. Fourcot, A. *et al.* Gas6 deficiency prevents liver inflammation, steatohepatitis, and fibrosis in mice. *Am J Physiol Gastrointest Liver Physiol* **300,** G1043-53; 10.1152/ajpgi.00311.2010 (2011).

122. Yamamoto, T. *et al.* Narrowing of the responsible region for severe developmental delay and autistic behaviors in WAGR syndrome down to 1.6 Mb including PAX6, WT1, and PRRG4. *American journal of medical genetics. Part A* **164A,** 634–638; 10.1002/ajmg.a.36325 (2014).

123. Pan, D. The hippo signaling pathway in development and cancer. *Developmental cell* **19,** 491–505; 10.1016/j.devcel.2010.09.011 (2010).

List of publications

- **Suvoshree Ghosh**, Katrin Kraus, Arijit Biswas, Jens Müller, Anna-Lena Buhl, Francesco Forin, Heike Singer, Klara Höning, Veit Hornung, Matthias Watzka, Katrin J. Czogalla-Nitsche and Johannes Oldenburg. **GGCX mutations show different responses to vitamin K thereby determining the severity of the hemorrhagic phenotype in VKCFD1 patients.** January 2021, *Journal of Thrombosis and Haemostasis*. doi: 10.1111/jth.15238

- **Suvoshree Ghosh**, Katrin Kraus, Arijit Biswas, Jens Müller, Francesco Forin, Heike Singer, Klara Höning, Veit Hornung, Matthias Watzka, Katrin J. Czogalla-Nitsche and Johannes Oldenburg. **GGCX variants leading to biallelic deficiency to γ-carboxylate GRP cause skin laxity in VKCFD1 patients**. October 2021, *Human mutation*. doi: 10.22541/au.161908504.42031882/v1

- Behnaz Pezeshkpoor, Katrin J Czogalla, Michael Caspers, Ann-Cristin Berkemeier, Kerstin Liphardt, **Suvoshree Ghosh**, Marco Kellner, Silvia Ulrich, Anna Pavlova, Johannes Oldenburg. **Variants in FIX propeptide associated with vitamin K antagonist hypersensitivity: functional analysis and additional data confirming the common founder mutations.** February 2018, *Annals of Hematology*. doi: 10.1007/s00277-018-3264-2

Acknowledgement

I would like to thank Prof. Dr. Johannes Oldenburg for providing his supervision and giving me the opportunity to work in the Institute of Experimental Haematology and Transfusion medicine. I would also like to thank my second supervisor Prof. Dr. Diana Imhof for her support and guidance.

I would like to express my immense gratitude towards my supervisor and mentor Dr. rer. nat. Katrin J. Czogalla-Nitsche for giving me this project and for providing all the required guidance. I would also thank Ms. Katrin Kraus for the technical help, without her assistance creating 400 plasmids would not have been easy.

I would like to thank PD. Dr. Arijit Biswas and PD. Dr. Jens Mueller for their support with *in silico* modeling and ELISA establishment. I thank PD. Dr. Matthias Watzka for assisting with the patient data.

Furthermore, I would like to thank my wonderful colleagues Dr. Heike Singer and Dr. Kerstin Liphardt for their support.

I am highly obliged to my parents Mr. Kajal Ghosh and Mrs. Babi Ghosh and my husband Dr. Rajiv Sundaramoorthy for their constant support. They are the sole reason for all of my achievements.